TECHNISCHE UNIVERSITÄT MÜNCHEN

Fakultät für Chemie
Bayerisches NMR–Zentrum
Arbeitsgruppe für Strukturelle Membranbiochemie

Analysis of the dynamics and interactions of an inhibitory Gα subunit and thermostabilized neurotensin receptor variants by NMR spectroscopy

DAVID GORIČANEC

Vollständiger Abdruck der von der Fakultät für Chemie der Technischen Universität München zur Erlangung des akademischen Grades eines

Doktors der Naturwissenschaften

genehmigten Dissertation.

Vorsitzende(r):   Priv. Doz. Dr. Gerd Gemmecker
Prüfer der Dissertation:

1. Prof. Dr. Franz Hagn
2. Prof. Dr. Bernd Reif

Die Dissertation wurde am 20.05.2020 bei der Technischen Universität München eingereicht und durch die Fakultät für Chemie am 14.07.2020 angenommen.

Analysis of the dynamics and interactions of an inhibitory Gα subunit and thermostabilized neurotensin receptor variants by NMR spectroscopy

Untersuchung der Dynamik und der Interaktionen einer inhibitorischen Gα Untereinheit und thermisch stabilisierten NTR1 Varianten mittels NMR Spektroskopie

Dissertation

zum Erlangen des akademischen Grades

Doktor der Naturwissenschaften (Dr. rer. nat.)

vorgelegt von

David Goričanec

geboren am 11.03.1988 in München

Technische Universität München

Fakultät für Chemie

Bayerisches NMR–Zentrum

Arbeitsgruppe für Strukturelle Membranbiochemie

Garching bei München, 2020

Contents

Abstract/Zusammenfassung

Abstract

One of the most important classes of membrane proteins are G-Protein-coupled-receptors (GPCRs). GPCRs represent a big part of the protein coding genome and are responsible for many biochemical processes, ranging from cancer to neurology. Due to their big role in physiology and pathophysiology, many drugs target GPCRs, to date approximately 1/3 of all FDA approved drugs. In order to understand these processes better and to develop drugs targeting those signaling pathways, it is from biggest importance to get a deeper understanding of the structure and dynamics of GPCRs and their corresponding G-proteins.

In this work, I used evolutionary stabilized Neurotensin 1 Receptor (NTR1) variants with different signaling capacity as a model system for the investigating the dynamics and interactions of a GPCR by NMR spectroscopy. The reason for this choice is an easy and effective production of this GPCR in *E. coli*, which is needed for isotope labeling for nuclear magnetic resonance (NMR) spectroscopy experiments. On the G-protein side, either the heterotrimeric G-protein extracted from insect cells or the alpha subunit (Gα) produced in *E.coli* was used. The key goal was to understand the effects of the dynamics of GPCRs and G-proteins on their interaction with each other.

The first goal was to study the role of the nucleotide state of Gα on its structure and dynamics and therefor on its interaction with an activated GPCR. Thereby I showed that Gα in an apo state has the highest affinity to an activated GPCR as well as an open conformation enhancing GTP binding. In line with these findings, GTP-bound Gα shows no significant affinity to an activated GPCR with a tightly closed conformation. I used NMR experiments for the investigation of labeled Gα in this project. The second part of my work was focused on the GPCR side. Therefore, different labeling strategies like ^{13}C methyl sulfide or selective isoleucine, leucine, valine and alanine (ILVA) labeling were used in order to facilitate NMR experiments to detect allosteric structural changes and dynamics during signaling. I could show that GPCR activation affects the whole GPCR with an allosteric mechanism, resulting in a helix 6 rearrangement on the cytosolic side. This is essential for the interaction of a GPCR with G-proteins. Furthermore, I could verify the importance of the ionic lock motif GPCR signaling.

In summary, I was able to obtain a deeper understanding of the interaction between GPCRs and G-proteins, with a focus on each binding partner. Nonetheless, future experiments are required to further characterize GPCR plasticity and determine the allosteric structural changes that are required to transfer the signal induced by ligand binding through the membrane to activate a bound G-protein.

Zusammenfassung

Eine der wichtigsten Klassen von Membranproteinen sind G-Protein-gekoppelte Rezeptoren (GPCRs). GPCRs stellen einen großen Teil des Protein-kodierenden Genoms dar und sind für viele biochemische Prozesse verantwortlich, die von Krebs bis zur Neurologie reichen. Aufgrund ihrer großen Rolle in der Physiologie und Pathophysiologie zielen viele Medikamente auf GPCRs ab, bis heute etwa 1/3 aller von der FDA zugelassenen Medikamente. Um diese Prozesse besser zu verstehen und Medikamente zu entwickeln, die auf diese Signalwege abzielen, ist es von größter Bedeutung, ein tieferes Verständnis der Struktur und Dynamik von GPCRs und ihren entsprechenden G-Proteinen zu erlangen.

In dieser Arbeit verwendete ich evolutionär stabilisierte Neurotensin-1-Rezeptor (NTR1) - Varianten mit unterschiedlicher Signalkapazität als Modellsystem für die Untersuchung der Dynamik und Wechselwirkungen eines GPCR mittels NMR-Spektroskopie. Der Grund für diese Wahl ist eine einfache und effektive Herstellung dieses GPCR in *E. coli*, die für die Isotopenmarkierung für Kernspinresonanz (nuclear magnetic resonance, NMR) – Spektroskopieexperimente benötigt wird. Auf der G-Protein-Seite wurde entweder das aus Insektenzellen extrahierte heterotrimere G-Protein oder die in *E. coli* hergestellte Alpha-Untereinheit (Gα) verwendet. Das Hauptziel war es, die Auswirkungen der Dynamik von GPCRs und G-Proteinen auf ihre Wechselwirkung miteinander zu verstehen.

Das erste Ziel war es, die Rolle des Nukleotidzustands von Gα auf seine Struktur und Dynamik und damit auf seine Wechselwirkung mit einem aktivierten GPCR zu untersuchen. Dabei habe ich gezeigt, dass Gα in einem Apo-Zustand die höchste Affinität zu einem aktivierten GPCR sowie eine offene Konformation aufweist, die die GTP-Bindung verstärkt. In Übereinstimmung mit diesen Befunden zeigt GTP-gebundenes Gα keine signifikante Affinität zu einem aktivierten GPCR mit einer eng geschlossenen Konformation. Ich habe in diesem Projekt NMR-Experimente zur Untersuchung von markiertem Gα verwendet. Der zweite Teil meiner Arbeit konzentrierte sich auf die GPCR-Seite. Daher wurden verschiedene Markierungsstrategien wie ^{13}C-Methylsulfid oder selektive Isoleucin-, Leucin-, Valin- und Alanin-Markierung (ILVA) verwendet, um NMR-Experimente zum Nachweis allosterischer Strukturänderungen und -dynamiken während der Signalübertragung zu erleichtern. Ich konnte zeigen, dass die GPCR-Aktivierung den gesamten GPCR mit einem allosterischen Mechanismus beeinflusst, was zu einer Helix-6-Umlagerung auf der zytosolischen Seite führt. Dies ist wesentlich für die Wechselwirkung eines GPCR mit G-Proteinen. Darüber hinaus konnte ich die Bedeutung des „ionic lock" Motivs bestätigen für die GPCR-Signalübertragung.

Zusammenfassend konnte ich ein tieferes Verständnis der Wechselwirkung zwischen GPCRs und G-Proteinen gewinnen, wobei ich mich auf jeden Bindungspartner konzentrierte. Dennoch sind zukünftige Experimente erforderlich, um die GPCR-Plastizität weiter zu charakterisieren und die allosterischen Strukturänderungen zu bestimmen, die erforderlich sind, um das durch Ligandenbindung induzierte Signal durch die Membran zu übertragen und ein gebundenes G-Protein zu aktivieren.

1. Introduction

1.1. G-Protein-coupled-receptors (GPCRs)

G-Protein-coupled-receptors (GPCRs) play an important role in cell physiology. They are membrane proteins consisting of seven transmembrane (TM) α-helices. Due to their importance in human physiology, they represent an important drug target. So far, more than 30 % of all drugs which have been approved by the US Food and Drug Administration (FDA) target GPCRs (Hauser et al., 2017; Wacker et al., 2017). These drugs are used to treat various diseases like cardiovascular diseases, inflammatory diseases or problems with the central nervous system (CNS). Still, only 27 % of all human non-olfactory GPCRs have been targeted so far (Santos et al., 2017). This number shows that there is still a lot of potential for the discovery of new drugs, treating GPCR-linked diseases.

Generally activated GPCRs induce heterotrimeric G protein induced downstream signaling. There also exists G protein independent signaling pathways like β-Arrestin mediated downstream signaling (Peterson and Luttrell, 2017). As this thesis is focused on the structure and dynamics of GPCRs and G proteins, the attention will be directed to G protein dependent downstream signaling. Figure 1.1 shows a schematic overview of GPCR mediated signaling.
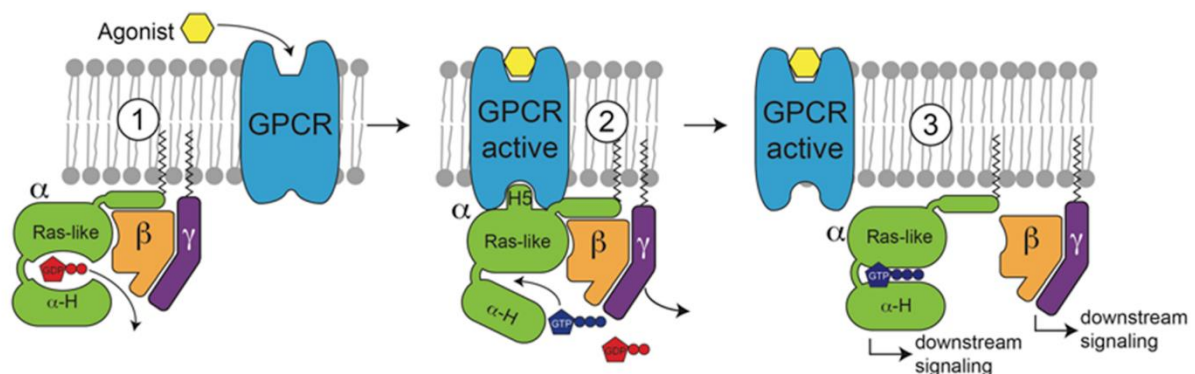

Figure 1.1: G-protein-coupled receptor (GPCR) mediated signaling
The GPCR signaling starts with agonist binding to the GPCR. Thereby the GPCR changes its conformation and is active. GDP bound heterotrimeric G protein is inactive, but has an increased affinity to bind active GPCRs (1). Upon binding between the activated GPCR and the G protein, a conformational change in the α subunit (especially helix 5 of the Ras domain) of the G protein enhances the dissociation of the GDP in the nucleotide binding pocket. This apo state of the G protein has the highest affinity to the activated GPCR and GTP (2). As soon as GTP binds to the α subunit of the G protein, the G protein dissociates from the activated GPCR. The two major subunits dissociate into the α subunit and the βγ subunit. Both are responsible for downstream signaling and have no significant affinity to the activated GPCR (3). When the α subunit hydrolyzes the GTP to GDP with its intrinsic enzymatic activity, the heterotrimeric G protein can reassemble and the cycle can start again. Figure shown as in the original publication (Goricanec et al., 2016).

In the Guanosine diphosphate (GDP) bound state, the G Protein α subunit forms a heterotrimer with the βγ subunit. This GDP bound heterotrimeric G Protein is signaling inactive. If a GPCR is activated by an agonist, the nucleotide exchange from GDP to Guanosine triphosphate (GTP) is catalyzed in the α subunit. This results in the dissociation of the heterotrimeric G protein (Oldham and Hamm, 2008). The GTP bound α subunit as well as the βγ subunit are both activating various effectors, i.e. adenylyl cyclase, Ca^{2+} channels, phospholipase C, cGMP (cyclic guanosine monophosphat) phosphodiesterase or phospho-inosite 3 kinase (Khan et al., 2013; Milligan and Kostenis, 2006; Smrcka, 2008). As soon as GTP is hydrolyzed to GDP due to the intrinsic GTPase activity of the α subunit, the heterotrimer is formed again. This stops the signaling potency of both subunits and completes the GPCR G protein activation cycle.

It was shown that certain receptors had in common that they catalyze the nucleotide exchange in heterotrimeric G proteins (Gilman, 1987). Over time, genome wide sequencing displayed that more than 800 such receptors can be classified as GPCRs (Fredriksson et al., 2003). These GPCRs can then be divided in 5 different classes. The by far biggest class is the "rhodopsin-like" family (class A) consisting over 700 different members (Alexander et al., 2017). It has receptors selective for biogenic amines, peptides, lipids, nucleotides and odorants to only name some ligand types. The "secretin-like" family (class B) usually binds long α-helical peptides like the glucagon receptor. The third family is the "adhesion-like" one. So far it is fairly little known about these receptors. The "glutamate-like" family (class D) has the glutamate receptor and γ-amino butyric acid (GABA) receptor as most known members. Finally, the least understood GPCR family is the "frizzled-like" (class F) which plays important roles in developmental biology.

To improve the comparability of class A GPCRs, the "Ballesteros Weinstein nomenclature" was developed (Ballesteros and Weinstein, 1995). Thereby the most conserved residue in each transmembrane helix is given the number 50 and the number of the TM helix is put in front (i.e. R3.50 for the arginine of the ionic lock in helix 3). All other are residues numbered relative to this position. For each individual GPCR the position in the sequence can be added in brackets after the amino acid identifier (i.e. R3.50(167) in the case of the neurotensin receptor 1 (NTR1)). The chosen conserved residues as well as their relative position in the NTR1 are shown in Table 1.1.

Table 1.1. Generalized numbering scheme according to Ballesteros and Weinstein 1995

Transmembrane helix (TMH)	100% conserved in neurotransmitter GPCR	AA identifier	AA No. in rat NTR1	AA identifier in rat NTR1
1	Asn	N1.50	82	N1.50(82)
2	Asp	D2.50	113	D2.50(113)
3	Arg	R3.50	167	R3.50(167)
4	Trp	W4.50	194	W4.50(194)
5	Pro	P5.50	249	P5.50(249)
6	Pro	P6.50	323	P6.50(323)
7	Pro	P7.50	366	P7.50(366)

The first solved structure of a GPCR was bovine rhodopsin (Palczewski et al., 2000). It was extracted from cow retinas and it is the reference structure of an inactive class A GPCR as it shows no basal activity at all.

The first GPCR for which a structure with a diffusible ligand was solved, was the beta-2 adrenergic receptor (β2AR) with Carazolol, a high affinity inverse agonist. To enable the structure determination, β2AR had to be stabilized. This was done with two different approaches. One of the approaches for the structure determination was to use a Fab5 antibody fragment (Day et al., 2007) binding to the very flexible 3rd intracellular loop (IC3) to stabilize the Carazolol bound structure of β2AR in lipid bicelles (Rasmussen et al., 2007). The other approach was to genetically engineer a T4 lysozyme (T4L) into the GPCR which then replaces most of the IC3 of β2AR. With this construct, the structure of Carazolol bound β2AR in lipidic cubic phases was also solved (Cherezov et al., 2007). Both approaches were compared and showed a very similar structure (Rosenbaum et al., 2007). The latter study also compared the Carazolol bound β2AR structures to the structure of bovine rhodopsin. It was shown that the interaction in the ionic lock between the E(D)RY motif and the E6.30 is only present in the bovine rhodopsin, but not in the case of β2AR. This shows that Carazolol does not inhibit the basal activity of β2AR completely.

These methods were also applied to other GPCRs and lead to structures being solved, i.e. the M3 muscarinic acetylcholine receptor with T4L fusion bound to the antagonist tiotropium (Kruse et al., 2012) or the δ-opioid receptor with T4L fusion bound to the antagonist naltrindole (Granier et al., 2012). All these structures showed the distinct features of class A GPCRs.

Experiments to solve agonist bound structures of GPCRs with the previously shown methods (either the T4L or the Fab) failed. This can be explained by lower stability of the active state of a GPCR in the absence of a G protein. In order to stabilize these GPCRs in their active state, nanobodies can be designed which show a G protein-like behavior (Manglik et al., 2017; Steyaert and Kobilka, 2011). For β2AR a screening showed that Nb80 behaves like a G protein and therefor was used to obtain the active structure (Rasmussen et al., 2011a). In this study BI-167107 was used as agonist, as it showed better efficacy, affinity and off-rate profile than isoproterenol.

This method has led to many solved active-state GPCR structures. In the case of β2AR it was also possible to compare multiple different agonists and their effect on the structure (Ring et al., 2013). Other examples for known structures of GPCRs in an active state are the M2 muscarinic acetylcholine receptor (Kruse et al., 2013) and μ-opioid receptor (Huang et al., 2015).

Most GPCRs have a basal signaling activity, which can be influenced by ligands. Ligands can be defined according to their influence on the signaling: a full agonist promotes maximum signaling, a partial agonist leads to submaximum signaling, an inverse agonist causes reduced basal activity whereas a neutral antagonist has no influence on the basal activity but competitively binds to the receptor (see Figure 1.2).
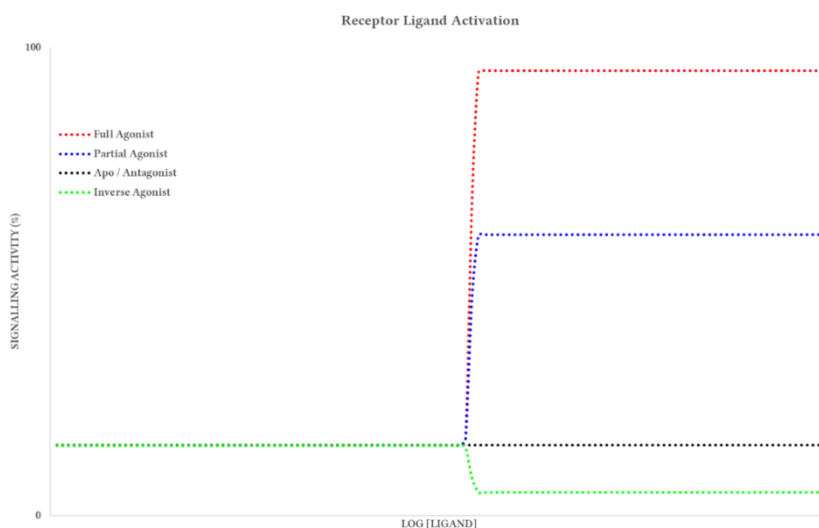

Figure 1.2: Influence of various ligand types on receptor signaling
This figure shows exemplary signaling activities of various different ligands on receptors. The apo or antagonist state represents the basal state. This should not be misunderstood as the state with the lowest activity. Inverse agonists decrease the signaling activity even further than the activity of the basal state. Full agonists maximize the signaling activity. Partial agonists can be anywhere between full agonists and the apo/antagonist state. This one showed in the figure is only randomly chosen for a better representation.

Ligands can also be differentiated depending on the selectivity of downstream signaling they promote (i.e. which G protein is favored or if there is a preference for G protein or β-Arrestin signaling). If any type of selectivity exists, the ligands causing it are called biased ligands (Kenakin, 2013; Smith et al., 2018).

The way how ligands influence GPCR signaling is by stabilizing certain populations of the receptor. This phenomenon is called the conformational selection. Thereby the signal intensity (Ye et al., 2016) as well as the signal bias (Liu et al., 2012) are influenced.

Ligand bias plays an important role in GPCR drug discovery as many side effects of drugs are caused by certain downstream signaling pathways which are not necessarily the same as for the desired effect of the drug (Kenakin, 2011; Smith et al., 2018). A prominent example for this in the case of GPCRs are opioid receptors, as they are one of the most drugged targets worldwide with severe problems caused by the side effects of the available drugs. It was shown that in the case of the μ-OR G protein biased ligands show fewer side effects than β-arrestin biased ligands (Majumdar and Devi, 2018; Manglik et al., 2016; Soergel et al., 2014).

To better understand, how ligands alter GPCR dynamics and therefor select certain conformations, various class A GPCRs were compared. Thereby the most conserved sequence motifs were compared in the active and inactive state. As an exemplary GPCR, the β2-AR has been described in this context (Weis and Kobilka, 2018).

One of the most conserved sequences is the D(E)3.49-R3.50-Y3.51 motif, which is present near the cytosolic side and close to the G protein binding site. If the GPCR is not active, the R3.50 is stabilized by an intrahelical salt bridge to D(E)3.49 and additionally by interhelical hydrophobic interactions with L6.34 and L6.37. R3.50 also interacts with E6.30 and forms a salt bridge in dark rhodopsin. This motif is also called the ionic lock (Ballesteros et al., 2001). In most inactive GPCRs, this interactions form only transiently (Dror et al., 2009), which also explains a low basal activity for these GPCRs.

As mentioned earlier, this work focuses on G proteins as effector molecules activated by GPCRs. Compared to the big diversity in GPCRs, heterotrimeric G proteins show only a small variety in the human genome. Based on their genetic homology, the human α subunit of G proteins (Gα) consists of 16 different genes which can be organized into 4 G protein families (Gα$_s$, Gα$_{i/o}$, Gα$_{q/11}$ and Gα$_{12/13}$). The human βγ subunit (Gβγ) is composed of 5 different β genes and 12 different γ genes (Downes and Gautam, 1999). Due to the big difference in the diversity of GPCRs and G proteins, it is assumed, that there is a conserved mechanism of GPCR mediated G protein acitivation.

The nucleotide binding site is between the two domains of Gα, the Ras-like (Ras) GTPase domain and the α-helical domain (AHD) (Oldham and Hamm, 2006; Sprang, 1997). Most interactions between the nucleotide and the Gα are present between the Ras domain and the nucleotide. The second part of the binding pocket is built by the AHD. Various biophysical studies have indicated that domain separation in Gα plays an important role in nucleotide release (Dror et al., 2015; Van Eps et al., 2011; Yao et al., 2016). Nevertheless, it also has been shown by deletion of the AHD, that even in the absence of the AHD, GDP still binds to the Ras domain and can activate downstream signaling (Markby et al., 1993). This finding is further supported by molecular dynamics (MD) simulations and double electron-electron resonance (DEER) distance measurements of GDP-bound heterotrimeric G proteins, showing even in case of domain separation or AHD deletion, that the nucleotide was still bound to the Ras domain (Dror et al., 2015). All these findings lead to the assumption that nucleotide release needs to be stimulated in the Ras domain via an activated receptor.

As described earlier, many structures of inactivated as well as activated GPCRs haven been solved in recent years. In order to obtain a better understanding of GPCR signaling and dynamics, it was tried to obtain a structure of a GPCR and a G protein in complex. So far this only succeeded once via crystallography with a heterotrimeric G protein in complex with β2AR T4L and a G protein stabilizing nanobody (Rasmussen et al., 2011b). This structure also shows that the AHD of GDP-bound Gα flips out after binding to an activated GPCR. It was also the first structure showing the interactions between the cytoplasmic GPCR side and the G protein. Especially helix 5 (α5) of the nucleotide free Gα shows strong interactions with intracellular GPCR surface and displacement compared to GTP-bound Gα. Compared to the activated structure which has been only stabilized with a nanobody (Rasmussen et al., 2011a), the differences are neglectable. A common feature in activated class A GPCRs is the outward movement of TM6 (Latorraca et al., 2017) making it accessible to the G protein. The importance of TM6 movement for the interaction with the G protein is further supported by a comparison of 5 different class A GPCRs in their active as well as inactive state (Venkatakrishnan et al., 2016).

Another advance in the investigation of GPCR G protein interaction was the use of optimized Ras domains, also called mini-G proteins (Carpenter and Tate, 2016; Nehme et al., 2017), instead of full length Gα to crystalize the complexes. When comparing the β2AR Gs structure (Rasmussen et al., 2011b) with A2AR in complex with a mini-Gs many similarities in the binding interface could be determined (Carpenter et al., 2016).

The most recent breakthrough in the structure determination of GPCR G protein complexes is the emerging of high resolution cryo electron microscopy (cryo-EM). The first solved cryo-EM structure of a GPCR in complex with a heterotrimeric G protein was the calcitonin receptor (Liang et al., 2017), shortly followed by the glucagon-like peptide-1 receptor (Zhang et al., 2017). Since then the structure of many GPCRs from different families in complex with heterotrimeric G proteins have been solved (see Table 1.2).

Table 1.2. Cryo-EM structures of different GPCRs in complex with heterotrimeric G proteins

Receptor	GPCR class	G protein	Res.	Reference
Calcitonin receptor (CALCR)	B1	G_s	4.1 Å	(Liang et al., 2017)
Glucagon like peptide 1 receptor (GLP1R)	B1	G_s	4.1 Å	(Zhang et al., 2017)
Adenosine receptor A2a ($A_{2A}R$)	A	G_s	4.1 Å	(Garcia-Nafria et al., 2018a)
μ-opioid receptor (μ-OR)	A	$G_{i/o}$	3.5 Å	(Koehl et al., 2018)
Serotinin receptor 1B (5-$HT_{1B}R$)	A	$G_{i/o}$	3.8 Å	(Garcia-Nafria et al., 2018b)
Adenosine receptor A1 (A_1R)	A	$G_{i/o}$	3.6 Å	(Draper-Joyce et al., 2018)
Rhodopsin	A	$G_{i/o}$	4.5 Å	(Kang et al., 2018)
Cannabinoid receptor 1 (CNR1)	A	$G_{i/o}$	3.0 Å	(Krishna Kumar et al., 2019)
Parathyroid hormone 1 receptor (PTH1R)	B1	G_s	3.0 Å	(Zhao et al., 2019)
Muscarinic acetylcholine receptor M2 (CHRM2)	A	$G_{i/o}$	3.6 Å	(Maeda et al., 2019)
Muscarinic acetylcholine receptor M1 (CHRM1)	A	$G_{q/11}$	3.3 Å	(Maeda et al., 2019)
Smoothened	F	$G_{i/o}$	3.9 Å	(Qi et al., 2019)
Neurotensin receptor 1 (NTR1)	A	$G_{i/o}$	3.0 Å	(Kato et al., 2019)

1.2. Neurotensin Receptor 1 (NTR1)

The Neurotensin receptor 1 (NTR1) is a class A GPCR involved in many physiological processes, i.e. cancer (Wu et al., 2012), central nervous system (CNS) disorders (Boules et al., 2013) or diabetes (Mustain et al., 2011). Therefor NTR1 is a promising drug target with big therapeutic potential (Kitabgi, 2002). The natural agonist for the NTR1 is Neurotensin (NTS), a 13 amino-acid peptide ligand (ELYENKPRRPYIL), being a neurotransmitter in the CNS as

well as a hormone in the periphery, especially the digestive tract (Vincent et al., 1999). NTR1 preferably interacts with G_q, but is also capable to promote downstream signaling via all other G protein families (Besserer-Offroy et al., 2017). Various structures of the rat NTR1 bound to NTS_{8-13} (RRPYIL) have been solved, the first by the Grisshammer lab (White et al., 2012). In the group of Andreas Plückthun, the structure of NTS bound evolutionary stabilized rat NTR1 variants have been solved (Egloff et al., 2014). The evolutionary stabilization has been described in earlier studies (Sarkar et al., 2008; Schlinkmann et al., 2012). An overview of the mutations in the different stabilized variants is shown in Table 1.3.

Table 1.3. Comparison of the two evolutionary stabilized NTR1 variants TM86V and HTGH4 to wild type NTR1

Sequential numbering	Ballesteros Weinstein	NTR1 (rat)	TM86V	HTGH4
83	1.51	S	S	G
86	1.54	A	L	L
101	2.38	T	T	R
103	2.40	H	D	D
105	2.42	H	Y	Y
119	2.56	L	L	F
121	2.58	M	M	L
124	2.61	E	E	D
143	3.26	R	R	K
150	3.33	D	D	E
161	3.44	A	V	V
167	3.50	R	L	L
213	4.69	R	L	L
234	5.35	V	L	L
235	5.36	K	K	R
240	5.41	V	V	L
253	5.54	I	A	A
260	5.61	I	I	A
262	5.63	N	N	R
263	5.64	K	K	R
305	6.32	H	R	R
332	6.59	C	C	V
342	7.26	F	F	A
354	7.38	T	T	S
358	7.42	F	V	V
362	7.46	S	A	A

In a recent study, the structure of NTR1 in complex with G_{i1} has been solved via cryo-EM (Kato et al., 2019). It was shown that two distinct conformations of activated NTR1 exist when bound to the G protein, with a canonical-state promoting the nucleotide exchange and a non-canonical state which resembles an intermediate during the activation process.

1.3. Aim of the Thesis

The main biological aim of this thesis was to get a better understanding of the GPCR and G protein dynamics and their interaction with each other. The structures are already known for each of the used proteins, in the case of the NTR1 the first structure is available for nearly a decade (White et al., 2012) and even for the thermostabilized variants the crystal structures were solved (Egloff et al., 2014). The reason for the choice of NTR1 as a GPCR model for this thesis, is its possible production in *Escherichia coli* (*E. coli*). Expression in *E. coli* enables high yield and the potential of isotope labeling. Both advantages are needed for the use in nuclear magnetic resonance (NMR) spectroscopy. For $G\alpha_{i,1}$ the structure was even earlier solved (Coleman et al., 1994) due to the fact that it is not a membrane protein. With only crystal structures solved, little was known about their dynamics and interaction with each other. To this day only one GPCR G protein complex had been solved via x-ray crystallography (Rasmussen et al., 2011b), and even the emergence of cryo-EM helps only to solve the complex structures, but gives little information about the underlying dynamics of the activation process. Therefore, NMR spectroscopy is a powerful tool as shown for other GPCRs (Liu et al., 2012). Two main goals should be achieved in this thesis:

- Obtain deeper knowledge about the structure and dynamics of $G\alpha_{i,1}$ in its different nucleotide states and the effects on its interaction with an activated GPCR

- Get a better understanding about the structure and dynamics of the different NTR1 variants in its different ligand states and how it affects the G protein activation

The optimization of the size homogeneity and thermal stability of lipid bilayer nanodiscs for structural studies was an additional goal of this thesis.

2. Methods

2.1. Expression and purification of recombinant proteins

2.1.1. Neurotensin Receptor 1 (NTR1)

The NTR1 constructs used in this thesis are thermostabilized *Rattus norvegicus* NTR1 variants (Egloff et al., 2014). A. Plückthun kindly provided the NTR1 vectors used for this work, as well as the vector for the production of an NTR1 specific purification column (Egloff et al., 2015). Thereby the NTR1 vectors contain an N-terminal maltose binding protein (MBP) followed by a hexa-histidine tag. This is then connected to a human rhinovirus (HRV) 3C protease site followed by the truncated (G50-G390, ΔIC3A (V280-I295)) and thermostabilized NTR1 variants HTGH4 or TM86V. C-terminally of the NTR1, an HRV 3C site is present, followed by a penta-asparagine linker, a di-glycine-serine linker and terminally connected to thioredoxin A (TrxA), which has a C-terminal deca-histidine tag.

The NTR1 variants were expressed in NEB Express I^q cells containing the corresponding plasmid. After transformation the cells were grown at 37 °C overnight in double yeast tryptone (dYT) medium containing 100 μg/mL ampicillin and 2% (w/v) of glucose. The next morning the preculture was then used with a 1:40 dilution to inoculate the main culture (dYT with 100 μg/mL ampicillin) at 28°C. As soon as the OD_{600} of the main culture reached a value of 0.6-0.8, the expression was induced with 1 mM isopropyl-β-D-Thiogalactopyranoside (IPTG) and the culture was incubated overnight. The cells were harvested the next morning at 6000 x g for 15 minutes at 4 °C and the bacterial pellets (approximately 3g cells/1L expression) were stored an -80 °C until usage. The purification of the NTR1 variants was performed as described (Egloff et al., 2014) with some variations. During lysis, liquid stocks of DNase I (5μl of 0.1mg/ml stock for 10 ml lysis volume) were used instead of lyophilized DNase I powder. 0.6% (w/v) 3-[(3-cholamidopropyl)dimethylammonio]-1-propanesulfonate (CHAPS) and 0.12% (w/v) cholesteryl hemisuccinate (CHS) were added as powder to the stirring lysis instead as a liquid stock. The buffers for the different purifications steps were also different (Table 2.1).

Table 2.1. Purification buffers for unlabeled NTR1 variants

	NT W1	NT W2	SP Bind	SP Wash	SP Elu	SEC
HEPES pH 8.0	25 mM	-	-	-	-	10 mM
HEPES pH 7.0	-	25 mM	10 mM	-	10 mM	-
HEPES pH 7.7	-	-	-	10 mM	-	-
Glycerol	10% (v/v)	10% (v/v)	10% (v/v)	10% (v/v)	10% (v/v)	-
NaCl	600 mM	150 mM	-	35 mM	350 mM	150 mM
DTT	-	2 mM	2 mM	2 mM	2 mM	2 mM
DM	0.5% (w/v)	0.3% (w/v)	-	-	-	-
DDM	-	-	0.05% (w/v)	0.05% (w/v)	0.05% (w/v)	0.02% (w/v)
NT1	-	-	-	-	0.5 μM	0.1 μM

If the NTR1 variants were purified in an Antagonist bound state, neurotensin (NT1) was omitted from the sulphopropyl (SP) Elution buffer, as well as the size exclusion chromatography (SEC) buffer.

In the case of isotope labeled expressions (see 2.1.4), the purification was identical except for the used buffers during the SP chromatography and SEC (Table 2.2)

Table 2.2. Purification buffers for isotope labeled NTR1 variants

	NT W1	NT W2	SP Bind	SP Wash	SP Elu	SEC
HEPES pH 8.0	25 mM	-	-	-	-	-
HEPES pH 7.0	-	25 mM	10 mM	-	10 mM	-
HEPES pH 7.7	-	-	-	10 mM	-	-
NaP_i pH 7.0	-	-	-	-	-	20 mM
Glycerol	10% (v/v)	10% (v/v)	10% (v/v)	10% (v/v)	10% (v/v)	-
NaCl	600 mM	150 mM	-	35 mM	350 mM	50 mM
DTT	-	2 mM	2 mM	2 mM	2 mM	2 mM
EDTA	-	-	-	-	-	0.5 mM
DM	0.5% (w/v)	0.3% (w/v)	0.3% (w/v)	-	-	-
d26-DH7PC	-	-	-	0.5% (w/v)	0.2% (w/v)	0.2% (w/v)
NT1	-	-	-	-	0.5 μM	0.1 μM

2.1.2. Guanine nucleotide-binding protein G(i) subunit alpha 1 (Gα$_{i,1}$)

In this work, Guanine nucleotide-binding protein G(i) subunit alpha-1 (Gα$_{i,1}$) variants from *Homo sapiens* were used. The used vector for all Gα$_{i,1}$ constructs is a pQE30 vector into which the Gα$_{i,1}$ gene was cloned via polymerase chain reaction (PCR) methods. All variants contain an N-terminal hexa-histidine tag, either directly followed by a tobacco etch virus (TEV) cleavage site, or immunoglobulin-binding protein G domain B1 (GB1) and then the TEV cleavage site. After the TEV cleavage site either the full length protein of Gα$_{i,1}$ follows, which is the case without the GB1 fusion protein, or a truncated Gα$_{i,1}$ variant missing the first 31 amino acids (Δ31Gα$_{i,1}$)

The protein production is described in detail in the published journals (Goricanec and Hagn, 2019; Goricanec et al., 2016) and was adapted from an already available protocol (Greentree and Linder, 2004). Isotope labeling was done as described in chapter 2.1.4.

2.1.3. Apolipoprotein A-I

For the use in Nanodisc (ND) production in this work, various membrane scaffold protein (MSP) constructs were used. MSP1D1 is a modified protein derived from Apolipoprotein A1. The two main constructs were MSP1D1 and the truncated version MSP1D1ΔH5 (Hagn et al., 2013). Protein expression and purification of MSP1D1 and its variants is explained in detail in a recent publication (Hagn et al., 2018; Klopfer and Hagn, 2019). Additionally, a method was developed to produce circularized MSP1D1 variants *in vivo* during expression. The corresponding cloning, protein expression, protein purification and Nanodisc assembly is described in detail in a recent publication (Miehling et al., 2018).

2.1.4. Isotope labeling Strategies

In contrast to unlabeled protein expression in *E. coli*, isotope labeling requires a different approach to expression. The transformation of the desired plasmid and the first preculture overnight have been done the same way as unlabeled protein expression. As the medium had to be changed to D$_2$O from H$_2$O, a careful adaption process had to be done. After the first overnight culture has grown densely, it was gently centrifuged (2000 x g for 10 minutes at 30 °C) so that the bacteria are not put under stress or even damaged. The used medium was discarded and, the *E. coli* were carefully resuspended under sterile conditions with prewarmed

(37 °C) LB (D_2O) or dYT (D_2O) containing the corresponding antibiotic and 2% Glucose (w/v) both dissolved in D_2O. The resuspended culture was then poured into a sterile dry shaking flask and again incubated overnight at 37 °C. The next morning the procedure to remove the medium was repeated as described previously. The *E. coli* were now gently resuspended in prewarmed (37 °C) "M9 (D_2O) general" minimal medium supplemented with the corresponding antibiotic and 2% Glucose (w/v) both dissolved in D_2O.

All variants of M9 medium used for different labeling strategies are listed in Table 2.3. The liquid stocks were dissolved in D_2O and the composition of the used trace elements solution is shown in Table 2.4. The solid components as well as the Biotin, Thiamin and antibiotic were mixed together in D_2O. After complete dissolving of the ingredients, the medium was sterile filtered. After sterile filtration the remaining liquid stocks (sterile filtered during preparation) were added and the final M9 (D_2O) minimal medium properly mixed. If the medium was not instantly used, it was sealed with parafilm and stored at 4 °C until usage.

Table 2.3. Different M9 media used for isotope labeling in E. coli

	M9 (D_2O) general	M9 (D_2O) double labeling	M9 (D_2O) triple labeling
Na_2HPO_4	6 g/L	6 g/L	6 g/L
KH_2PO_4	3 g/L	3 g/L	3 g/L
NaCl	0.5 g/L	0.5 g/L	0.5 g/L
$^{15}NH_4Cl$	1 g/L	1 g/L	1 g/L
$^1H^{12}C$ Glucose	2 g/L	-	-
$^2H^{12}C$ Glucose	-	2 g/L	-
$^2H^{13}C$ Glucose	-	-	2 g/L
Biotin (1 mg/ml)	1 mL/L	1 mL/L	1 mL/L
Thiamin (1 mg/ml)	1 mL/L	1 mL/L	1 mL/L
Trace elements solution (1000x)	1 mL/L	1 mL/L	1 mL/L
1 M $MgSO_4$	2 mL/L	2 mL/L	2 mL/L
0.5 M $CaCl_2$	0.2 mL/L	0.2 mL/L	0.2 mL/L

Table 2.4. Trace elements solution 1000x

	Per 100 mL D_2O
EDTA	5 g
$FeCl_3$ x 6 H_2O	0.83 g
ZnCl2	84 mg
$CuCl_2$ x 2 H_2O	13 mg
$CoCl_2$ x 6 H_2O	10 mg
H_3BO_3	10 mg
$MnCl_2$ x 6 H_2O	1.6 mg

The first M9 preculture was incubated for approximately eight hours at 37 °C and then directly added to the prewarmed (37 °C) final preculture, which corresponds to either "M9 (D_2O) double labeling" or "M9 (D_2O) triple labeling" minimal medium, supplemented with the needed antibiotic and additional 0.5% of the used glucose type. The final preculture is then incubated overnight at 37 °C and the next morning added in a 1:20 ratio to the prewarmed (37 °C) corresponding medium. When the OD_{600} reached a value of 0.6 to 0.7, the main cultures were cooled down to the needed expression temperature. In the case of ^{13}C methyl labeling via specific precursors for isoleucin, leucin, valin and alanin (ILVA labeling, see below), the precursors were added at this same time to the culture, as they should be added approximately one hour prior to induction. As soon as the OD_{600} was 0.8 the cells were induced with IPTG, the concentration depending on the expressed protein. The induced bacteria were grown for 20 h until harvest, which is identical as described for the NTR1 in 2.1.1.

For the ^{13}C methyl labeling of the proteins, specific precursors were used, depending on which amino acids should be selectively labeled (see Figure 2.1).
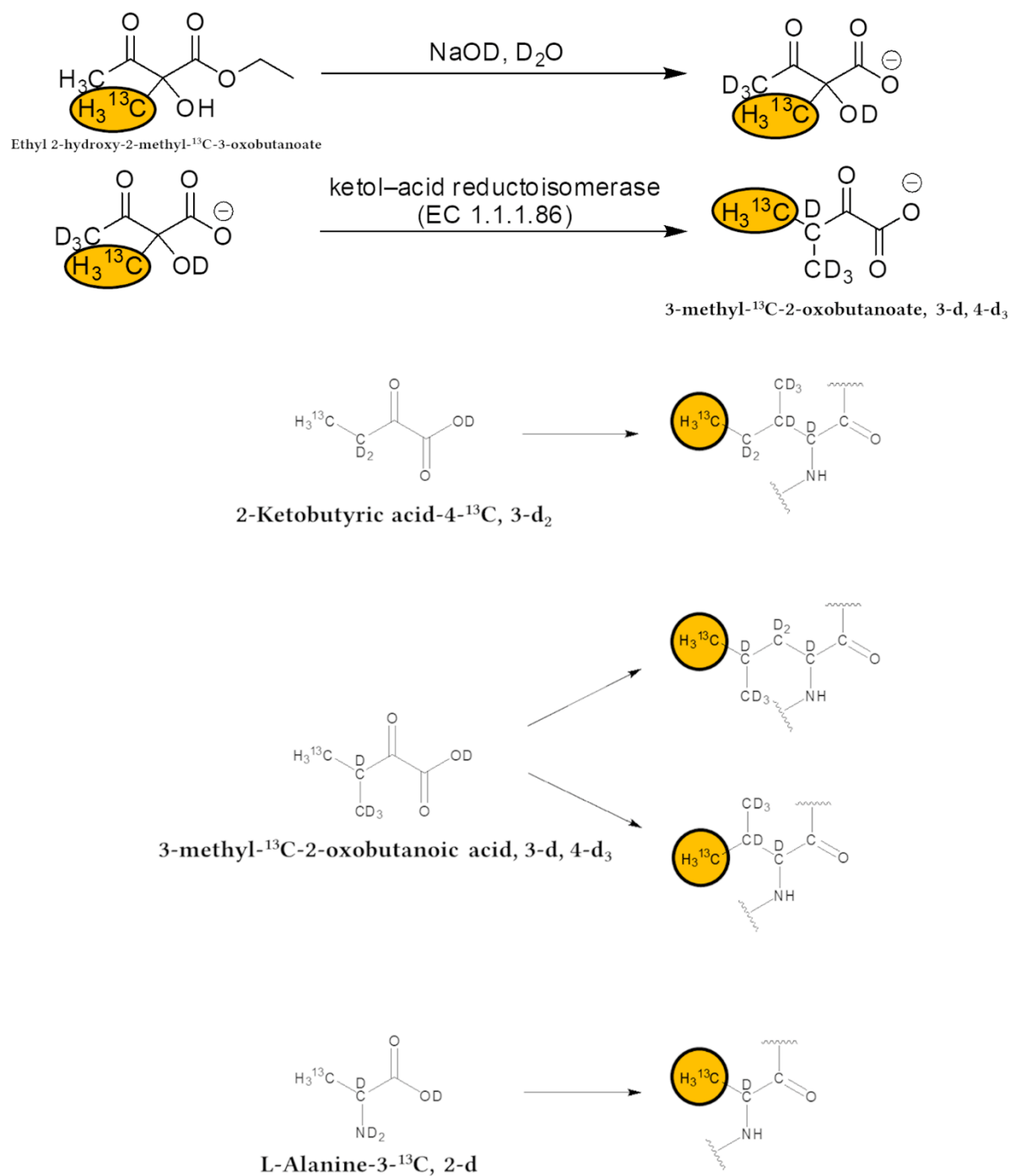

Figure 2.1: Precursors used for the selective isotope labelling of methyl groups and their incorporated position in the protein
These figures show the precursors used for selective ILVA ^{13}C methyl labelling. The precursors 2-ketobutyric acid-4-^{13}C and ethyl 2-hydroxy-2-methyl-^{13}C-3-oxobutanoate for ILV had to be treated with sodium deuteroxide prior to the addition of the bacterial culture. This resulted in the precursors 2-ketobutyric acid-4-^{13}, 3-d₂ and 3-methyl-^{13}C-2-oxobutanoic acid, 3-d, 4-d₃ which were then used by the E. coli for the incorporation of ^{13}C methyl labeled isoleucine and leucine/valine respectively. Alanine was added directly as powder and is not needed to be treated prior to its use

Various studies describe the method for selective methyl labelling in detail (Proudfoot et al., 2019; Tugarinov et al., 2006). In this work, the precursors used for the ILVA labelling scheme had to be prepared for their use depending on each precursor. As both the precursor for isoleucine (2-ketobutyric acid-4-^{13}C) as well as the precursor for valine/leucine (ethyl 2-hydroxy-2-methyl-^{13}C-3-oxobutanoate) were obtained in a protonated state at the carbon next to the ^{13}C labeled methyl, they had to be treated with NaOD in M9(D_2O) to facilitate proton deuterium exchange. For this, the precursors which were needed per liter of final medium (see Table 2.5) were dissolved in 15 mL/L culture of the medium used. For the isoleucine precursor, the pH of the medium was titrated to 10 prior to its addition. After the precursor was added, the solution was incubated at 37 °C overnight. The next morning the pH was titrated back with DCl to the initial value of the M9 medium and was ready to use. In the case of the leucine/valine precursor, the medium was titrated to pH 12 prior to its addition. For this precursor, the incubation time at high pH was only 1h at 37 °C. Afterwards the solution was titrated back as in the case of the isoleucine precursor. As the alanine precursor was bought with complete isotope labeling, it could be directly added without prior treatment. Due to the potential for amino acid scrambling of alanine, deuterated succinic acid had to be added to the cultures. 2.5 g succinic acid were dissolved in 45 mL of the used medium and the pH had to be titrated back to its original value.

Table 2.5. Amount of deuterated precursors used for ILVA labeling

	Per 1 L M9 D_2O
2-Ketobutyric acid-4-^{13}C	80 mg
Ethyl 2-hydroxy-2-methyl-^{13}C-3-oxobutanoate	300 mg
L-Alanine-3-^{13}C, 2-d	800 mg
Succinic acid-2,2,3,3-d_4	2.5 g

In order to obtain ^{13}C methyl labelled samples, a second method was also used. Unlabeled proteins can be tagged with S-Methyl-^{13}C methanethiosulfonate (^{13}C MMTS). Thereby all accessible cysteines are tagged with a ^{13}C methyl group (see Figure 2.2).
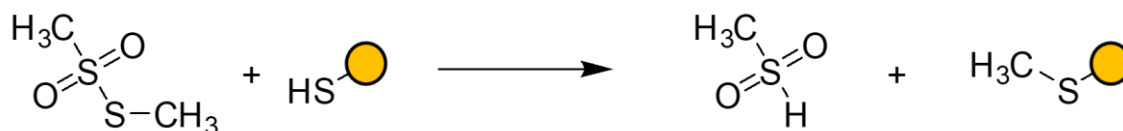
S-Methyl-methanethiosulfonate (MMTS)

*Figure 2.2: Tagging of accessible cysteines with MMTS*
Here, the chemical basis of MTS tagging of cysteines with MMTS is shown. This reaction is also reversible to a certain degree,
but the methanesulfonyl hydride is not stable in H₂O and reacts to methanesulfonate (not shown in this figure).

In a first step, the protein to be tagged (in this work the NTR1 variants in n-Dodecyl β-D-maltoside (DDM)) needs to be buffer exchanged to no dithiothreitol (DTT). This is accomplished by centricon buffer exchange. The relevant fractions of the NTR1 variant are pooled (3 mL total volume for 6 S200a fractions) and then filled to 15 ml with MMTS tagging buffer (50 mM NaPi pH 7.5, 1 mM EDTA, 0.02 % (w/v) DDM) and concentrated to 1 mL at 3400 x g and 4 °C. The concentrated sample is again filled up to 15 mL with MMTS tagging buffer and again concentrated to 1 mL at 3400 x g and 4 °C. This step is repeated 2 more times. Then the concentration of the NTR1 variant is determined and a 10-fold molar excess (relative to the cysteines) of MMTS (100 mM stock in dimethyl sulfoxide (DMSO)) is added. This reaction mixture is then incubated at 4 °C overnight on a shaking plate. The next morning the reaction is stopped by buffer exchange via centricon concentration. The 1 mL reaction mixture is filled to 15 mL with NMR buffer (20 mM NaPi pH 7.0, 50 mM NaCl, 1 mM EDTA, 0.02 % (w/v) DDM). These 15 mL are then concentrated to 1 mL at 3400 x g and 4 °C. This is repeated 3 more times and during the last centrifugation step, the sample is concentrated to the lowest possible volume in the centricon (250 μL). After this final step, the samples are ready for NMR measurement. This protocol was adapted from a previous published work in the group of Prof. Lewis Kay (Religa et al., 2011).

2.2. Nanodisc assembly

Membrane proteins outside of lipid bilayers tend to denature or show a not physiological behavior. Before the emergence of nanodiscs only lipid vesicles could be used as a native-like membrane mimetic. Their disadvantages in the use of structural biology are the big size, the lack of size homogeneity, solubility and stability. Therefor nanodiscs present an effective way for structure determination of membrane proteins in a lipid environment (Bayburt and Sligar, 2010; Denisov and Sligar, 2016, 2017).

Nanodiscs consist of a phospholipid bilayer wrapped by two amphipathic helical belt proteins called membrane scaffold proteins (MSPs), schematically shown in Figure 2.3. The structure of nanodiscs was confirmed via NMR spectroscopy (Bibow et al., 2017). MSP is derived from human Apolipoprotein A1 (ApoA1) which is part of high density lipoprotein (HDL) particles (Brouillette et al., 2001).
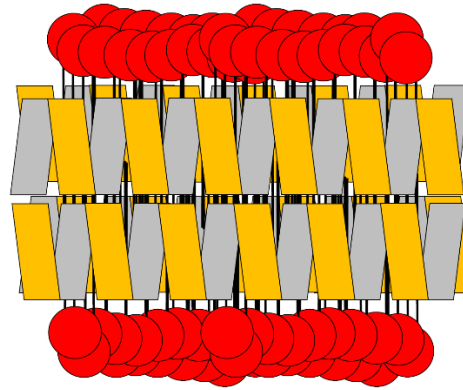
Figure 2.3: Structural model of a nanodisc
In this figure an empty nanodisc is shown schematically. Two alphahelical proteins (orange/grey) form a belt around the lipid bilayer. These proteins are derived from Apolipoprotein A1 (ApoA1) and are called membrane scaffold proteins (MSPs). The length of the MSPs determines the diameter of the nanodiscs. The lipids used for nanodiscs can be varied in their fatty acid chain length as well as in their head groups (red). Also, mixtures of lipids or even extracts from biological material can be used as source for the lipids.

Nanodiscs are mainly used for 2 different applications in biochemistry. They are suitable for the reconstitution of membrane proteins in a lipid bilayer. Additionally, nanodiscs can be used as a model membrane surface of defined lipid composition.

Empty nanodiscs as well as membrane protein containing nanodiscs can be assembled via gradual detergent removal of detergent solubilized assembly mixtures consisting of lipids, MSP and optionally membrane proteins. The detergent removal is accomplished via hydrophobic adsorption (bio beads) or dialysis (Bayburt et al., 2002; Bayburt and Sligar, 2010).

The protocol for the assembly of nanodiscs is flexible and therefor it can be optimized for each membrane protein. Parameters which can be optimized are the temperature, time, amount of adsorbent or choice of detergent to name only some. An important factor in nanodisc assemblies is the determination of the correct stoichiometric ratio of MSP, lipid and the membrane protein, especially if a desired monomeric or oligomeric state of the membrane protein is desired.

The basic MSP variant MSP1D1 has been optimized for NMR by the creation of truncated variants resulting in nanodiscs of smaller diameter (Hagn et al., 2013; Hagn et al., 2018; Klopfer and Hagn, 2019).

2.2.1. Assembly of empty Nanodiscs

In order to assemble empty nanodiscs, MSP and lipids are mixed in MSP buffer (20 mM Tris pH7.5, 100 mM NaCl, 0.5 mM EDTA). Depending on the MSP variant and which lipids were used, the assembly ratios had to be adapted. The final concentration of cholate during assembly was always 20 mM. For empty MSP1D1 nanodiscs with 1-palmitoyl-2-oleoyl-sn-glycero-3-phosphocholine (POPC) as lipid, the ratio between MSP and lipid was 1:35. In the case of MSP1D1dH5 and 1,2-dimyristoyl-sn-glycero-3-phosphocholine (DMPC) or 1,2-dimyristoyl-sn-glycero-3-phosphoglycerol (DMPG), the ratio between MSP and lipid was 1:50. Upon pipetting the nanodisc assembly mixture, the reactions were left to incubate for 1 h. POPC containing nanodisc assembly mixtures needed to be incubated on ice due to the phase transition point of POPC. In the case of DMPC, the assemblies could be performed at room temperature. Afterwards polystyrene bio beads were added to the reaction mixtures (0.7 g bio beads/1 mL reaction mixture) and incubated for 3 h on a shaking plate. Then the bio beads were removed from the reaction mixture and latter was applied to a S200 size exclusion chromatography column. The fractions containing the empty nanodiscs were pooled and ready for further work. The procedure is described in more detail a recently published work (Hagn et al., 2018).

2.2.2. Reconstitution of NTR1 into Nanodiscs

To obtain nanodiscs containing NTR1 variants, the above-mentioned protocol had to be modified. Additional to MSP1D1 and the lipids (POPC in the case of NTR1), the GPCR had to be added to the reaction mixture. In order to obtain nanodiscs with monomeric NTR1, an excess of MSP1D1 had to be used. The molar ratio between MSP and the GPCR was 1:20, so only 1 nanodisc contains the NTR1 per 9 empty discs. As the nanodiscs are not completely empty, a different lipid to MSP ratio was used. Only 25 POPC per 1 MSP was added to the reaction mixture. Also, the MSP buffer was modified by an addition of 10 mM β-mercaptoethanol (β-ME) as the GPCR contains cysteines. The assembly was incubated on ice for 2 h. Afterwards 0.5 g Biobeads/1 mL assembly were added and incubated at 4 °C on a shaking plate for 2 h. Then 0.3 g bio beads/1 mL assembly were added additional to the mixture with another 2 h incubation time at 4 °C. Afterwards, the bio beads were separated via an empty gravity flow column and washed with 5-fold excess (relative to the assembly volume) of MSP buffer with β-ME. The assembly mixture with the wash fraction were pooled and dialyzed against SP binding buffer (10 mM HEPES pH 7, 10 mM β-mercaptoethanol (β-ME)) overnight at 4 °C. The dialyzed nanodisc pool was then applied onto a SP FF hiTrap

column and washed and eluted with a NaCl gradient from 10 mM to 1 M. At around 300 mM the NTR1 containing nanodisc eluted, whereas the empty nanodiscs could be found in the flow through. The final purification step was a size exclusion chromatography (S200a) of the concentrated pool of NTR1 nanodiscs.

2.3. Biophysical methods

2.3.1. Circular dichroism spectroscopy

Circular dichroism (CD) spectroscopy reveals information about the secondary structure of proteins (Greenfield, 2006b). If circularly polarized light interacts with asymmetric molecules, the left-handed circularly polarized light is absorbed differently than the right-handed circularly polarized light (Beychok, 1966). The angle of the rotated plane of light is defined as degree ellipticity θ. The molar ellipticity [θ] is defined as

$$[\theta] = \frac{deg \cdot cm^2}{dmol}$$

Different structural elements show different CD spectra (see Figure 2.4).
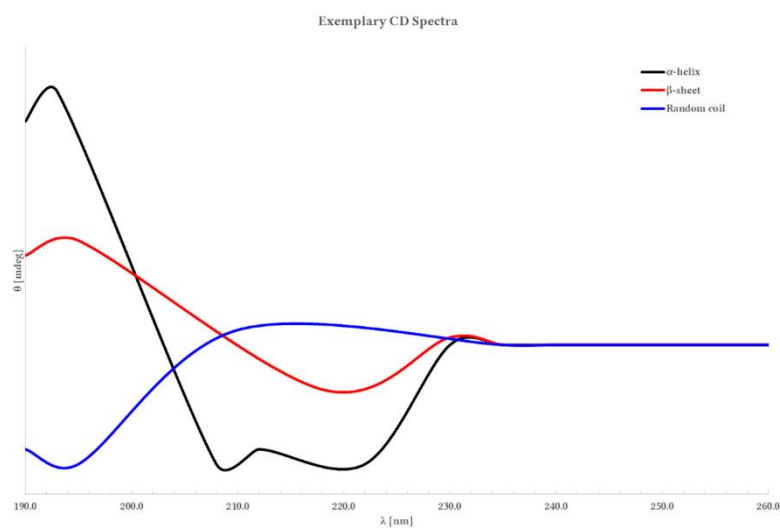
Figure 2.4: Exemplary CD spectra for different secondary structure elements
These CD spectra are examples, depending on the predominant secondary structure which is mainly present in the investigated proteins. As GPCRs are nearly pure alpha helical proteins, they show a classic alpha helical CD spectrum. Therefor they always showed two distinct minima around 222 nm and 209 nm. The former was used as a reference wave length for thermal denaturation experiments in CD spectroscopy.

α-helical proteins show minima at 208 nm and 222 nm and a maximum at 193 nm (Holzwarth and Doty, 1965). Proteins with β-sheet secondary structures show a minimum at 218 nm and

a maximum at 195 nm (Greenfield and Fasman, 1969). Disordered proteins show a minimum at 195 nm and a weak maximum at 210 nm (Venyaminov et al., 1993).

As the proteins have different sizes, their molar ellipticity needs to be normalized in order to compare different proteins via CD spectroscopy. This is done with the mean residue molar ellipticity:

$$\theta_{MRE} = \frac{\theta(mdeg) \cdot 10^6}{d(mm) \cdot c(\mu M) \cdot n}$$

In this formula d is the pathlength in mm, c is the protein concentration in µM and n is the number of peptide bonds in the protein.

CD spectroscopy can also be used to determine the thermal stability of proteins (Greenfield, 2006a).

The CD spectra were recorded on a Jasco J-715 spectropolarimeter. The concentration of the samples recorded was 5 µM, dissolved in CD buffer (10 mM NaPi pH 7.0, 10 mM β-ME; for NTR1 samples in detergent micelles additional 0.02 % (w/v) DDM or 0.2 % (w/v) DH$_7$PC was added).

The wavelength spectra were recorded from 260 nm to 190 nm in 0.5 nm intervals at 20 °C. 5 measurements were accumulated. Points recorded with a voltage of higher than 800 were excluded from analysis.

Thermal denaturation spectra were recorded at a wavelength corresponding to the global minimum of the protein, in the case of α-helical proteins at 220-222 nm. The temperature was ramped at a rate of 1 °C/min from 20 °C to 100 °C.

2.3.2. Fluorescence spectroscopy

The Förster resonance energy transfer (FRET) is a mechanism of radiationless energy transfer from a fluorescence donor to a fluorescence acceptor (Lakowicz, 2013). Thereby the fluorescence donor is excited by a specific wavelength and transfers its energy to the fluorescence acceptor reach the ground state. The fluorescence acceptor emits the energy through a distinct wavelength in order to get also back to its ground state. This emission is then detected. The phenomenon was first described by Theodor Förster more than 70 years ago (Förster, 1948). The efficiency of the FRET depends correlates to the distance between the donor fluorophore and acceptor fluorophore. This enables to map the distance between both or to check binding kinetics. In this study, the binding kinetics of fluorescence labeled

nucleotides to Gα$_{i,1}$ were investigated. The fluorescence label used was N-Methylanthraniloyl (MANT) bound to the 3'-OH of the ribose from the nucleotide. In order to obtain the K$_D$ values for the binding affinity of the nucleotides, Gα$_{i,1}$ was titrated in increasing concentrations to a buffer containing the MANT labeled nucleotide. Another experiment performed was the determination of the binding and dissociation kinetics of GDP or GTP to GNAI. Therefor presatured Gα$_{i,1}$ with MANT-GDP or MANT-GTP was incubated with an excess of unlabeled GDP or GTP and the decay of the Fluorescence signal was measured. The exact method was described in a recent work (Goricanec et al., 2016).

2.4. NMR Spectroscopy

NMR is a powerful tool to investigate the structure and dynamics of biomolecules. The physical basis of NMR is the magnetic dipolar momentum (μ). μ consists of the gyromagnetic ratio (γ) and the spin quantum number (I) and in this formula only the z-component is shown:

$$\mu_z = \gamma \cdot I_z$$

The gyromagnetic ratio is a nucleus specific factor, whereas the spin quantum number depends on the number of unpaired protons (p) and neutrons (n) in the nucleus. If p = n then I is zero and therefore not detectable via NMR. In biomolecular NMR, only nuclei with I=1/2 are used (i.e. ^{1}H, ^{13}C, ^{15}N).

If an external magnetic field (B) acts on the magnetic dipolar momentum (μ), the resulting magnetic moment (M = E) can be described as:

$$E = \mu \cdot B$$

Putting both equations together and defining $I_z = \hbar \cdot m_z$ leads to the following equation:

$$E = \gamma \cdot B \cdot \hbar \cdot m_z$$

For spin ½ nuclei, two energy states can be defined:

$$E_\alpha = \frac{1}{2} \cdot \gamma \cdot B \cdot \hbar \qquad \text{and} \qquad E_\beta = -\frac{1}{2} \cdot \gamma \cdot B \cdot \hbar$$

The spins with these energy levels precise along the magnetic field B in the Larmor frequency:

$$\omega_{Larmor} = \gamma \cdot B$$

If the low spin state is excited with a radio frequency pulse according to the Larmor frequency, it is flipped to the high spin state. This difference in energy between the 2 states can be

detected via the fast induction decay (fid) when the high spin state flips back to the low spin state:

$$\Delta E = \gamma \cdot B \cdot \hbar \qquad \text{or} \qquad \Delta E = \omega_{Larmor} \cdot \hbar$$

In order to maximize the energy difference, the magnetic field strength can be increased as well as using nuclei with a high gyromagnetic ratio (especially ^{1}H) for excitation and detection.

The population of the spin states is distributed according to the Boltzmann distribution:

$$\frac{N_\beta}{N_\alpha} = e^{\frac{-\cdot \gamma \cdot B \cdot \hbar}{k_B \cdot T}}$$

As each nucleus has a small difference in its frequency depending on the electron distribution in his surrounding, with the effect being called chemical shift.

This chemical shift difference is normalized relative to sodium trimethylsilylpropane-sulfonate (DSS) in the case of ^{1}H and [13]C. As the frequency differences are small, they are multiplied by 10^6 for an easier handling and therefor called ppm.

$$\delta = \frac{\nu - \nu_{DSS}}{\nu_{DSS}} \ [ppm]$$

All performed NMR experiments were acquired on the following instruments: Bruker AvanceIII spectrometers operating at 950, 900, 800 and 600 MHz proton frequency, each equipped with a cryo TCI triple resonance (^{1}H, ^{13}C, ^{15}N) z gradient probe.

The general NMR buffer contained 20 mM sodium phosphate with a pH of 7.0 and 50 mM sodium chloride. If the sample contained cysteines and should be in a reduced state, 2 mM DTT was added. In the presence of $G\alpha_{i,1}$ no EDTA could be added as $MgCl_2$ (concentration twice the nucleotide concentration in the sample) was needed as cofactor. Nucleotides for $G\alpha_{i,1}$ were added in a twofold molar excess relative to the protein. The concentration of EDTA was 0.5 mM if no $G\alpha_{i,1}$ was present in order to improve long term stability (inhibition of metalloproteases). 7-10% D_2O were added to gain a lock for the sample.

The spectra were recorded and processed with Bruker TopSpin 3.5 pl7. NMRFAM-SPARKY was used to analyze and display the NMR spectra (Lee et al., 2015).

2.4.1. NMR resonance assignment

NMR does not only provide information via the chemical shift but also due to magnetic coupling. Magnetic coupling can happen through covalent bonds or through space. This information can then be used to determine the structure on an atomic level.

Couplings through electrons of covalent bonds are called J-couplings or scalar couplings. J-couplings lead to multiplet splitting of the corresponding peaks, dependent on the chemical environment. The distance in the splitting is corresponding to the coupling constant J of the observed coupling and the size depends on the strength of the coupling. Typically, J-couplings are observed between 1 and 3 covalent bonds. Typically, the first recorded NMR experiment is a ^{1}H 1D. This gives a first overview about the sample quality and can be used to determine the presence of small molecules in the sample like detergents or nucleotides.

The next step is to record a 2D NMR of the labeled sample. Thereby the magnetization is transferred from the proton to the heteronucleus via an insensitive nuclei enhanced by polarization transfer (INEPT) pulse sequence (Morris and Freeman, 1979). For backbone assignment experiments, this is usually a ^{1}H^{15}N heteronuclear single quantum coherence (HSQC) spectrum. For each proton bound to a nitrogen, one specific peak arises. This is true for all backbone amides (except for prolines which are imides and therefore not detectable) which also explains why this spectrum is called the fingerprint spectrum of proteins. Additionally, sidechain amides are visible, but due to their distinct chemical shifts they appear in different regions of the spectrum.

For big proteins, signal overlap can be a problem. This is circumvented mainly by two methods. The signal overlap caused by line broadening originates from increased relaxation rates due to the ^{13}C-^{1}H dipolar interactions. By deuterating the carbon at not exchangeable positions, this effect can be decreased by approximately factor 15, resulting in narrower peaks and therefor better resolution (Gardner and Kay, 1998). Also, the pulse sequence can be optimized in order to minimize the transverse relaxation of ^{1}H, ^{13}C and ^{15}N. The pulse sequence used to accomplish this goal is the transverse relaxation-optimized spectroscopy (TROSY) which minimizes the dipole-dipole coupling and chemical shift anisotropy causing the transverse relaxation in a ^{1}H ^{15}N 2D NMR spectrum (Pervushin et al., 1997). It could also be shown that this TROSY effect can also be observed in ^{1}H ^{13}C heteronuclear multi quantum coherence HMQC spectra compared to ^{1}H ^{13}C HSQC spectra, therefor the HMQC with improved sensitivity for high molecular weight (MW) proteins is called "methyl TROSY" (Tugarinov et al., 2003).

The next step in the assignment of proteins is accomplished by using 3D NMR experiments. Thereby the magnetization is additionally transferred a second time, from the first heteronucleus (^{15}N) to the second heteronucleus (^{13}C). A big set of heteronuclear multidimensional NMR experiments can then be used to assign the resonances for the protons, amide nitrogen and alpha and beta carbon for each amino acid in the protein (Sattler et al., 1999). The 3D experiments can also be combined with the TROSY pulse sequence for further improvement of sensitivity. This was shown for the [^{15}N,^{1}H]-TROSY-HN(CO)CA, [^{15}N,^{1}H]-TROSY-HN(CA)CO, [^{15}N,^{1}H]-TROSY-HNCACB, [^{15}N,^{1}H]-TROSY-HN(CO)CACB (Salzmann et al., 1999), [^{15}N,^{1}H]-TROSY-HNCA and [^{15}N,^{1}H]-TROSY-HNCO (Salzmann et al., 1998). In this work, the TROSY type 3D NMR experiments were used for the assignment of G$\alpha_{i,1}$. With the residue specific C$_\alpha$ and C$_\beta$ chemical shifts, a secondary structure prediction can be done (Spera and Bax, 1991).
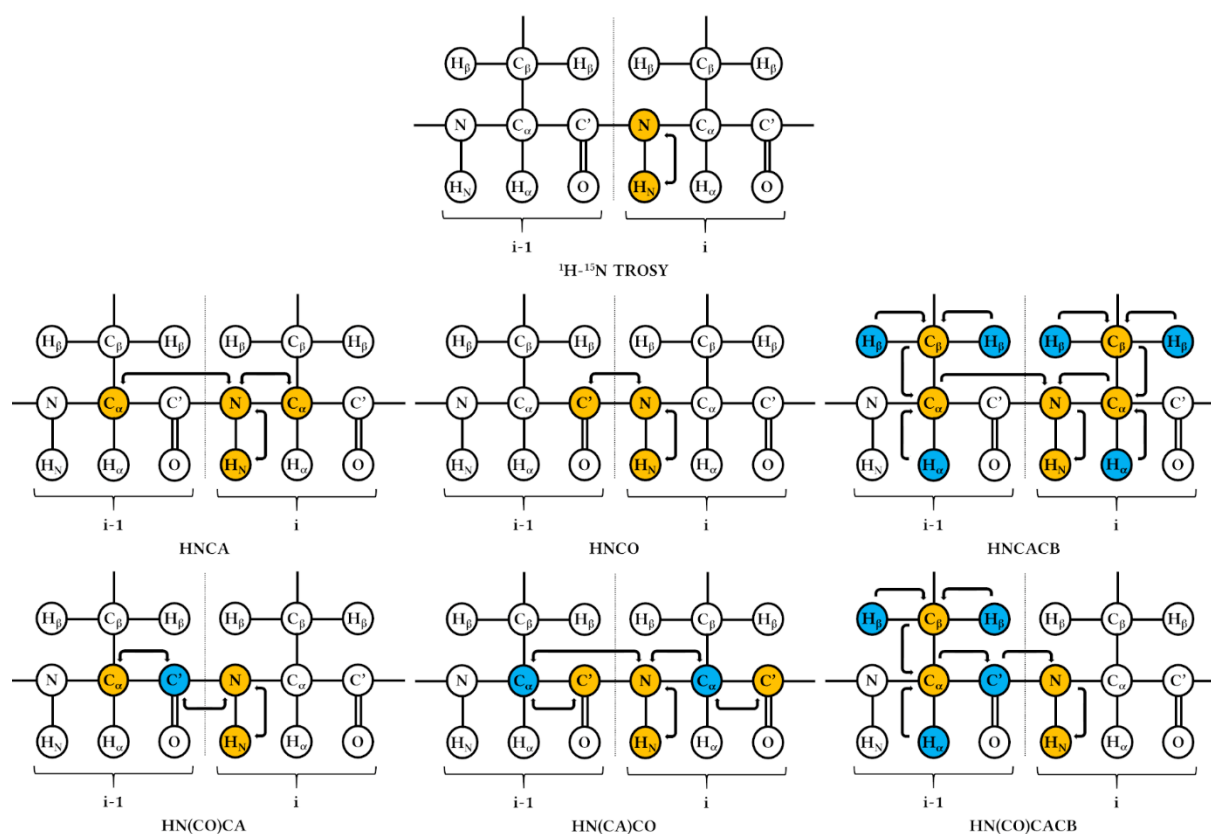
Figure 2.5: Assignment strategy
This is an overview of the NMR assignment experiments which were performed for the proteins in this work. The starting point is always a 2D ^{1}H-^{15}N fingerprint spectrum. There is also always a pair of two experiments for each carbon to be assigned. The HNCA experiment correlates C$_\alpha$ and C$_{\alpha-1}$ chemical shifts with the corresponding ^{1}H and ^{15}N chemical shift. In the case of the HN(CO)CA only the C$_{\alpha-1}$ chemical shift is correlated with the corresponding ^{1}H and ^{15}N chemical shift. The HNCO experiment correlates C$_{carbonyl}$ and C$_{carbonyl-1-1}$ chemical shifts with the corresponding ^{1}H and ^{15}N chemical shift. In the case of the HN(CA)CO only the C$_{carbonyl-1}$ chemical shift is correlated with the corresponding ^{1}H and ^{15}N chemical shift. The HNCACB experiment correlates C$_\alpha$ and C$_{\alpha-1}$ as well as C$_\beta$ and C$_{\beta-1}$ chemical shifts with the corresponding ^{1}H and ^{15}N chemical shift. In the case of the HN(CO)CACB only the C$_{\alpha-1}$ as well as C$_{\beta-1}$ chemical shift is correlated with the corresponding ^{1}H and ^{15}N chemical shift.

2.4.2. NMR relaxation experiments

Relaxation in NMR is the phenomenon of the excited spins returning to their Boltzmann equilibrium magnetization. In an external magnetic field B (along z-axis), the spins align along to this field. This results in a net magnetization M_0. This bulk magnetization along z is unaligned in x and y direction, so no transverse magnetization is present. If a 90° radio frequency pulse is applied to M_0, the magnetization flips into the xy-plane and precesses around the z-axis in the Larmor frequency causing transverse magnetization. Due to relaxation mechanisms like dipolar spin-spin interactions or chemical shift anisotropy, this transverse magnetization decays over time and finally coherence is lost. The time for this loss of coherence in the xy plane is called the T_2 relaxation time, or spin-spin relaxation time. Parallel to the T_2 relaxation, the magnetization is also going back to its equilibrium along the z-axis. The time needed to reach the net magnetization M_0 is called the T_1 relaxation time, or spin-lattice relaxation time see Figure 2.6.
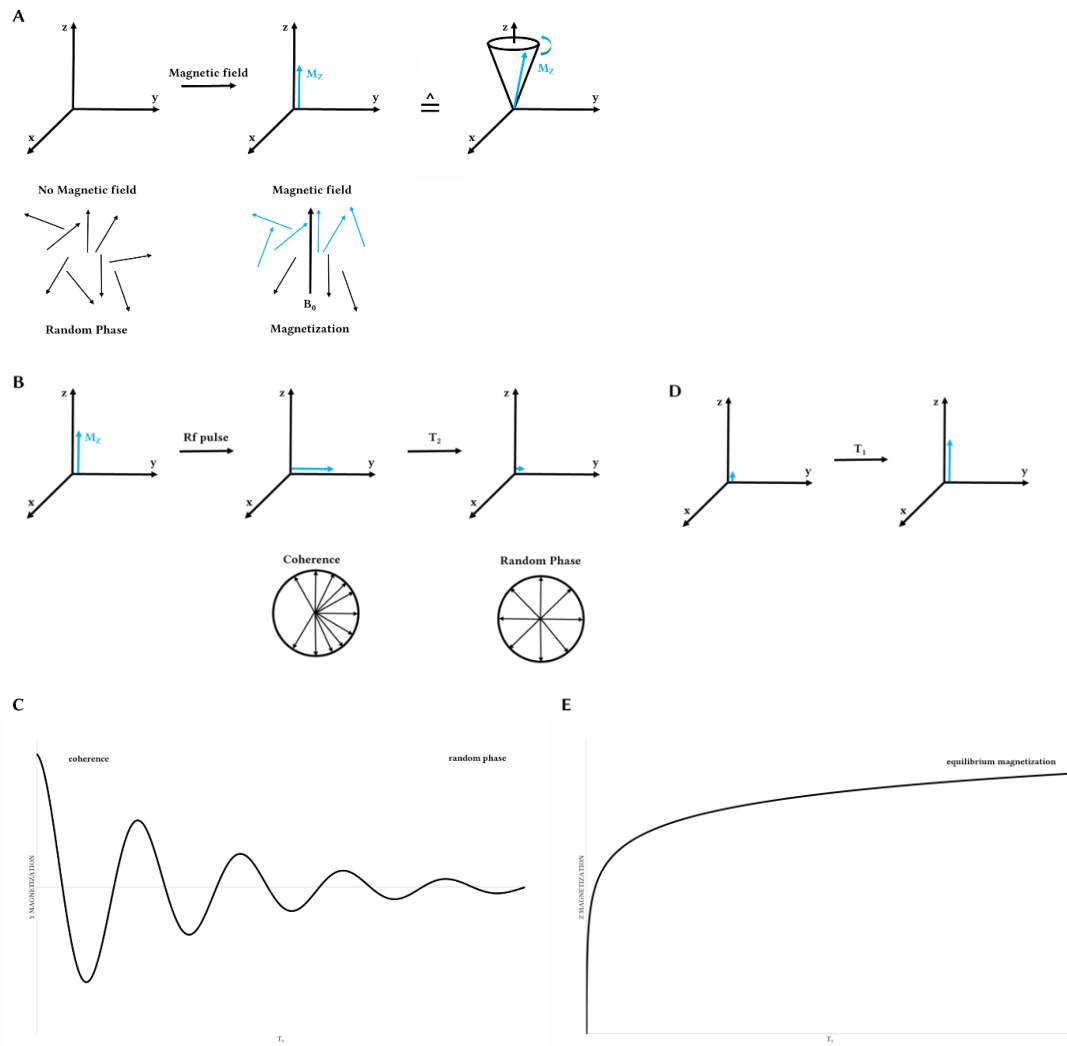
Figure 2.6: T₁ and T₂ relaxation

These are the physical basis of the NMR experiments. (A) Without an external magnetic field, the spins are randomly oriented in a random phase and therefor no net magnetization is detected. As soon as an external magnetic field B0 is applied, the spins align to the magnetic field and magnetization can be observed. Thereby the spins precess around the z axis. (B) If a radio frequency (rf) pulse is applied, the spins flip into the xy plane. As the spins are precessing, the coherence is lost and the spins are randomly distributed over time in the xy plane. The time to reach this equilibrium is the T₂ relaxation time. (C) This graph shows exemplary the T₂ relaxation over time. (D) The spins which have no magnetization in z direction reach again the starting net magnetization in an external magnetic field. The time to reach this equilibrium is the T₁ relaxation time. (E) This graph shows exemplary the T₁ relaxation over time.
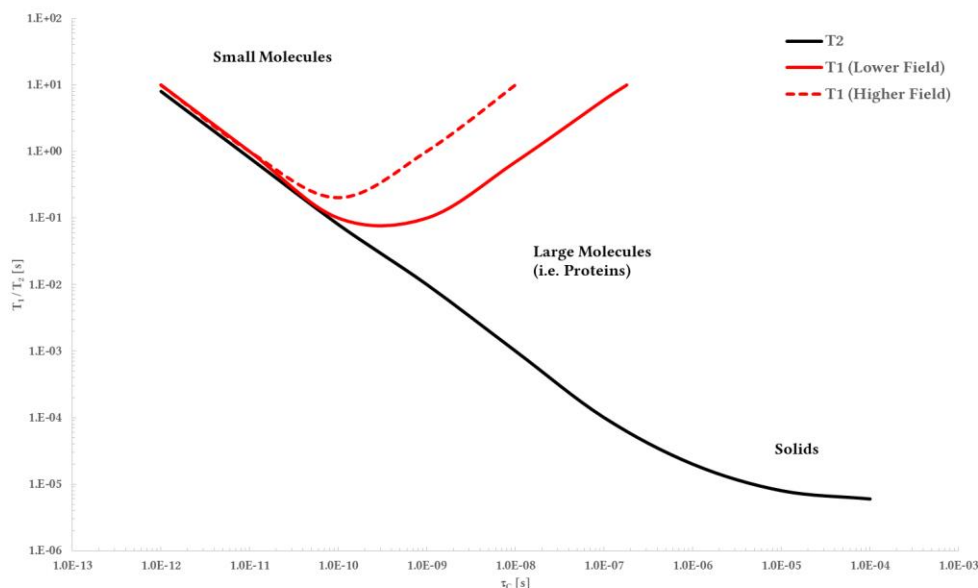
Figure 2.7: Correlation of T_1 and T_2 with varying τ_c
Here is a representation on how the relaxation rates T_1 and T_2 correlate with different correlation times τ_c. T_1 represents the time needed to reach the net magnetization in z, therefor it is dependent on the magnetic field B. T_2 in contrast is only dependent on the molecular size and viscosity of the sample

The correlation time (τ_c) defines the time needed for a molecule to rotate on average 1 rad. The bigger the molecule, the bigger is the correlation time. Figure 2.7 shows the correlation between correlation time (and therefore molecular size) and relaxation times T_1 and T_2. As T_1 is the time needed to reach the net magnetization in z direction it is dependent on the magnetic field B.

In order to get a better understanding of protein dynamics in the µs to ms range, Carr-Purcell-Meiboom-Gill (CPMG) relaxation dispersion (RD) NMR experiments can be done (Neudecker et al., 2009). A protein existing in two discrete conformations (A and B), means that certain nuclei will have different chemical shifts, correlating to different rotation frequencies ω_A and ω_B (see Figure 2.8 A). If after an evolution time of T/2 a 180° pulse is applied to this sample, the phase is inverted and after another T/2 evolution time and the phases are refocused (see Figure 2.8 B). This pulse sequence is also known as CPMG pulse sequence. In the case where exchange is occurring between state A and state B, the precession frequency will fluctuate between ω_A and ω_B. This leads to an incomplete refocusing of the magnetization with the 180° pulse (see Figure 2.8 C). The more refocusing pulses are applied during the delay T, the better the refocusing works and therefore the effects of chemical exchange are decreased (see Figure 2.8 D).
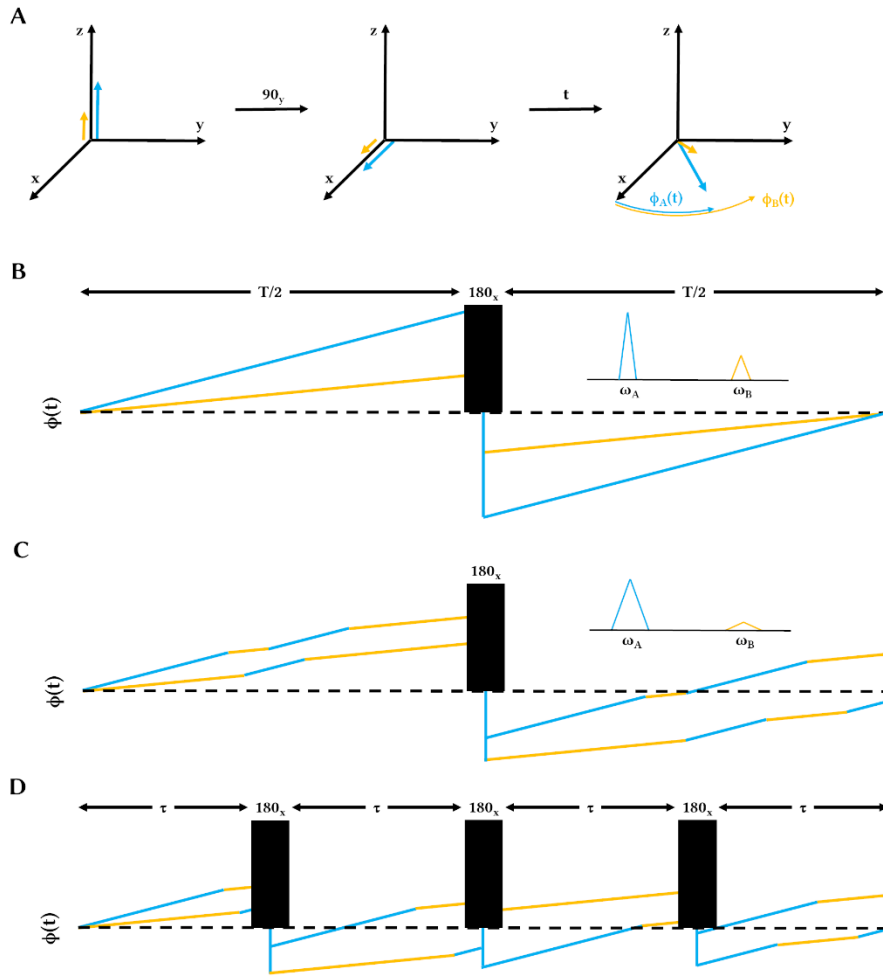
Figure 2.8: Theoretical background to relaxation dispersion NMR spectroscopy.
(A) Certain nuclei will have two different chemical shifts, correlating to two different rotation frequencies ω_A and ω_B, in a protein having two discrete conformations (here named A and B). (B) This means that, if after an evolution time of T/2 a 180° pulse is applied to this sample, the phase is inverted and after another T/2 evolution time and the phases are refocused (CPMG pulse sequence). (C) When exchange occurs between state A and state B, the precession frequency will fluctuate between ω_A and ω_B resulting in an incomplete refocusing of the magnetization with the 180° pulse. (D) With more refocusing pulses during the delay T, the refocusing is improved and therefor the effects of chemical exchange are decreased.

In CPMG relaxation dispersion NMR experiments the signal intensity I of the ground state A for a certain spin probe is observed with varying repetition rates of the refocusing pulses. This function is $I(\nu_{CPMG})$ with $\nu_{CPMG} = 1/(2\tau)$ and τ being the time between the 180° pulses. $I(\nu_{CPMG})$ can then be converted to a site specific effective transverse relaxation rate $R_{eff}(\nu_{CPMG})$ = $-\ln(I(\nu_{CPMG})/I_0)/T$ with I_0 being a reference signal intensity. With $R_{eff}(\nu_{CPMG})$ the exchange rates k_{AB} and k_{BA} can be calculated via the Bloch-McConnell equations (McConnell, 1958). The probes used for CPMG RD NMR experiments can be backbone HN groups or methyls, where preferably protonated and ^{13}C-labeled methyls in a highly deuterated background are being used for large (membrane-)protein systems.

2.4.3. NMR RDC experiments

The magnetic field of a nucleus depends due to dipole-dipole interactions on the magnetic field of its neighboring nuclei. This interaction is the dipolar interaction. The strength of the dipolar interaction depends on the distance (r), the relative orientation (θ) of the nuclei to the external magnetic field and their gyromagnetic ratios (γ):

$$D_{IS}(\theta) = \frac{\hbar \cdot \gamma_I \cdot \gamma_S}{4 \cdot \pi^2 \cdot r_{IS}^3} \cdot (1 - 3 \cdot \cos^2 \theta)$$

In solution state NMR, the dipolar interaction is on average zero due to the molecular motion. If alignment media are used, the molecular motion can be slowed down and partial alignment can be achieved (Tjandra and Bax, 1997). In this study liquid crystalline medium was used to achieve partial alignment but also other alignment media like the filamentous bacteriophage 1 (Pf1) have been used for alignment (Zweckstetter and Bax, 2001). As not only the distance can be calculated by residual dipolar couplings (RDCs) but also the relative orientation, a precise determination of relative domain orientation is possible. In order to determine the RDCs, two NMR measurements (TROSY and semi-TROSY) need to be done with alignment medium (showing J coupling and dipolar coupling) and without alignment medium (showing only J coupling). With the TROSY and semi-TROSY the J coupling can be determined whereas the comparison of the isotropic and anisotropic state leads to the dipolar coupling. To perform the structure calculation XPlor-NIH was used (Schwieters et al., 2003), the back calculation of RDCs was accomplished via PALES (Zweckstetter, 2008). The resulting R factor, representing the correlation between the experimental and back-calculated RDCs, allows an estimation of the agreement of the couplings with a specific 3D structure.

3. Publications

As my doctoral work will be written as a publication-based dissertation, I will summarize all published articles I was part of. Special focus will be put on the articles where I am the first author. All relevant data, which have not been published so far, will be presented in detail in the appendix.

3.1. Conformational dynamics of a G-protein α subunit is tightly regulated by nucleotide binding

This article (Goricanec et al., 2016) has been published on the 13th of June 2016 in the journal PNAS. "Conformational dynamics of a G-protein α subunit is tightly regulated by nucleotide binding" can be accessed online via http://doi.org/10.1073/pnas.1604125113. David Goricanec contributed as the 1st author to this publication. Due to summarizing the article in the following, I will not mention the citations of the original article (Goricanec et al., 2016).

Heterotrimeric G-proteins are important transducers of GPCR signaling. To get a better understanding of this signaling pathway, the structure and dynamics of the involved proteins have to be better understood. A key role in this signaling process is the interaction between the heterotrimeric G-protein and the corresponding GPCR. This work mainly focused on the G-protein side, to be more precise on the inhibiting G-protein α subunit 1 ($G\alpha_{i,1}$) and its structure and dynamics, depending on its ligand state and if there is an activated GPCR present.

In this work I produced the ^2H ^{13}C ^{15}N labeled $\Delta 31G\alpha_{i,1}$ for the planned NMR studies. Via FRET measurements it was by previous work shown that $\Delta 31G\alpha_{i,1}$ has a very similar nucleotide binding behavior compared to the full length $G\alpha_{i,1}$, but with preferable spectral quality in NMR measurements. The labeled $\Delta 31G\alpha_{i,1}$ was purified by myself in three different ligand states: apo, GDP-bound and GMPPNP-bound (GMPPNP was used as a more hydrolysis stable GTP analogue). Additionally, I produced unlabeled agonist bound HTGH4-L167R as active NTR1 for the studies. With this GPCR I made nanodiscs as well as empty nanodiscs as an empty membrane reference. With all the material I produced, nine different NMR samples were made, each containing either apo, GDP-bound or GMPPNP-bound $\Delta 31G\alpha_{i,1}$ combined with either only NMR buffer, empty MSP1D1 POPC nanodiscs or MSP1D1 POPC nanodiscs containing NT1-bound HTGH4-L167R. Those samples were used for the backbone

assignment of Δ31Gα$_{i,1}$ as well as for the mapping of chemical shift perturbations and peak intensities for the different ligand states and for the presence or absence of an activated GPCR.

These results, as well as the results of the other experiments, lead to the conclusion that GTP-bound Δ31Gα$_{i,1}$ (or bound to GTP analogues) shows little dynamics due to tight binding of the nucleotide. It was also shown that it has little to no affinity to the activated GPCR, as one would suspect due to signaling physiology. In line with this result, apo and GDP-bound Δ31Gα$_{i,1}$ showed a higher degree of flexibility and a more open conformation. This led to the finding of two distinct conformational states of Δ31Gα$_{i,1}$, to be more precise of its Ras domain. The population levels are defined by the ligand state and the presence of a GPCR. The open state has a high affinity to an activated GPCR and is even more stabilized by the binding to the GPCR. In contrast to this, the closed state does not interact with the GPCR.

3.2. NMR backbone and methyl resonance assignments of an inhibitory G-alpha subunit in complex with GDP

This article (Goricanec and Hagn, 2019) has been published on the 11th of December 2018 in the journal Biomolecular NMR Assignments. "NMR backbone and methyl resonance assignments of an inhibitory G-alpha subunit in complex with GDP" can be accessed online via https://doi.org/10.1007/s12104-018-9865-9. David Goricanec contributed as the 1st author to this publication. Due to summarizing the article in the following, I will not mention the citations of the original article (Goricanec and Hagn, 2019).

As shown in 3.1, NMR analysis of proteins is necessary to obtain high quality data on the dynamics and conformational states of proteins, in this case of Δ31Gα$_{i,1}$. But to be able to perform these experiments, a detailed assignment of the relevant protein is needed. In the first study (Goricanec et al., 2016), only the GMPPNP bound Δ31Gα$_{i,1}$ was assigned in detail. For the GDP-bound Δ31Gα$_{i,1}$, some assignments were missing, due to severe resonance broadening of this dynamic ligand state.

In this study, I published the backbone and methyl group resonance assignments for the GDP-bound form using an ILVA-labeled protein sample. The main focus of this work, was to report a detailed assignment of Δ31Gα$_{i,1}$ in the GDP-bound form, to complement the already published detailed assignment of the GMPPNP-bound form of Δ31Gα$_{i,1}$ from the previous study (Goricanec et al., 2016).

With those two assignments, future research in the GPCR G-protein interaction as well as the dynamic processes is enabled. For the necessary NMR studies in this context, the resonance assignments are of elementary need.

3.3. A Split-Intein-Based Method for the Efficient Production of Circularized Nanodiscs for Structural Studies of Membrane Proteins

This article (Miehling et al., 2018) has been published on the 27th of June 2018 in the journal CHEMBIOCHEM. "A Split-Intein-Based Method for the Efficient Production of Circularized Nanodiscs for Structural Studies of Membrane Proteins" can be accessed online via https://doi.org/10.1002/cbic.201800345. David Goricanec contributed as the 2nd author to this publication. Due to summarizing the article in the following, I will not mention the citations of the original article (Miehling et al., 2018).

To study the structural biology of membrane proteins, phospholipid nanodiscs have recently gained in popularity. In contrast to detergent micelles, nanodiscs resemble a native-like environment. Although they exist for nearly two decades, only recently their use in structural biology increased. One of the reasons was their optimization for structural biology via different sizes. Still their thermal stability as well as their size homogeneity varied from MSP to MSP variant. An approach to overcome this problem are covalently circularized nanodiscs. There were already methods available to produce covalently circularized nanodiscs, but they were difficult to produce and it was a time-consuming process. The aim of this project was an easy and fast method, preferably *in vivo*, to produce circularized membrane scaffold protein (cMSP) of different sizes for a covalently circularized nanodisc preparation.

I was involved in the design of the cMSP constructs in the beginning and for the establishment of the first protein production and purification steps. The initial step, was to design the PCR to clone the *Nostoc punctiforme* DnaE split-inteins before and after the MSP sequence. To stablish this method, MSPΔH5 was used as a scaffold. After successful cloning, I optimized the expression of cMSP in *E. coli*, especially under the goal to maximize monomeric cMSP expression. As a last step, the first steps of the purification have been established. Following this ground laying work, Jonas Miehling continued and finished the project completely by himself.

In this work it could be seen via electron microscopy, that the circularized nanodiscs showed better size homogeneity. Additionally, they had a higher thermal stability as CD data proofed. Both effects were leading to better spectra in NMR. The membrane proteins used in the circular nanodiscs to confirm this phenomenon were bacterial outer membrane protein X (OmpX) and human voltage-dependent anion channel subtype 1 (VDAC1). Both showed better spectra in circularized than linear MSP derived nanodiscs. With VDAC1 containing nanodiscs it could also be seen that higher measurement temperatures for NMR are possible, what also enabled better spectral quality.

3.4. Stabilization and structural analysis of a membrane-associated hIAPP aggregation intermediate

This article (Rodriguez Camargo et al., 2017) has been published on the 17th of November 2017 in the journal eLIFE. "Stabilization and structural analysis of a membrane-associated hIAPP aggregation intermediate" can be accessed online via https://doi.org/10.7554/eLife.31226.001. David Goricanec contributed as the 5th author to this publication. Due to summarizing the article in the following, I will not mention the citations of the original article (Rodriguez Camargo et al., 2017).

Many diseases are caused by protein aggregation and amyloid formation, i.e. human islet amyloid polypeptide (hIAPP) in the case of type II diabetes. It is also known that many of those proteins interact with cell membranes causing unique protein folding patterns or even promote amyloid formation. In this work it has been shown that nanodiscs can be used to mimic membrane-associated protein aggregation. The used amyloigenic polypeptide in this study was hIAPP and the structural analysis has been done mostly via solid state NMR spectroscopy.

My part of this work was to produce different types of nanodiscs, varying in size but especially in lipid composition. First it was checked which size of nanodiscs is needed, what could be concluded to be MSP1D1ΔH5, as MSP1D1 would have been unnecessarily too big. The next step was the screening of different lipid ratios, to influence the charge of the membrane surface. Whereas DMPC has a net charge of zero, DMPG has a negative net charge. Therefor I produced the nanodiscs with the following three ratios (90% DMPC/10% DMPG, 75% DMPC/25% DMPG, 50% DMPC/50% DMPG). From those nanodiscs, the one with the ratio 90% DMPC/10% DMPG caused the most stable nanodisc hIAPP intermediate.

It was shown that nanodiscs are suitable to study amyloid membrane interactions in a native like environment and this could also be used for the investigation of other amyloigenic polypeptides.

4. Discussion

The main goal of this thesis was to get a better understand in the GPCR G protein signaling process (see Figure 4.1).

The first part of the work mainly focused on the G-protein side, to be more precise on the inhibiting G-protein α subunit 1 (G$\alpha_{i,1}$) and its structure and dynamics, depending on its ligand state and if there is an activated GPCR present. Thereby I first labeled $\Delta 31$G$\alpha_{i,1}$ (^{2}H ^{13}C ^{15}N) for the planned NMR studies. FRET measurements done by prior to this thesis have shown that $\Delta 31$G$\alpha_{i,1}$ has a very similar nucleotide binding behavior compared to the full length G$\alpha_{i,1}$. The reason $\Delta 31$G$\alpha_{i,1}$ is preferred for NMR measurements is due to its smaller hydrodynamic radius resulting in a shorter correlation time (τ_C) which equals improved relaxation behavior. I successfully purified the labeled $\Delta 31$G$\alpha_{i,1}$ in three different nucleotide states: apo, GDP-bound and GMPPNP-bound (GMPPNP was used as a more hydrolysis stable GTP analogue). For this work I additionally produced unlabeled NT1 bound HTGH4-L167R in nanodiscs as active GPCR for the studies. Along to the GPCR loaded nanodiscs I produced empty nanodiscs as an empty membrane reference. This resulted in nine different NMR samples I measured, each containing either apo, GDP-bound or GMPPNP-bound $\Delta 31$G$\alpha_{i,1}$ combined with either only NMR buffer, empty MSP1D1 POPC nanodiscs or MSP1D1 POPC nanodiscs containing NT1-bound HTGH4-L167R. The G$\alpha_{i,1}$ NMR samples only in buffer were used for the backbone assignment of $\Delta 31$G$\alpha_{i,1}$. All samples were used for the mapping of chemical shift perturbations and peak intensities for the different nucleotide states and for the presence or absence of an activated GPCR.

Here I could show that GTP-bound $\Delta 31$G$\alpha_{i,1}$ (or bound to GTP analogues) shows little dynamics due to tight binding of the nucleotide. In line with this finding I showed that GTP-bound $\Delta 31$G$\alpha_{i,1}$ has little to no affinity to the activated GPCR. As GTP-bound G alpha subunits promote downstream signaling one would expect this finding. Additionally I could determine that apo and GDP-bound $\Delta 31$G$\alpha_{i,1}$ showed a higher degree of flexibility and a more open conformation. These two distinct conformations led to the finding of two distinct populations of $\Delta 31$G$\alpha_{i,1}$. The nucleotide state of G$\alpha_{i,1}$ as well as the presence of NTR1 influenced the population levels of G$\alpha_{i,1}$. There it could be showed that G$\alpha_{i,1}$ in its open conformation has a high affinity to an activated GPCR, most pronounced for the apo state of G$\alpha_{i,1}$. The population of the open conformation of the GDP-bound state is stronger increased by the binding to the GPCR than for the apo state. In contrast to this, the closed state doesn't interact with the GPCR and the closed conformation is the only present population.
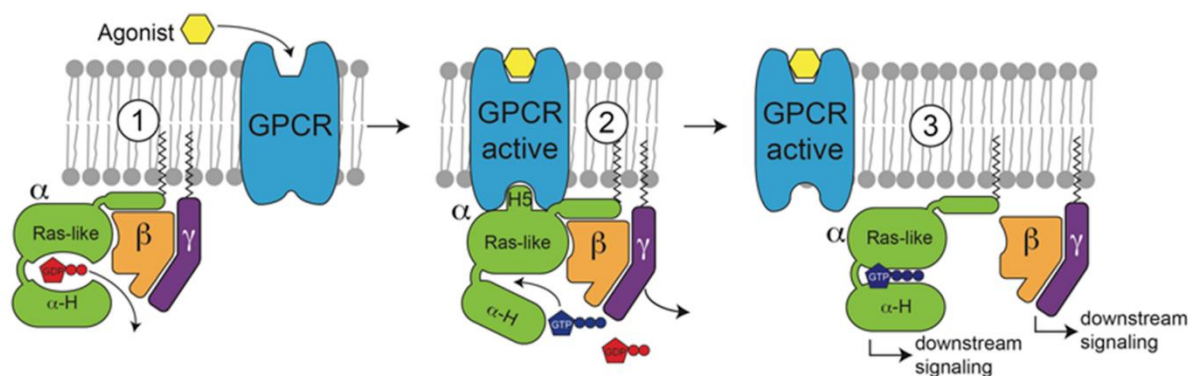
Figure 4.1: GPCR G protein interaction
The GPCR signaling starts with agonist binding to the GPCR. Thereby the GPCR changes its conformation and is active. GDP bound heterotrimeric G protein is inactive, but has an increased affinity to bind active GPCRs (1). Upon binding between the activated GPCR and the G protein, a conformational change in the α subunit (especially helix 5 of the Ras domain) of the G protein enhances the dissociation of the GDP in the nucleotide binding pocket. This apo state of the G protein has the highest affinity to the activated GPCR and GTP (2). As soon as GTP binds to the α subunit of the G protein, the G protein dissociates from the activated GPCR. The two major subunits dissociate into the α subunit and the βγ subunit. Both are responsible for downstream signaling and have no significant affinity to the activated GPCR (3). When the α subunit hydrolyzes the GTP to GDP with its intrinsic enzymatic activity, the heterotrimeric G protein can reassemble and the cycle can start again. Figure shown as in the original publication (Goricanec et al., 2016).

In chapter 1.1 (G-Protein-coupled-receptors (GPCRs)) I showed many examples of GPCR structures solved in different ligand states and with various G proteins or G protein mimetics bound to them. But in order to get a better understanding in their activation and how they promote downstream signaling via G protein activation, NMR spectroscopy is big importance. Only via NMR spectroscopy, dynamics in the µs to ms range can be observed on an atomic level as well as the determination of different states being present at the same time.

Many different methods are used in NMR spectroscopy to investigate the dynamics as well as the allosteric changes of GPCRs. This is either accomplished by the use of special tags i.e. the ^{19}F labelling of cysteines (Horst et al., 2013; Liu et al., 2012; Susac et al., 2018), by the use of ^{13}C methyl labelling of proteins during expression (Kofuku et al., 2014; Solt et al., 2017; Toyama et al., 2017; Xu et al., 2019). Even selective ^{15}N labelling strategies (Eddy et al., 2018b; Isogai et al., 2016) have been applied as well as tryptophan mutagenesis for extrinsic NMR probes (Eddy et al., 2018a).

In recent years, a lot of insight was gained on the receptor activation mechanisms and allostery (Bostock et al., 2019; Casiraghi et al., 2019; Flock et al., 2015; Shimada et al., 2019; Thal et al., 2018). With all this knowledge, we wanted to determine the dynamics and the allosteric activation of the NTR1 variants.

The first project involved the use of ILVA labeled NTR1 variants in different ligand states and with the presence or absence of a G protein. The assignments have been done prior to my work and will not be discussed in detail here. My part of the project was to express HTGH4 wt, HTGH4 L167R and TM86V L167R in M9 (D_2O) for ILVA labelling. After successful expression, all 3 variants were purified in an agonist as well as antagonist bound state. Thereby only for HTGH4 wt, the apo form as well as the antagonist bound receptors were produced. As described in the appendix, the apo as well as the 2nd antagonist state were omitted for further studies. This decision was made, due to the fact that the differences between those three ligand states were nearly non exisiting. Due to its favorable handling properties, SR-142948 bound NTR1 was used to study the inactive GPCR form. Additionally, the 2 step G protein titration step was also skipped, as the 50% G protein relative to agonist bound NTR1 showed nearly identical spectra as only agonist bound NTR1. Therefor only one G protein NTR1 complex was measured via NMR, with an excess of G protein added to the GPCR (see Figure A.1). All the NTR1 variants were measured in d_{26}-DH$_7$PC due to smaller micelle size compared to DDM micelles.

As expected from previous results of the signaling activity of the NTR1 (Egloff et al., 2014), no significant differences between all ligand states can be observed for HTGH4 wt (see Figure A.2). This can be explained with the impaired signaling potency of HTGH4 wt, which is caused by the thermostabilizing mutation of Arginine to Leucine at position 167 (R$^{3.50}$L). The mutation of Arginine in this class A GPCR conserved region (D/ERY) causes a not functional ionic lock. HTGH4 L167R shows the opposite signaling behavior. Hereby big differences between the agonist and antagonist bound form can be seen (see Figure A.2). Comparing these spectra shows chemical shifts for many peaks, with some peaks disappearing completely. The number of affected peaks surpasses the labeled residues in the ligand binding pocket, which can then only be explained by allosteric changes throughout the GPCR. Additionally, the spectrum of HTGH4 L167R titrated with an excess of heterotrimeric G protein is fairly distinct, compared to the spectra of antagonist and agonist bound forms. This could be explained by an interaction of the NTR1 and G protein, either with peaks being affect via direct interaction, as well as conformational selection of the GPCR via the G protein and therefor allosteric effects. The dynamics of TM86V L167R are between the two extremes of HTGH4 wt and HTGH4 L167R. In general it shows a similar signaling behavior like the HTGH4 L167R, but in a smaller extent. The differences between the agonist and antagonist bound state are smaller for the TM86V L167R in contrast to HTGH4 L167R, which is also the case if the agonist state is compared with and without G protein. This could be explained by

a less stable transient opening of the ionic lock, due to allosteric effects in TM86V L167R, as it is more NTR1 wild type like. These findings are also supported by comparing the different ligand states directly for each NTR1 variant (see Figure A.3).

A second method which I used to get insight into the GPCR activation mechanism, was the use of ^{13}C-MMTS as a cysteine specific methyl label. This label was already successfully used in NMR (Religa et al., 2011), and I had similar or even identical tagging positions compared to the ^{19}F studies on β_2AR (Horst et al., 2013; Liu et al., 2012). The first part of the project was to establish the tagging of the unlabeled GPCR. For this I adapted an already published protocol (Religa et al., 2011) to the NTR1 variants. Via electrospray ionization mass spectrometry (ESI-MS, see Figure A.4) I could prove complete tagging of the GPCR. In order to track the helix 6 movement of the GPCR, valine at position 300 (6.27 according to Ballesteros Weinstein) was mutated to a cysteine. With this construct I completed the assignment of all cysteines which could be tagged (see Figure A.8 and Figure 4.2)
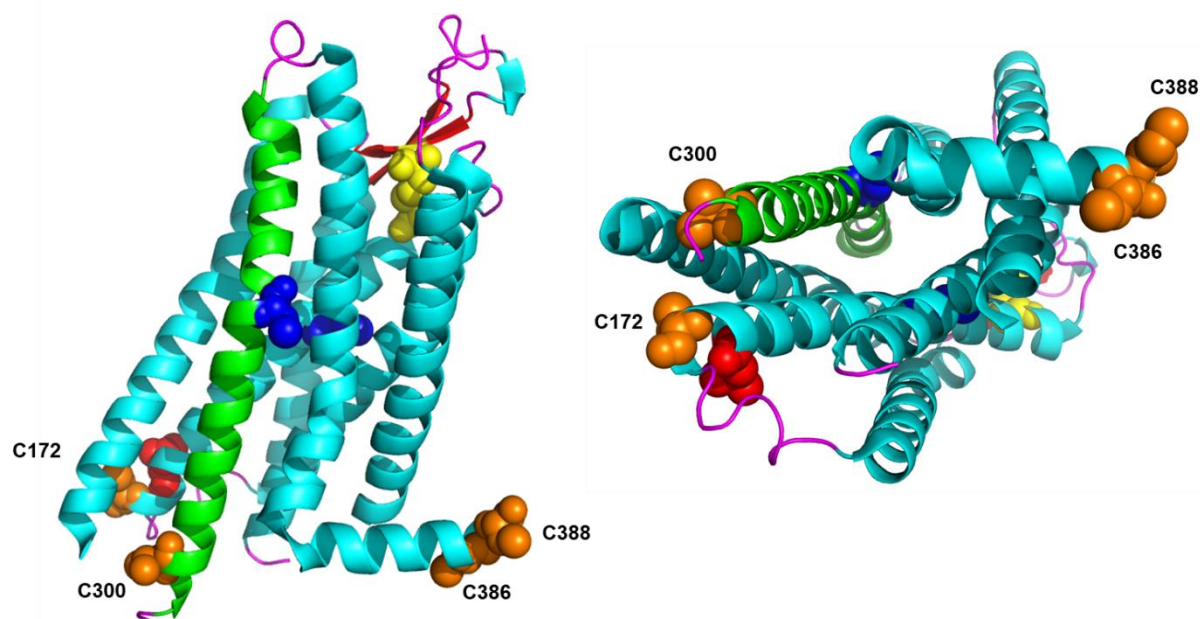
Figure 4.2: Structure of HTGH4 with the cysteines and leucine 167 showed as spheres (here C300 is shown as V)
This is a cartoon representations of the crystal structure of HTGH4 (pdb: 4BWB). Inaccessible cysteines for tagging with MMTS are shown as blue and yellow spheres, with the former being isolated inside the helical bundle whereas the latter form a disulfide bridge. The orange spheres represent cysteines which have been tagged with MMTS in this work. The cysteine in position 300 is obtained via mutagenesis as a valine is present in the wildtype in this position. The red spheres show the position of the amino acid 167 in HTGH4, 3.50 in Ballesteros/Weinstein nomenclature. This is a conserved residue in class A GPCRs. In this figure the amino acid at 167 is a leucine (as the structures was solved for the thermostabilized HTGH4 variant), whereas in the wildtype this amino acid is an arginine.

As we know from already published studies, TM86V L167R is in contrast to HTGH4 L167R switchable. The latter is active in G protein activation independent of the ligand state,

whereas TM86V L167R is only active while NT1 bound. I wanted to know which of the 15 mutations difference between both NTR1 constructs is responsible for this behavior. Our collaboration partners at the Universität Zürich provided us with information about the 4 most promising mutations. These 4 mutations were then cloned by myself into the HTGH4 L167R V300C vector to obtain 4 additional single mutants, the HTGH4 L167R V300C A260I/R101T/D124E/E150D.

In the next step, their thermal stability depending on the ligand and tagging state was checked via CD spectroscopy (see Figure A.5 until Figure A.7). All HTGH4 L167R V300C variants show nearly identical behavior as HTGH4 L167R. Two findings were of particular interest. First, TM86V variants show inverted tendencies for the stability of tagged versus untagged constructs if compared to HTGH4 constructs. This could be explained by the fact, that HTGH4 is more hydrophobic close to the ionic lock than TM86V due to the evolutionary stabilization process. Therefor a methyl tagged cysteine would stabilize this region even further, whereas this effect is opposite in the less hydrophobic region for TM86V. Second, for each ligand state as well as tagging state, the R101T variant shows an increased stability. The exact details for this mechanism still have to be studied, which could be done via the ILVA experiments giving insight in the allosteric network.

I recorded ^{1}H-^{13}C methyl-TROSY NMR for each NTR1 variant in an agonist bound (NT1) active state as well as in an antagonist bound (SR-142948) inactive state. Except for C386, all labeled cysteines showed two peaks, each representing either the active or the inactive state. As the cysteine at position 386 did not change for any NTR1 variant or ligand state, it was used as a reference in all spectra. All spectra and their peak height analysis are shown in the Appendix (Figure A.9 until Figure A.15). For a better visual comparison of all spectra, their peak heights can be seen in Figure A.16. In this comparison it can be seen that HTGH4 L167R V300C D124E as well as TM86V L167R V300C show the most populated ground states in the agonist bound state. In contrast to this, HTGH4 L167R V300C E150D shows the most populated active states in the agonist bound state. The relative populations of the other observed NTR1 variants are somewhere between those two extremes. For the antagonist bound state, similar results are obtained. The most populated active state is detected for the NT1 bound state of HTGH4 L167R V300C E150D. The HTGH4 L167R V300C D124E variant shows the least populated active states in the antagonist bound form. A general tendency is that the other NTR1 variants vary more in the antagonist bound state compared to the agonist bound form. To get a better understanding of these results, further experiments are necessary. One possibility would be to create multiple mutations for one construct in order to investigate

their collaborative effects. Another direction for the investigation of key residues in signaling is a titration with heterotrimeric G protein and its effect on the population of the different states. Lastly, I want to mention, that ideally all experiments should be repeated without the presence of detergent, preferably in a native like environment like phospholipid nanodiscs.

An important aspect in studying the structural biology of membrane proteins, is the use of membrane mimetics. Even though detergents are easy to handle, they can alter the function of membrane proteins. Therefor the use of native-like membrane mimetics is the preferred choice. Recently the use of phospholipid nanodiscs got more and more popular. Their use in biochemistry exists for nearly two decades (Bayburt et al., 2002; Bayburt and Sligar, 2010), only recently their application in structural biology increased. One of the reasons was their optimization for structural biology via different sizes (Hagn et al., 2013; Hagn et al., 2018). As the MSP used for the nanodiscs was linear and not covalently bound, their thermal stability as well as their size homogeneity varied. A solved structure of nanodiscs via NMR (Bibow et al., 2017) could explain these problems. Therefor methods to overcome this problem were desired. One method to optimize the stability and size homogeneity is the use of covalently circularized nanodiscs. There were already methods available to produce covalently circularized nanodiscs *in vitro* (Nasr et al., 2017), but they were difficult to produce and it was a time-consuming process. The aim of this project was an easy and fast method, preferably *in vivo*, to produce circularized membrane scaffold protein (cMSP) of different sizes for a covalently circularized nanodisc preparation.

The first step in this project the cloning of the cMSP constructs Thereby I designed a PCR strategy to clone the *Nostoc punctiforme* DnaE split-inteins before and after the MSP sequence (see Figure 4.3). Following the successful cloning of the cMSP plasmids, I established the first protein production and purification steps with my intern Jonas Miehling. Following this ground laying work, Jonas Miehling continued and finished the project completely by himself (Miehling et al., 2018).

In this work we showed via electron microscopy, that the circularized nanodiscs have a better size homogeneity. They also had a higher thermal stability as determined via CD thermal melting curves. Both effects help to obtain better spectra in NMR as well as in cryo EM. As model membrane proteins to confirm the improved properties of circularized nanodiscs, bacterial outer membrane protein X (OmpX) and human voltage-dependent anion channel subtype 1 (VDAC1) have been used. In both cases better spectra could be obtained in circularized than linear MSP derived nanodiscs. With VDAC1 containing nanodiscs it could

also be seen that higher measurement temperatures for NMR are possible, what also enabled better spectral quality.
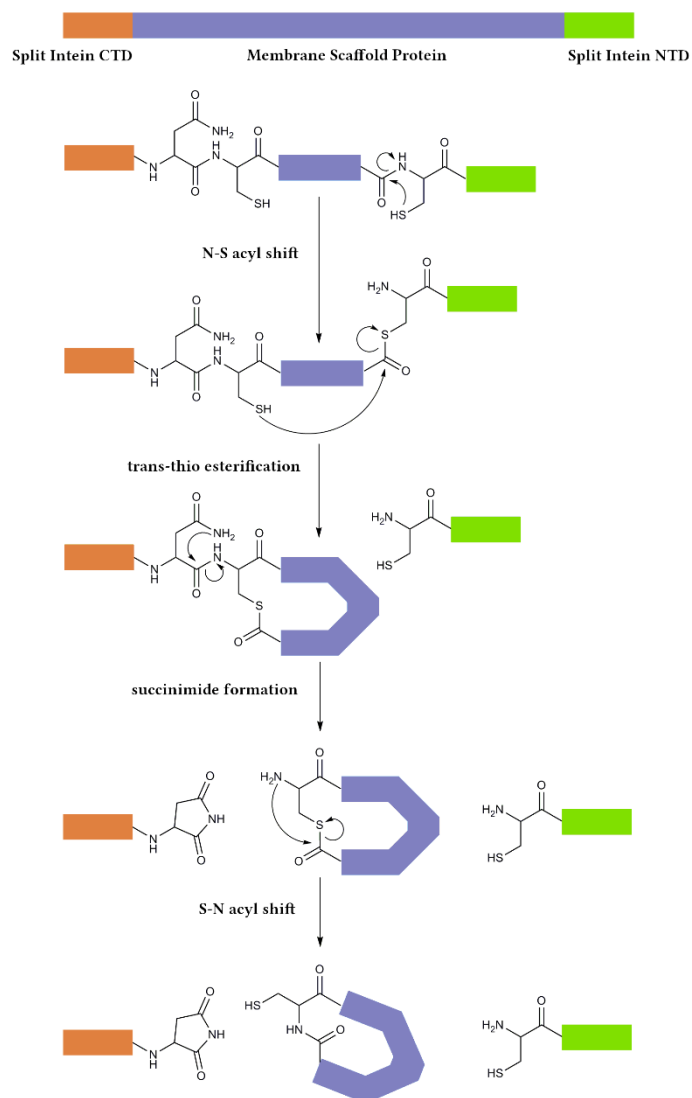

Figure 4.3: cMSP split intein splicing
Here, the molecular mechanism of split intein mediated MSP circularization is shown. Split inteins are cloned around linear MSP constructs. During expression, both split inteins align together and catalyze the circularization.

A. Appendix

The dynamics of the thermostabilized NTR1 were investigated in the second half of the PhD thesis as it was outlined in the aims of the thesis (see 1.31.3 "Aims of the Thesis"). Therefor the data acquired and analyzed for this part of the project is unpublished to date. Certain experiments still have to be done in the lab to get a better understanding on the dynamics of the NTR1 with the underlying mechanisms of GPCR activation and G protein interaction.

a. Unpublished Data

GPCR allostery mapped with ILVA labeled NTR1 variants

The main goal of this project is to get a deeper understanding of the allosteric network of NTR1 activation. In this context the influence of the thermostabilizing mutations on this process should be investigated. Therefore, 3 different NTR1 variants were used for the analysis:

- HTGH4 "wt" (L167)

- HTGH4 L167R

- TM86V L167R

We were also interested in the influence of the ligand state on the activation mechanism. In this regard we checked the following ligand states:

- Apo

- SR-48692: Non-peptide antagonist. It is selective for the neurotensin receptors, but not selective between subtypes (Gully et al., 1993)

- SR-142948: Non-peptide antagonist. It is selective for the neurotensin receptors, but not selective between subtypes (Nalivaiko et al., 1998)

- NT1: Truncated NT1 peptide containing the amino acid positions 8 to 13 with an N-terminal glycine linker and 3C cleavage rest: GPGGRRPYIL

As the apo state and both antagonists showed similar behavior in NMR, only SR-142948 was used in further studies to obtain the inactive NTR1 state. This antagonist was also solely used in the 2nd project of unpublished results.

Lastly the effect of unlabeled heterotrimeric G protein, obtained from insect cells by our collaboration partners in Harvard Medical School (Prof. Gerhard Wagner and Meng Zhang), on the NT1 activated NTR1 variants was analyzed. First two different concentrations of the G protein relative to the GPCR were used, a 1:2 ratio of G protein to GPCR and a 2:1 ratio of G protein relative to GPCR. As both showed identical behavior in NMR, the rest of the experiments were titrated with a 3:2 ratio of G protein to GPCR.

As the NTR1 variants were analyzed via NMR spectroscopy, it first had to be assigned. This has already been done before my involvement in this project by Prof. Franz Hagn and Prof. Joshua Ziarek (now Indiana University Bloomington) during their time at the Harvard Medical School (Prof. Gerhard Wagner). The assignments for the ^{1}H-^{13}C methyl groups from the ILVA labeling are nearly complete, whereas the ^{1}H-^{15}N assignments are incomplete (approximately 30% of all possible signals). This can be explained by the protein production. As the GPCR is directly folded and inserted into the membrane during expression in D2O containing M9 medium, all backbone amides are deuterated. During purification in aqueous solution, only the accessible amide deuterons are back exchanged to protons. All deuterons of the backbone amides in the transmembrane region cannot exchange with the protons.

My part of the project was to express the NTR1 variants in M9 (D$_2$O) ILVA medium, to purify the GPCRs in the different ligand states and to measure the NMR spectra for analysis. The labeled expression was done as described in chapter 2.1.4 (Isotope labeling Strategies). Following the expression, the NTR1 variants were purified as explained in chapter 2.1.1 (Neurotensin Receptor 1 (NTR1)). After successful purification, the samples were concentrated to the maximum and as described in chapter 2.4 (NMR Spectroscopy) prepared for NMR measurement. For each sample a [^{1}H-^{15}N] 2D TROSY and an optimized [^{1}H-^{13}C] 2D HMQC also called methyl-TROSY (Tugarinov et al., 2003) was recorded. The results are shown in Figure A.1 until Figure A.3.

In Figure A.1 six different [^{1}H-^{13}C] HMQC spectra of ILVA labeled HTGH4 wt in different ligand states and titrated with heterotrimeric G protein are overlayed. I am missing the assignments, therefor the spectra are analyzed in a qualitative manner. Three different peak regions are zoomed in as examples of changes in the spectra. The zoomed in region on top shows different peak shifts and intensities for all 6 variants. The middle zoomed in region shows no changes between the 6 different ligand states. The bottom one shows only peaks for the agonist bound state, but not for the apo or antagonist bound states. As the differences in the antagonist and apo spectra were neglectable and the yield of apo form NTR1 was really

low, only one spectrum was recorded for the inactive form of NTR1 in future experiments. The antagonist chosen for the studies was SR-142948. Additionally, only titrations with excess of heterotrimeric G protein were performed for the other NTR1 variants, as the 50% G protein spectrum was identical to the spectrum only with agonist bound to HTGH4 wt.

Figure A.2 shows the overlays of [^{1}H-^{13}C] HMQC spectra of ILVA labeled NTR1 variants for each investigated NTR1 variant. Thereby the SR-142948 bound NTR1 variants are shown in black, the NT1 bound NTR1 variants in red and the NT1 bound NTR1 variants titrated with an excess of G protein in blue. The NTR1 variants of this study are HTGH4 wt (left overlay), HTGH4 L167R (middle overlay) and TM86V L167R (right overlay). It can be seen that in the case of HTGH4 wt no differences are significantly visible for all three ligand and titration states. This is in line with the impaired signaling potency of HTGH4 wt due to the Leucine at position 167, leading to an impaired ionic lock. In line with these results, HTGH4 L167R shows the exact opposite effects. The differences between the antagonist bound form and the agonist bound form are very big. For many peaks a chemical shift can be observed, as well as peaks disappearing completely. This means that many residues are affected by the different ligands and therefor an allosteric effect is a plausible cause as only a small fraction of labeled residues is present in the ligand binding pocket. The spectrum with the titrated heterotrimeric G protein is also very distinct to the other two ligand states, as some peaks are only visible for one of both spectra. This could be explained by a strong interaction between the NTR1 and the G protein. In the case of TM86V L167R, similar observations can be made, but to a lower extent. The differences in the spectra for the antagonist as well as the agonist bound state are smaller compared to HTGH4 L167R, as well as the differences in the spectra for the agonist bound state with and without heterotrimeric G protein. A more transient activation of the "wild type" like TM86V L167R compared to HTGH4 L167R would be an explanation of this effect.

The overlays of [^{1}H-^{13}C] HMQC spectra of ILVA labeled NTR1 variants for each ligand state shown in Figure A.3 Thereby the HTGH4 wt spectra are shown in black, the HTGH4 L167R spectra in red and the TM86V L167R spectra in blue. The spectra of the SR-142948 bound NTR1 variants used in his study are overlaid on the left, The NT1 bound NTR1 variants of this study are overlaid in the middle and the NT1 bound NTR1 variants of this study titrated with heterotrimeric G protein are overlaid on the right. These results further underline the findings explained by Figure A.2. The differences between the spectra for the SR-142948 bound NTR1 forms are relatively big and each variant shows a distinct pattern. In contrast to

this, the NT1 bound states, both L167R variants are very similar, with only HTGH4 wt being significantly different.

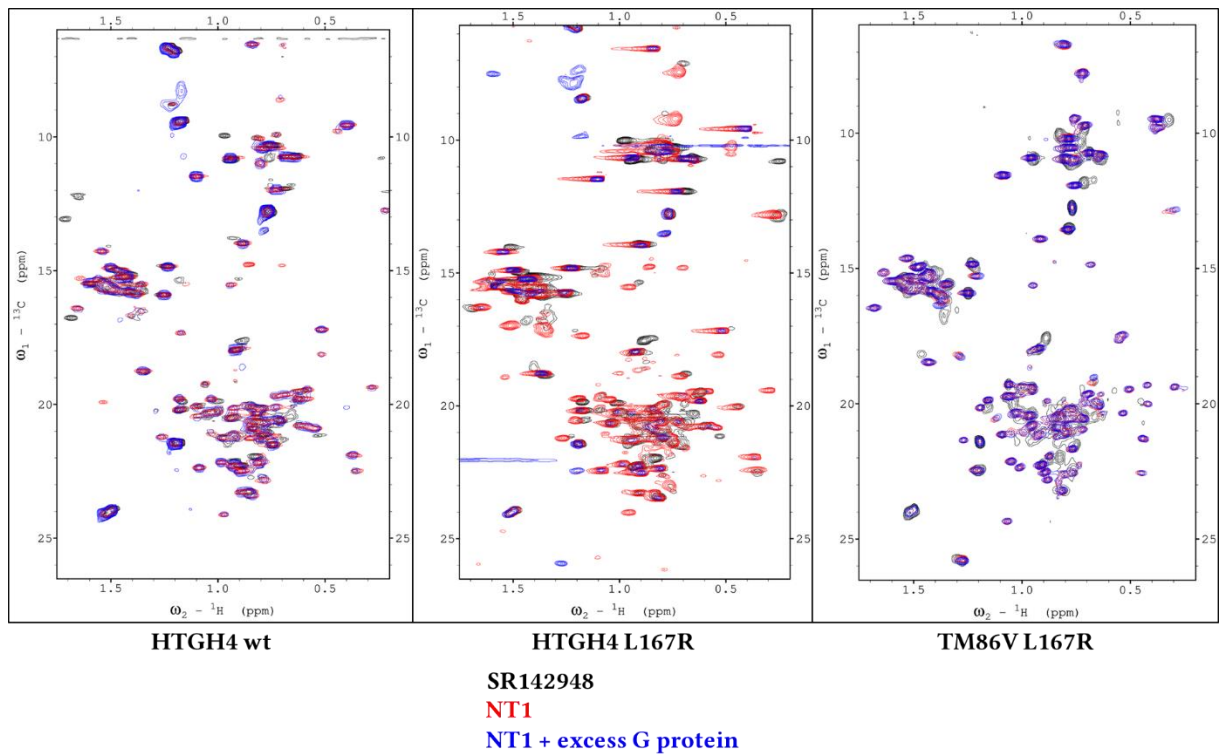| ILVA labeled NTR1 in DH₇PC		ILVA labeled NTR1 in DH₇PC	
HTGH4 wt apo	**Blue**	HTGH4 wt NT1	**Yellow**
HTGH4 wt SR-142948	**Red**	HTGH4 wt NT1 +50% G protein	**Pink**
HTGH4 wt SR-48692	**Green**	HTGH4 wt NT1 +200% G protein	**Black**
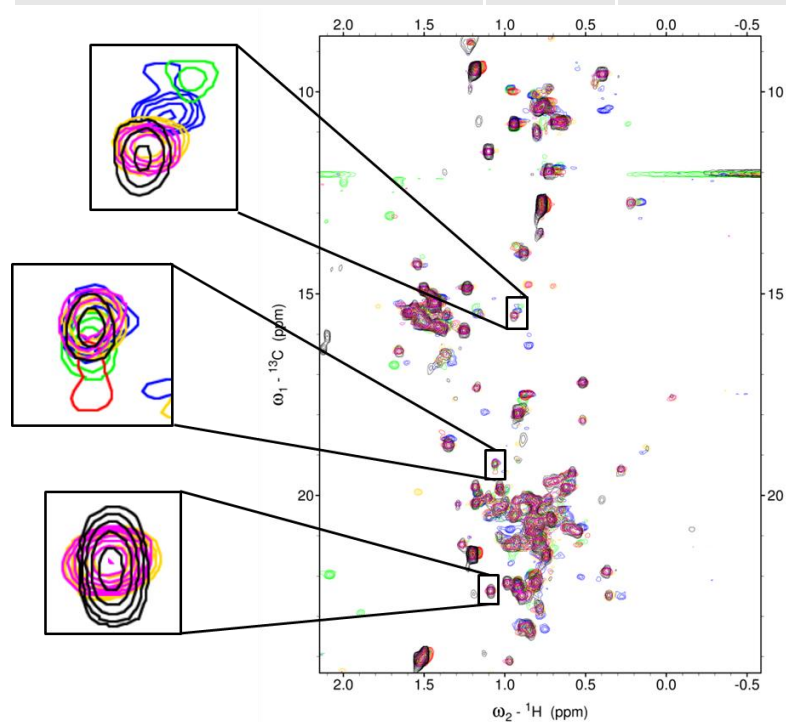
Figure A.1: [¹H-¹³C] HMQC of ILVA labeled HTGH4 wt in different ligand states and titrated with heterotrimeric G protein
This figure shows the overlay of 6 different [¹H-¹³C] HMQC spectra. Each spectrum represents ILVA labeled HTGH4 wt with different ligand conditions as described on top of the spectra. As the data is not complete so far, the spectra are analyzed in a qualitative manner. 3 Peaks are shown as examples of changes in the spectra (zoomed in). The top one shows different peak shifts and intensities for all 6 variants. The middle peak shows no changes between the 6 different ligand states. The bottom one shows only peaks for the agonist bound state, but not for the apo or antagonist bound states.

HTGH4 wt   **HTGH4 L167R**   **TM86V L167R**

SR142948
NT1
NT1 + excess G protein

Figure A.2: Overlays of [^{1}H-^{13}C] HMQC spectra of ILVA labeled NTR1 variants for each NTR1 variant
For each overlay the black spectrum represents the SR142948 bound NTR1 variant, the red spectrum represents the NT1 bound
NTR1 variant and the blue spectrum represents the NT1 bound NTR1 variant in complex with excess heterotrimeric G protein.
The overlay of NMR spectra on the left is showing the different ligand states of HTGH4 wt. The overlay of NMR spectra in the
middle is showing the different ligand states of HTGH4 L167R. The overlay of NMR spectra on the right is showing the different
ligand states of TM86V L167R.

SR142948 **NT1** **NT1 + excess G protein**

HTGH4 wt
HTGH4 L167R
TM86V L167R
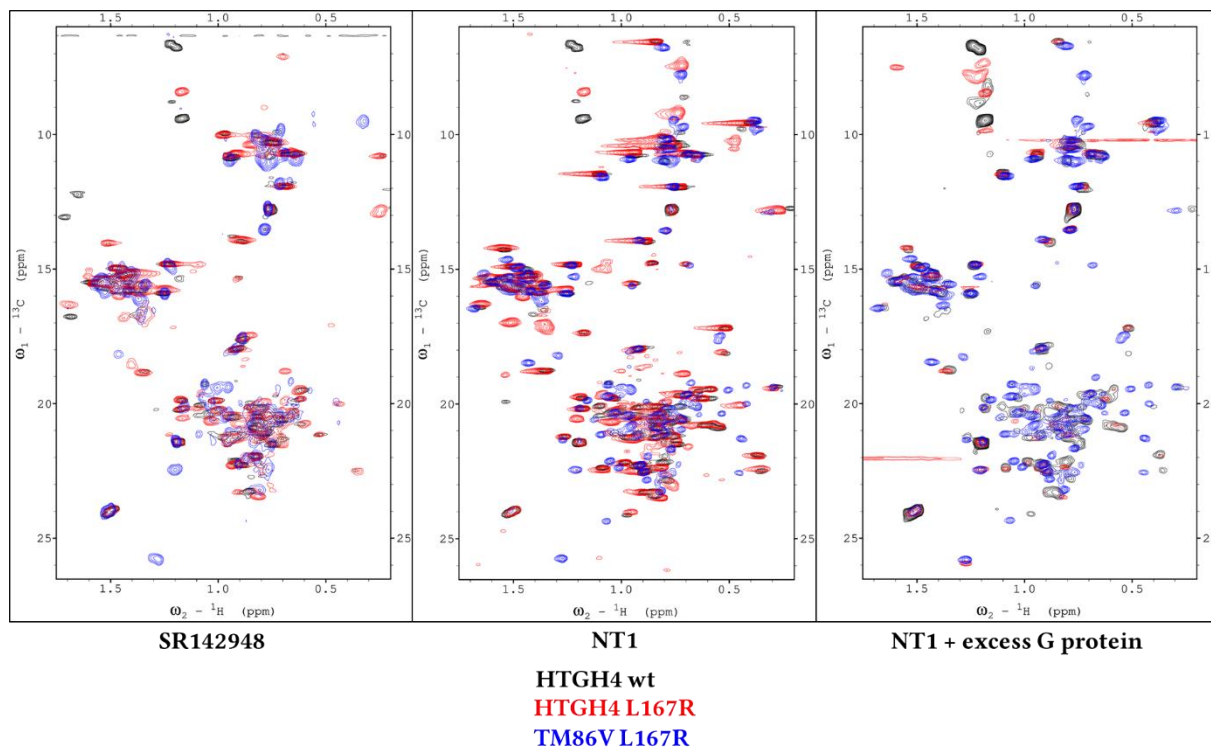
Figure A.3: Overlays of [^{1}H-^{13}C] HMQC spectra of ILVA labeled NTR1 variants for each ligand state
For each overlay the black spectrum represents HTGH4 wt, the red spectrum represents HTGH4 L167R and the blue spectrum
represents TM86V. The overlay of NMR spectra on the left is showing the different NTR1 variants in the SR142948 bound state.
The overlay of NMR spectra in the middle is showing the different NTR1 variants in the NT1 bound state. The overlay of NMR
spectra on the right is showing the different NTR1 variants in the NT1 bound state in complex with excess of heterotrimeric
G protein.

GPCR activation mapped with ^{13}C-MTS labeled NTR1 variants

The main goal of this project is to get a deeper understanding of the NTR1 activation. In this context the influence of the thermostabilizing mutations on the GPCR signaling was analyzed. As for the ILVA study, 3 different NTR1 variants were used for the analysis, but they all had an additional cysteine cloned in order to probe for helix 6 movement (V300C, 6.27 according to Ballesteros-Weinstein):

- HTGH4 "wt" (L167) V300C

- HTGH4 L167R V300C

- TM86V L167R V300C

In order to assign the cysteines which could be tagged with the ^{13}C-MMTS reagent, an additional variant was cloned:

- HTGH4 L167R C386S

I also wanted to get further insight in which mutations from the TM86V to the HTGH4 variant have an influence on the GPCR signaling. With the help of unpublished data from our collaboration partners at the University of Zürich (Prof. Andreas Plückthun), we also used four different mutants which they identified as strongly involved in the activation process:

- HTGH4 L167R V300C A260I

- HTGH4 L167R V300C R101T

- HTGH4 L167R V300C D124E

- HTGH4 L167R V300C E150D

In this project, I was also interested in the influence of the ligand state on the activation mechanism. In this regard we checked the following ligand states:

- SR-142948

- NT1

The reasoning behind only using SR-142948 to obtain the inactive NTR1 state has been explained in the previously shown unpublished results.

Expression and purification of the unlabeled NTR1 variants was done according to our adapted NTR1 purification protocol described in chapter 2.1.1 (Neurotensin Receptor 1

(NTR1)). After successful purification, the samples were concentrated to the maximum and as described in chapter 2.4 (NMR Spectroscopy) prepared for NMR measurement. For each sample a [^{1}H-^{13}C] 2D HMQC also called methyl-TROSY (Tugarinov et al., 2003) was recorded.

As the NTR1 variants needed to be tagged with ^{13}C-MMTS, I adapted and optimized the tagging procedure to our system as explained in chapter 2.1.4 (Isotope labeling Strategies). To verify the tagging efficiency determined by NMR spectroscopy, electrospray ionization mass spectrometry (ESI-MS) was used (see Figure A.4). Here the molecular weight difference of an exemplary NTR1 variant (HTGH4 L167R V300C) is determined, with being either tagged (37617 Da) or not tagged (37425 Da). For all HTGH4 variants with the V300C mutation the weight difference is 192 Da. As each tag has a molecular weight of 48 Da (S^{13}CH$_3$), 4 cysteines are accessible for tagging in HTGH4 V300C variants and therefor complete tagging was proven (4 tags à 48 Da equals 192 Da).

To obtain all the needed mutants of NTR1 described earlier, I used the QuikChange Lightning Site-Directed Mutagenesis Kit from Agilent according to the manufacturers instruction manual (see Appendix b: Material).

Additionally, I measured CD spectra and thermal denaturation curves of the newly generated NTR1 mutants to verify their structural integrity as well as to estimate their thermal stability (see Figure A.5 until Figure A.7). Four thermal melting curves were recorded for each analyzed NTR1 mutant. The four different CD measurements have been done with and without tag as well as in a NT1 and SR142948 bound state. In all CD melting curves, the dashed lines represent the tagged constructs, whereas the solid lines show the untagged constructs. These experiments show that tagged constructs are on average more stable than their untagged counterparts and they show also that TM86V variants are less stable than the HTGH4 variants. In order to simplify the analysis of the CD melting curves, only tagged or untagged NT1 bound NTR1 variants were compared in one figure (see Figure A.6), whereas their SR-142948 bound counterparts were compared in another figure (see Figure A.7). The CD data show that for the HTGH4 variants, the tagged constructs are more stable than the untagged counterparts. In contrast to this the TM86V variant which is tagged is less stable than the untagged one. For NT1 bound HTGH4 constructs all untagged variants have a similar melting point except for the R101T variant, having an increased stability. Antagonist bound HTGH4 constructs show the same behavior with an increased stability also for the A260I variant.

In order to be able to analyze the NTR1 variants via NMR spectroscopy, I first had to assign all accessible cysteines that could be tagged. Thereby I first measured the ^{13}C-methyl tagged

NTR1 variants HTGH4 wt and HTGH4 L167R which show the same residues being tagged, C172, C386 and C388. As the cysteines in helix 8 (386 and 388) are in a similar chemical environment, I mutated the cysteine at position 386 to serine and tagged this NTR1 variant, resulting in a loss of one of the two similar peaks. This enabled me to obtain all 3 residues being assigned. In the next step I used the ^{13}C-methyl tagged HTGH4 L167R and compared it to ^{13}C-methyl tagged HTGH4 L167R V300C to get the assignment of the cysteine at position 300 (V300C$^{6.27}$). Due to the fact, that the TM86V has one cysteine more than the HTGH4, I compared the ^{13}C-methyl tagged TM86V L167R V300C to the ^{13}C-methyl tagged HTGH4 L167R V300C. This gave me the final assignment needed, for the TM86V specific cysteine 332 (see Figure A.8).

With the assignments for the ^{1}H-^{13}C methyl groups from the ^{13}C-MMTS tagging now obtained, I measured a methyl-TROSY NMR for each NTR1 variant. Thereby each variant was also measured in an agonist bound (NT1) active state as well as in an antagonist bound (SR-142948) inactive state. For all labeled cysteines, two peaks were visible, each representing one state. In my nomenclature I used the asterisk to denominate the peak corresponding to the presumed active state. The cysteine at position 386 did not change for any NTR1 variant or ligand state and was there for used as a reference, i.e. for the analysis of the peak heights. It is also the only cysteine without a corresponding peak for the presumed active state. In order to visualize the populations for each peak, I also display the relative peak height for each pair of inactive and active state peaks. The resulting spectra and their peak height analysis are shown in Figure A.9 to Figure A.15. A comparison of all spectra can be seen in Figure A.16.

There by a comparison of all investigated NTR1 variants respective to their peak height is shown. The top graph is a comparison of agonist bound NTR1 variants, whereas the bottom graph is a comparison of antagonist bound NTR1 variants. All peak heights are normalized relative to C386 (therefor C386 = 1.00). The top graph shows that HTGH4 L167R V300C D124E as well as TM86V L167R V300C show the most populated ground states in the agonist bound state. Opposite to these tendencies, HTGH4 L167R V300C E150D shows the most populated active states in the agonist bound state. The other observed NTR1 variants are found between those two extremes. For the antagonist bound state, similar results are obtained. The most populated active state is detected for the NT1 bound state of HTGH4 L167R V300C E150D. The HTGH4 L167R V300C D124E variant shows the least populated active states in the antagonist bound form. A general tendency is that the other NTR1 variants vary more in the antagonist bound state compared to the agonist bound form.
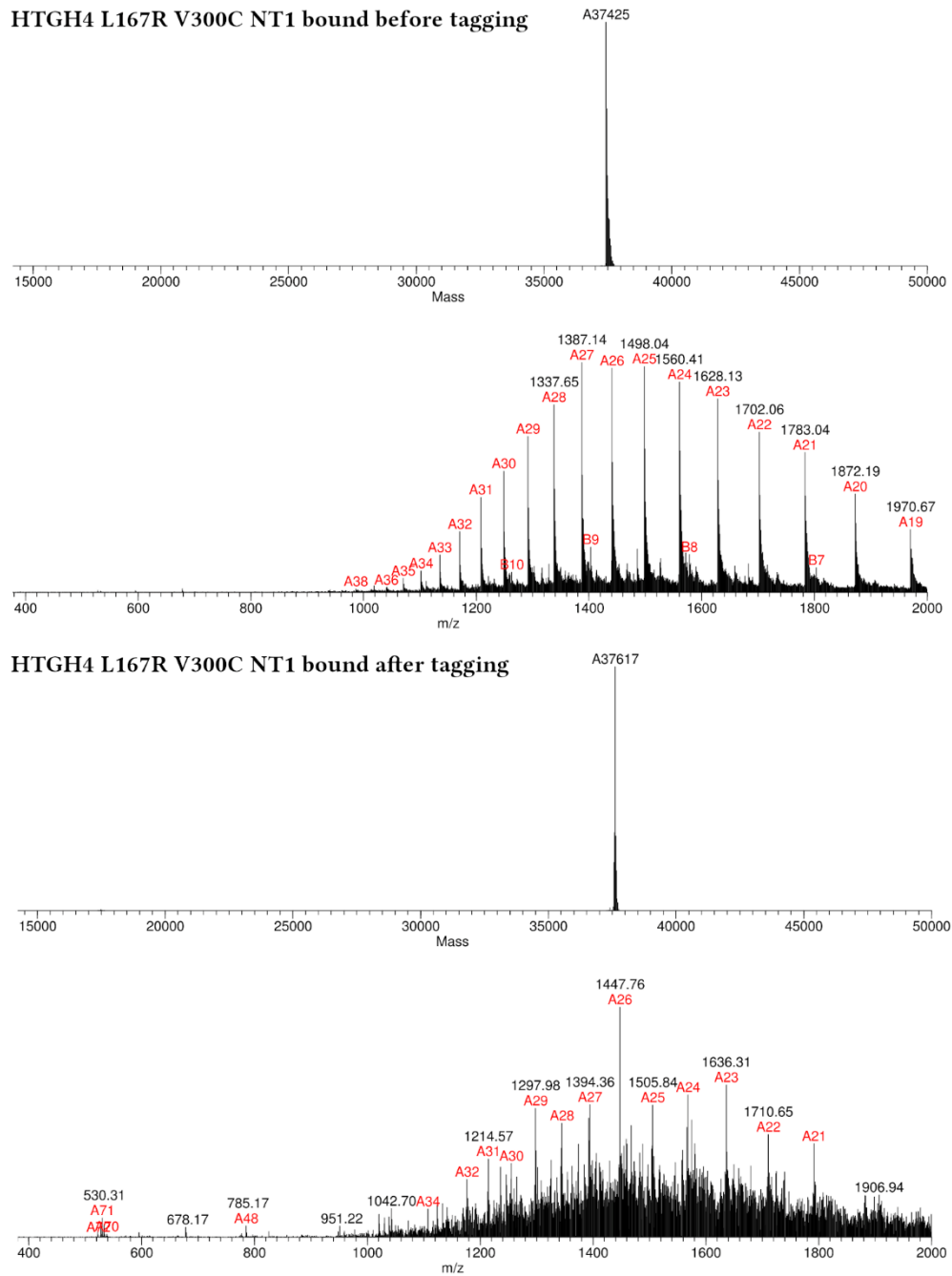
Figure A.4: Exemplary ESI-MS to verify NTR1 tagging
This is an exemplary ESI-MS data set, which have been used to verify complete MMTS tagging of the NTR1 variants. The molecular weight difference of the NTR1 variant (HTGH4 L167R V300C) which is tagged (37617 Da) and the one which is not tagged (37425 Da) is 192 Da. Each tag has a molecular weight of 48 Da ($S^{13}CH_3$). As 4 cysteines are accessible for tagging, complete tagging was proven (4 tags à 48 Da equals 192 Da)
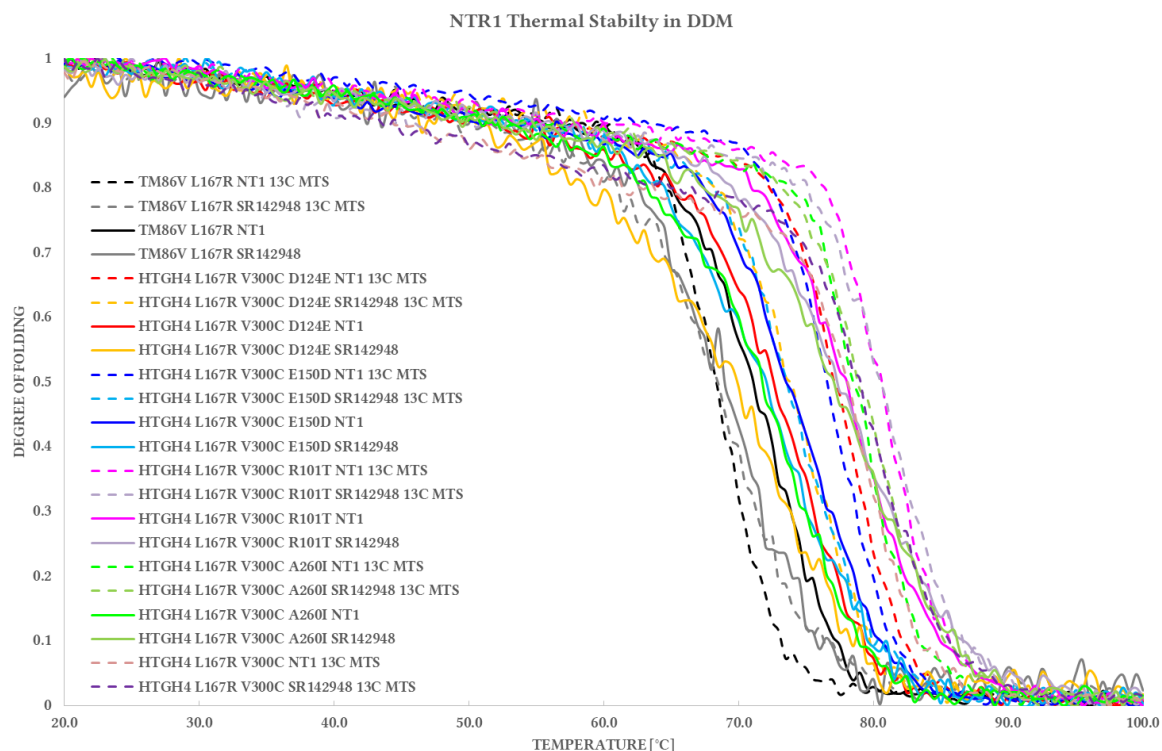
NTR1 Thermal Stabilty in DDM

Figure A.5: CD thermal melting curves of all the HTGH4 L167R V300C back mutation variants in DDM
All thermal melting curves recorded via CD spectroscopy of all newly generated NTR1 variants for the MMTS tagging are shown in this overlay. For each construct, 4 thermal melting curves were recorded, with and without tag as well as in NT1 and SR142948 bound state. The dashed lines show the tagged constructs, whereas the solid lines show the untagged constructs. Two observations can be directly made: tagged constructs are on average more stable than the untagged counterparts and the TM86V variants are less stable than the HTGH4 variants

Table A.1. List of melting termperatures obtained via CD spectroscopy

NTR1 Variant	NT1 + ^{13}C MTS	SR142948 + ^{13}C MTS	NT1	SR142948
HTGH4 L167R V300C	78 °C	79 °C	n/a	n/a
HTGH4 L167R V300C D124E	77 °C	74 °C	73 °C	70 °C
HTGH4 L167R V300C E150D	77 °C	74 °C	74 °C	72 °C
HTGH4 L167R V300C R101T	81 °C	81 °C	78 °C	77 °C
HTGH4 L167R V300C A260I	79 °C	79 °C	72 °C	77 °C
TM86V L167R	68 °C	68 °C	71 °C	69 °C
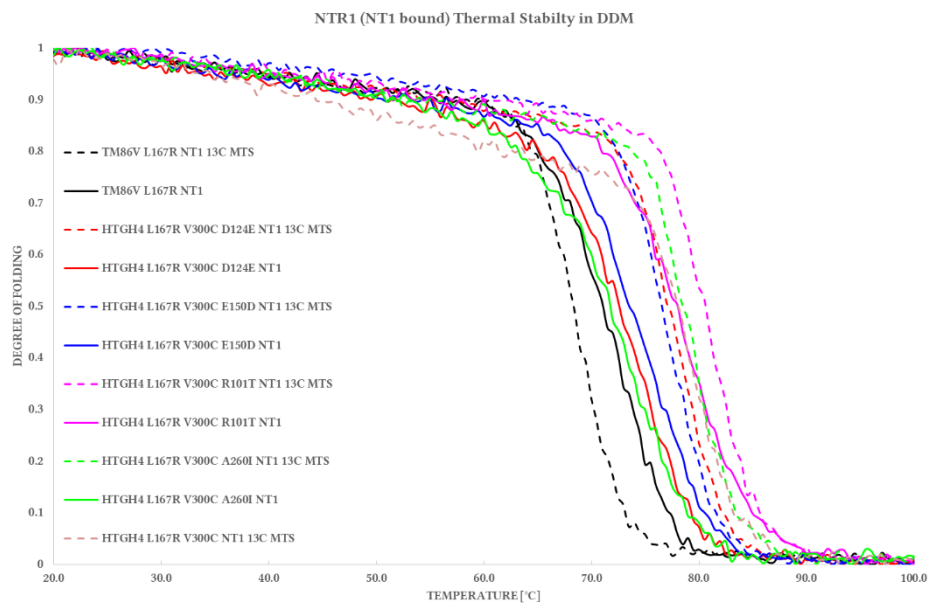
Figure A.6: CD thermal melting curves of the HTGH4 L167R V300C back mutation variants bound to NT1 in DDM
The thermal melting curves recorded via CD spectroscopy of NT1 bound NTR1 variants for the MMTS tagging are here overlaid. To simplify the analysis of the melting curves from Figure A.5, only 2 thermal melting curves are shown per construct: with and without tag. The dashed lines show the tagged constructs, whereas the solid lines show the untagged constructs. For the HTGH4 variants, the tagged constructs are on more stable than the untagged counterparts. In the case of TM86V the tagged variant is less stable than the untagged one. All untagged variants have a similar melting point except for the R101T variant, which shows increased stability. For this construct the tagged version is the most stable, too.
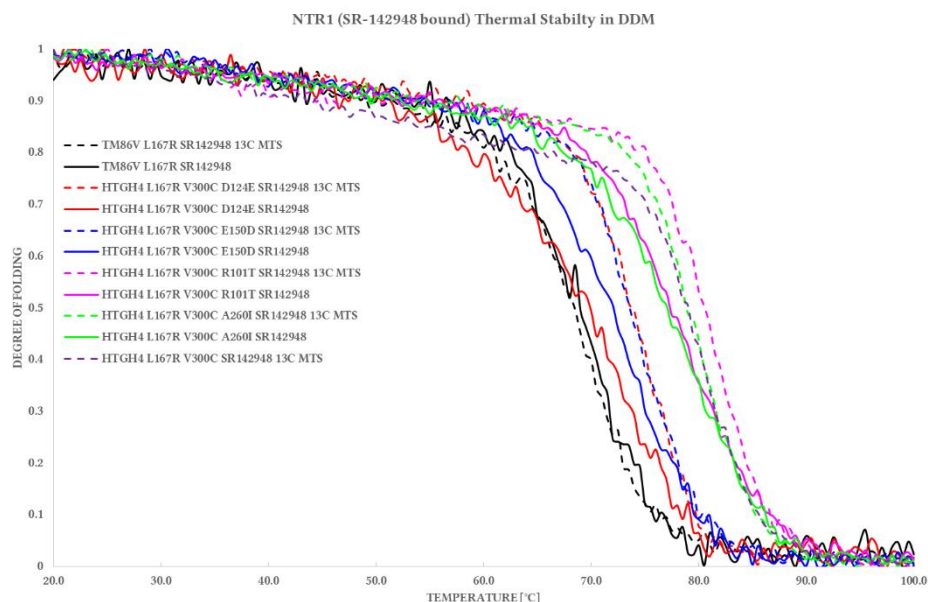
Figure A.7: CD thermal melting curves of the HTGH4 L167R V300C back mutation variants bound to SR-142948 in DDM
The thermal melting curves recorded via CD spectroscopy of SR142948 bound NTR1 variants for the MMTS tagging are here overlaid. To simplify the analysis of the melting curves from Figure A.5, only 2 thermal melting curves are shown per construct: with and without tag. The dashed lines show the tagged constructs, whereas the solid lines show the untagged constructs. For the HTGH4 variants, the tagged constructs are on more stable than the untagged counterparts. In the case of TM86V the tagged variant is less stable than the untagged one. All untagged variants have a similar melting point except for the R101T and the A260I variant, which show increased stability. For both of these constructs the tagged version is also more stable.
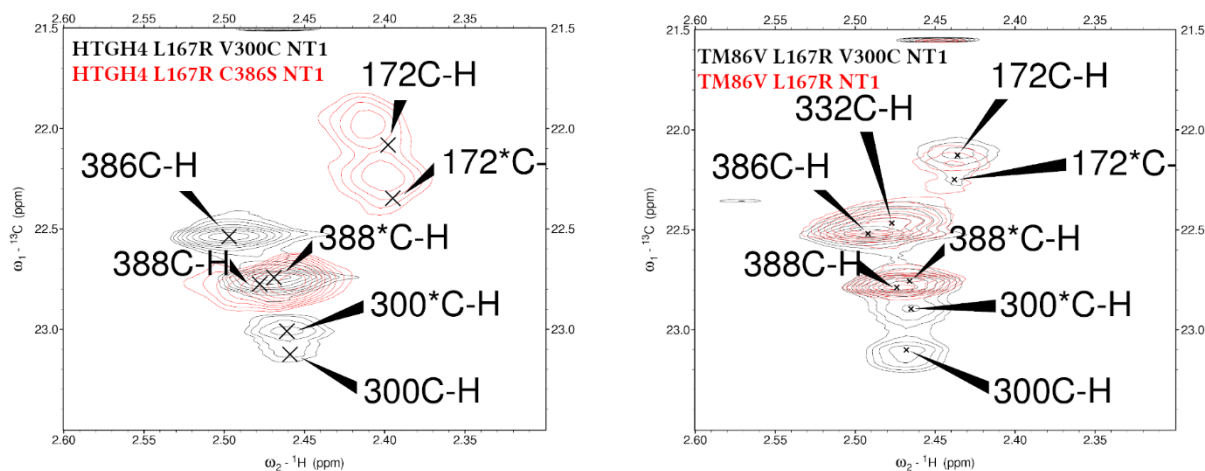
Figure A.8: ^{13}C-MMTS assignment spectra

These are the spectra which were used to assign all cysteines which could be tagged. On the left side, an overlay of HTGH4 L167R V300C (black) and HTGH4 L167R C386S (red) is shown. The peaks are always centered according to the reference spectrum in black. Peaks which are labeled with an asterisk correspond to an active conformation, whereas the ones without correspond to the ground state (assignment of inactive ground state peaks was done with the HTGH4 wt peaks (see Figure A.9)) as HTGH4 wt shows no signaling activity at all. It can be seen that 2 peaks are missing in the red spectrum as the V300C mutation is not present in this NTR1 variant and additionally the C386 is mutated to serine. For the C386, in all spectra only one peak is present, showing that it is completely unaffected by the conformational state of the NTR1. Therefor it is used as reference peak in all spectra. On the right side, TM86V L167R V300C (black) and TM86V L167R (red) are overlaid. With this experiment, the assignment of the 300C could be confirmed. Additionally, the C332 could be assigned, as this cysteine is only present in TM86V but not in HTGH4.
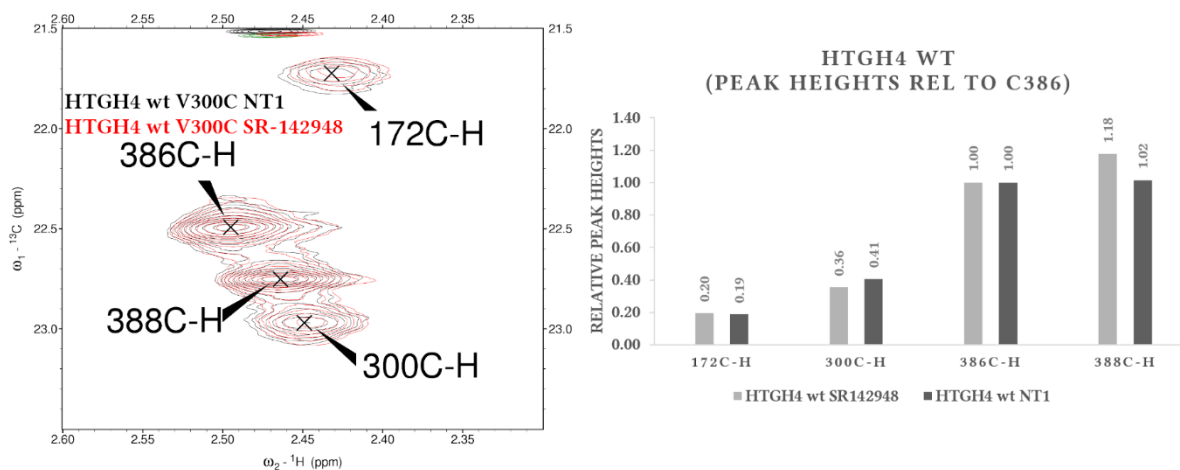
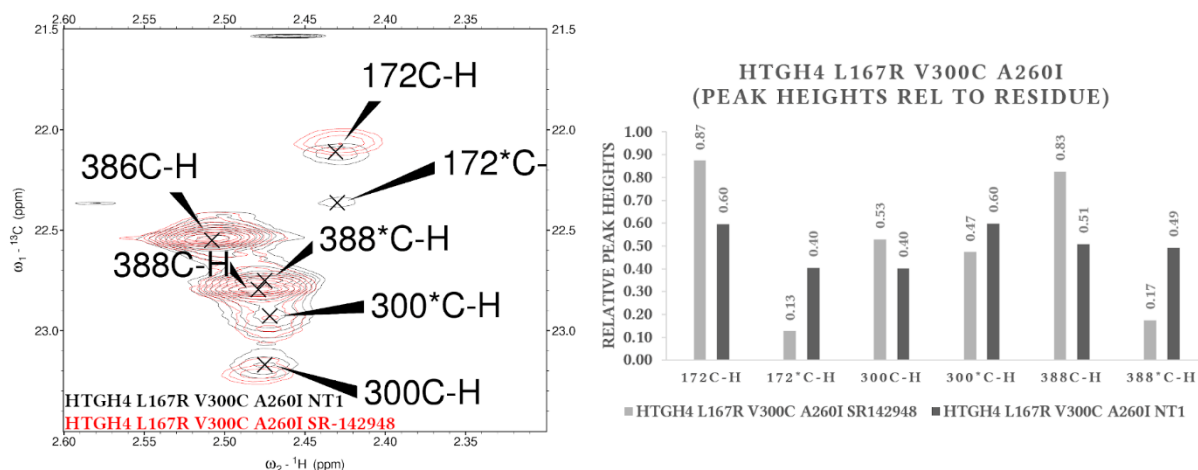*Figure A.9: ^{13}C-MMTS tagged HTGH4 wt V300C*

These are the spectra comparing HTGH4 wt V300C with different ligands. On the left side, an overlay of HTGH4 wt V300C NT1 (black) and HTGH4 wt V300C SR-142948 (red) is shown. The peaks are labeled as explained in Figure A.8. It can be seen that both spectra are identical in their peak shifts as well as peak heights. On the right side, the peak heights of the spectra shown in the left are displayed as bar diagram. They are normalized relative to C386 (therefor C386 = 1.00). Both graphical representations show that only ground state is present and that the populations are independent on the ligand state of this NTR1 variant.
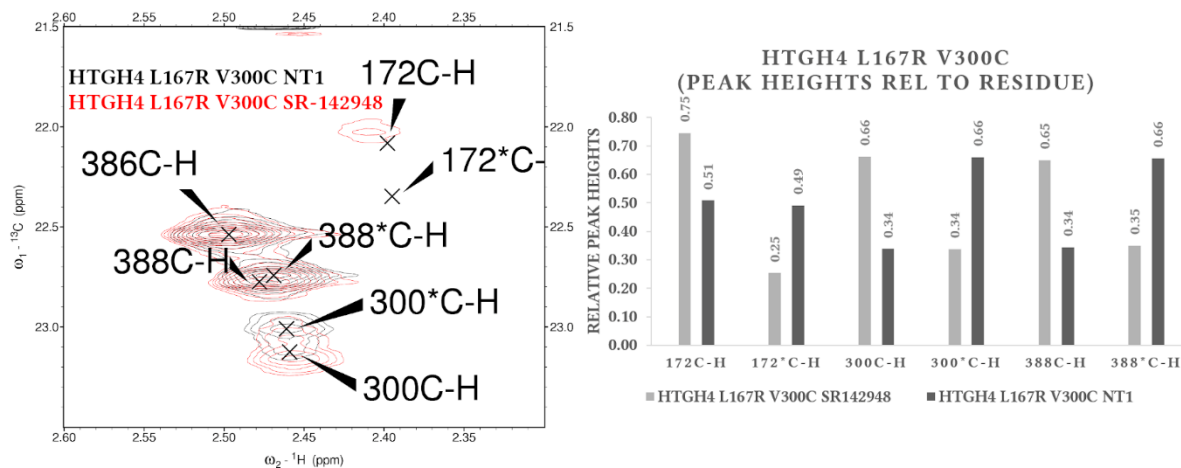
Figure A.10: ¹³C-MMTS tagged HTGH4 L167R V300C
These are the spectra comparing HTGH4 L167R V300C with different ligands. On the left side, an overlay of HTGH4 L167R
V300C NT1 (black) and HTGH4 L167R V300C SR-142948 (red) is shown. The peaks are labeled as explained in Figure A.8. It can
be seen that both spectra have different peak heights for all peaks except the constant C386 peak. On the right side, the peak
heights of the spectra shown in the left are displayed as bar diagram. They are normalized relative to C386 (therefor C386 =
1.00). Both graphical representations show that in the antagonist bound state the ground state peaks are more pronounced than
the active state peaks. If the HTGH4 L167R V300C is bound to the agonist NT1, the populations are populated inverse to the
*antagonist bound state, with the active state being more populated.*
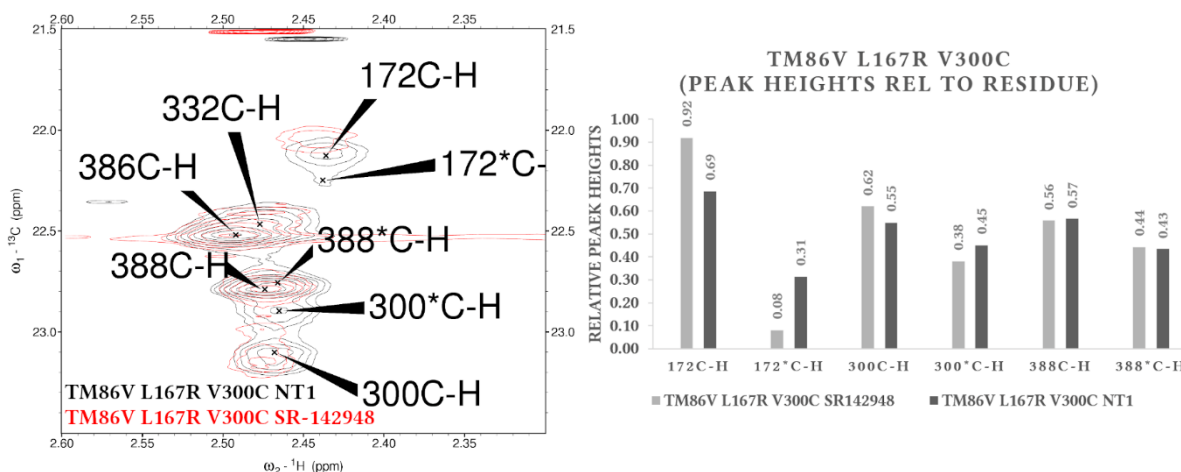
Figure A.11: ¹³C-MMTS tagged TM86V L167R V300C
These are the spectra comparing TM86V L167R V300C with different ligands. On the left side, an overlay of TM86V L167R
V300C NT1 (black) and TM86V L167R V300C SR-142948 (red) is shown. The peaks are labeled as explained in Figure A.8. It can
be seen that both spectra have different peak heights for all peaks except the constant C386 peak. On the right side, the peak
heights of the spectra shown in the left are displayed as bar diagram. They are normalized relative to C386 (therefor C386 =
1.00). In contrast to the HTGH4 L167R V300C variants (Figure A.10), the differences are not as strongly pronounced in the
populations. Still both graphical representations show that in the antagonist bound state the ground state peaks are more
pronounced than the active state peaks. If the TM86V L167R V300C is bound to the agonist NT1, the populations are populated
*inverse to the antagonist bound state, with the active state being more populated. The peak corresponding to C388 as well as the*
TM86V specific peak corresponding to C332 are not affected by the different ligands.

64

Figure A.12: ^{13}C-MMTS tagged HTGH4 L167R V300C A260I

These are the spectra comparing HTGH4 L167R V300C A260I with different ligands. On the left side, an overlay of HTGH4 L167R V300C A260I NT1 (black) and HTGH4 L167R V300C A260I SR-142948 (red) is shown. The peaks are labeled as explained in Figure A.8. It can be seen that both spectra have different peak heights for all peaks except the constant C386 peak. On the right side, the peak heights of the spectra shown in the left are displayed as bar diagram. They are normalized relative to C386 (therefor C386 = 1.00). Both graphical representations show that in the antagonist bound state the ground state peaks are more pronounced than the active state peaks. If the HTGH4 L167R V300C A260I is bound to the agonist NT1, the populations are populated inverse to the antagonist bound state, with the active state being more populated.
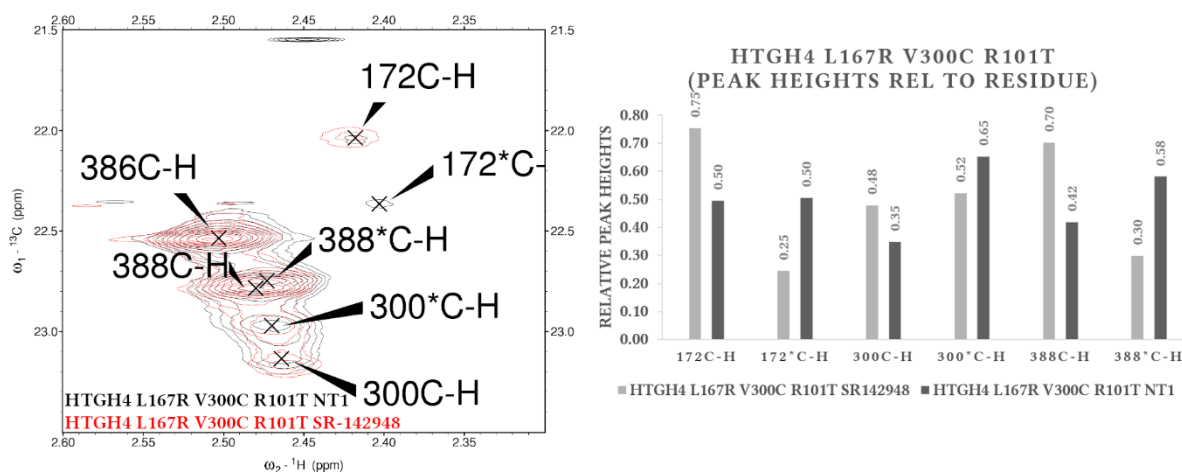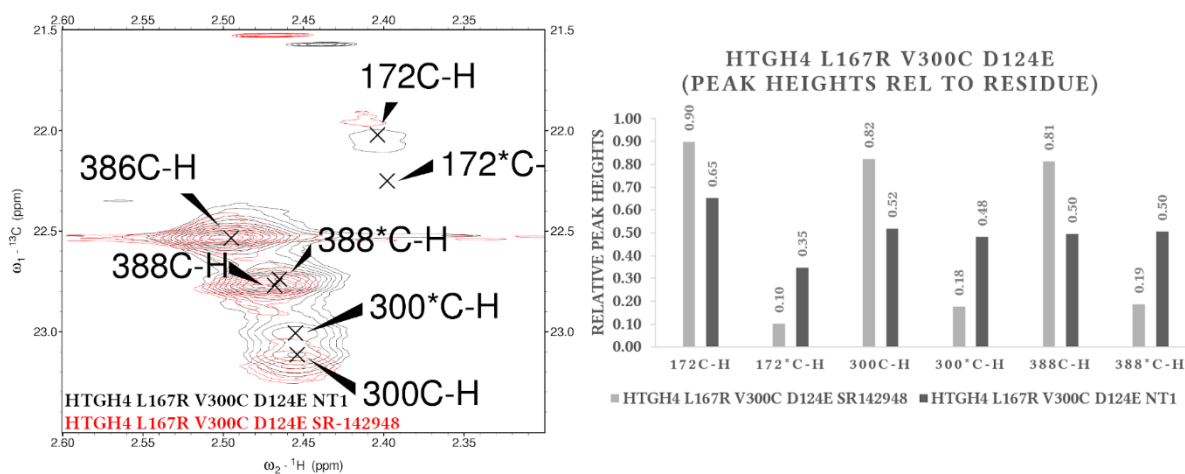

Figure A.13: ^{13}C-MMTS tagged HTGH4 L167R V300C R101T

These are the spectra comparing HTGH4 L167R V300C R101T with different ligands. On the left side, an overlay of HTGH4 L167R V300C R101T NT1 (black) and HTGH4 L167R V300C R101T SR-142948 (red) is shown. The peaks are labeled as explained in Figure A.8. It can be seen that both spectra have different peak heights for all peaks except the constant C386 peak. On the right side, the peak heights of the spectra shown in the left are displayed as bar diagram. They are normalized relative to C386 (therefor C386 = 1.00). Both graphical representations show that in the antagonist bound state the ground state peaks are more pronounced than the active state peaks. If the HTGH4 L167R V300C R101T is bound to the agonist NT1, the populations are populated inverse to the antagonist bound state, with the active state being more populated.
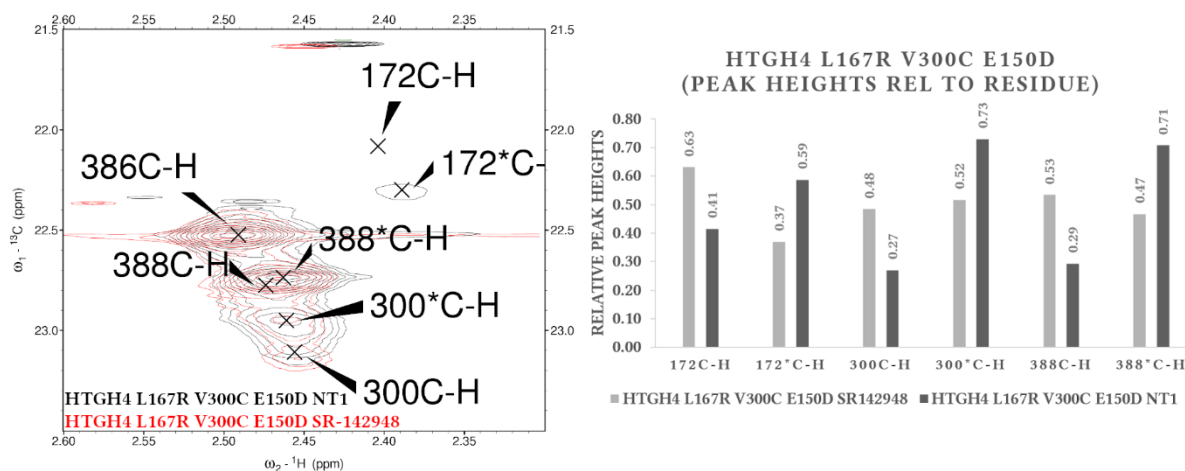
Figure A.14: ^{13}C-MMTS tagged HTGH4 L167R V300C E150D

These are the spectra comparing HTGH4 L167R V300C E150D with different ligands. On the left side, an overlay of HTGH4 L167R V300C E150D NT1 (black) and HTGH4 L167R V300C E150D SR-142948 (red) is shown. The peaks are labeled as explained in Figure A.8. It can be seen that both spectra have different peak heights for all peaks except the constant C386 peak. On the right side, the peak heights of the spectra shown in the left are displayed as bar diagram. They are normalized relative to C386 (therefor C386 = 1.00). Both graphical representations show that in the antagonist bound state the ground state peaks are more pronounced than the active state peaks. If the HTGH4 L167R V300C E150D is bound to the agonist NT1, the populations are populated inverse to the antagonist bound state, with the active state being more populated.

Figure A.15: ^{13}C-MMTS tagged HTGH4 L167R V300C D124E

These are the spectra comparing HTGH4 L167R V300C D124E with different ligands. On the left side, an overlay of HTGH4 L167R V300C D124E NT1 (black) and HTGH4 L167R V300C D124E SR-142948 (red) is shown. The peaks are labeled as explained in Figure A.8. It can be seen that both spectra have different peak heights for all peaks except the constant C386 peak. On the right side, the peak heights of the spectra shown in the left are displayed as bar diagram. They are normalized relative to C386 (therefor C386 = 1.00). Both graphical representations show that in the antagonist bound state the ground state peaks are more pronounced than the active state peaks. If the HTGH4 L167R V300C D124E is bound to the agonist NT1, the populations are populated inverse to the antagonist bound state, with the active state being more populated.

Figure A.16: Comparison ^{13}C-MMTS tagged NTR1 variant peak heights

In this figure we see the comparison of all investigated NTR1 variants respective to their peak height. The top graph is a comparison of agonist bound NTR1 variants, whereas the bottom graph is a comparison of antagonist bound NTR1 variants. The peaks are labeled as explained in Figure A.8. They are normalized relative to C386 (therefor C386 = 1.00). The top graph shows that HTGH4 L167R V300C D124E as well as TM86V L167R V300C show the most populated ground states in the agonist bound state. In contrast to this, HTGH4 L167R V300C E150D shows the most populated active states in the agonist bound state. The other NTR1 variants are between those two extremes. A comparable tendency can also be observed in the antagonist bound state. HTGH4 L167R V300C E150D is like in the NT1 bound state the one with the biggest population of the active state. And also the HTGH4 L167R V300C D124E variant shows the least populated active states in the antagonist bound form. But the other NTR1 variants vary more in the antagonist bound state compared to the agonist bound form.

b. Material

Reagent	Manufacturer
L-Alanine-3-^{13}C, 2-d	Sigma-Aldrich
Ammonium-^{15}N chloride	Sigma-Aldrich
CHAPS (3-[(3-cholamidopropyl)dimethylammonio]-1-propanesulfonate)	Sigma-Aldrich
Cholesteryl hemisuccinate	Sigma-Aldrich
Deuterium chloride solution	Sigma-Aldrich
DM (n-Decyl-β-D-Maltopyranoside)	Cube Biotech
d_{26}-DH7PC (1,2-Diheptanoyl-sn-glycero-3-phosphocholine)	FB Reagents
DDM (n-Dodecyl β-D-maltoside)	Cube Biotech
D-Glucose-1,2,3,4,5,6,6-d_7	Sigma-Aldrich
2-Keto-3-(methyl-d_3)-butyric acid-4-^{13}C	FB Reagents
2-Ketobutyric acid-4-^{13}C,3-d	FB Reagents
^{13}C-MMTS (S-Methyl-^{13}C methanethiosulfonate)	Sigma-Aldrich
NEB® Express Iq Competent E. coli (High Efficiency)	NEB
NHS-Activated Sepharose 4 Fast Flow	GE Healthcare
QuikChange Lightning Site-Directed Mutagenesis Kit, 10 Rxn	Agilent
Sodium deuteroxide solution	Sigma-Aldrich
SR 142948	Tocris
SR 48692	Sigma-Aldrich
Succinic acid-2,2,3,3-d_4	Sigma-Aldrich

c. List of Figures

d.   List of Tables

e.   List of Abbreviations

AA	Amino acid
AHD	α-helical domain
ApoA1	Apolipoprotein A1
CD	Circular dichroism
cGMP	Cyclic guanosine monophosphat
CHAPS	3-[(3-cholamidopropyl)dimethylammonio]-1-propanesulfonate
CHS	Cholesteryl hemisuccinate
cMSP	Circularized membrane scaffold protein
CNS	Central nervous system
CPMG	Carr-Purcell-Meiboom-Gill
cryo-EM	Cryo electron microscopy
DDM	n-Dodecyl β-D-maltoside
DEER	Double electron-electron resonance
DH$_7$PC	1,2-diheptanoyl-sn-glycero-3-phosphocholine
DM	n-Decyl β-D-maltoside
DMPC	1,2-dimyristoyl-sn-glycero-3-phosphocholine
DMPG	1,2-dimyristoyl-sn-glycero-3-phosphoglycerol
DMSO	Dimethyl sulfoxide
DSS	Sodium trimethylsilylpropane-sulfonate
DTT	Dithiothreitol
dYT	Double yeast tryptone
E. coli	*Escherichia coli*
EDTA	Ethylenediaminetetraacetic acid
ESI-MS	Electrospray ionization mass spectrometry
FDA	US Food and Drug Administration
FRET	Förster resonance energy transfer
GABA	γ-amino butyric acid
GB1	Immunoglobulin-binding protein G domain B1
GDP	Guanosine diphosphate
GPCR	G-Protein-coupled-receptor
GTP	Guanosine triphosphate
Gα	G protein α subunit
HDL	High density lipoprotein
HEPES	4-(2-hydroxyethyl)-1-piperazineethanesulfonic acid
hIAPP	Human islet amyloid polypeptide
HMQC	Heteronuclear multi quantum coherence
HRV	Human rhinovirus
HSQC	Heteronuclear single quantum coherence

IC	Intracellular
ILVA	Isoleucin, Leucin, Valin and Alanin
INEPT	Insensitive nuclei enhanced by polarization transfer
IPTG	Isopropyl-β-D-Thiogalactopyranoside
MANT	N-Methylanthraniloyl
MBP	Maltose binding protein
MD	Molecular dynamics
β-ME	β-mercaptoethanol
MMTS	S-Methyl-methanethiosulfonate
MSP	Membrane scaffold protein
MW	Molecular weight
ND	Nanodisc
NMR	Nuclear magnetic resonance
NT1	Neurotensin
NTR1	Neurotensin receptor 1
OD600	Optical density at 600 nm
OmpX	Bacterial outer membrane protein X
PCR	Polymerase chain reaction
POPC	1-palmitoyl-2-oleoyl-sn-glycero-3-phosphocholine
RD	Relaxation dispersion
RDC	Residual dipolar coupling
SEC	Size exclusion chromatography
SP	Sulphopropyl
T4L	T4 lysozyme
τc	Correlation time
TEV	Tobacco etch virus
TM	Transmembrane
TROSY	Transverse relaxation-optimized spectroscopy
TrxA	Thioredoxin A
VDAC1	Human voltage-dependent anion channel subtype 1

Bibliography

Alexander, S.P., Christopoulos, A., Davenport, A.P., Kelly, E., Marrion, N.V., Peters, J.A., Faccenda, E., Harding, S.D., Pawson, A.J., Sharman, J.L., *et al.* (2017). THE CONCISE GUIDE TO PHARMACOLOGY 2017/18: G protein-coupled receptors. British journal of pharmacology *174 Suppl 1*, S17-S129.

Ballesteros, J.A., Jensen, A.D., Liapakis, G., Rasmussen, S.G., Shi, L., Gether, U., and Javitch, J.A. (2001). Activation of the beta 2-adrenergic receptor involves disruption of an ionic lock between the cytoplasmic ends of transmembrane segments 3 and 6. The Journal of biological chemistry *276*, 29171-29177.

Ballesteros, J.A., and Weinstein, H. (1995). [19] Integrated methods for the construction of three-dimensional models and computational probing of structure-function relations in G protein-coupled receptors. In Methods in Neurosciences, S.C. Sealfon, ed. (Academic Press), pp. 366-428.

Bayburt, T.H., Grinkova, Y.V., and Sligar, S.G. (2002). Self-Assembly of Discoidal Phospholipid Bilayer Nanoparticles with Membrane Scaffold Proteins. Nano letters *2*, 853-856.

Bayburt, T.H., and Sligar, S.G. (2010). Membrane protein assembly into Nanodiscs. FEBS letters *584*, 1721-1727.

Besserer-Offroy, E., Brouillette, R.L., Lavenus, S., Froehlich, U., Brumwell, A., Murza, A., Longpre, J.M., Marsault, E., Grandbois, M., Sarret, P., *et al.* (2017). The signaling signature of the neurotensin type 1 receptor with endogenous ligands. European journal of pharmacology *805*, 1-13.

Beychok, S. (1966). Circular dichroism of biological macromolecules. Science *154*, 1288-1299.

Bibow, S., Polyhach, Y., Eichmann, C., Chi, C.N., Kowal, J., Albiez, S., McLeod, R.A., Stahlberg, H., Jeschke, G., Guntert, P., *et al.* (2017). Solution structure of discoidal high-density lipoprotein particles with a shortened apolipoprotein A-I. Nature structural & molecular biology *24*, 187-193.

Bostock, M.J., Solt, A.S., and Nietlispach, D. (2019). The role of NMR spectroscopy in mapping the conformational landscape of GPCRs. Current opinion in structural biology *57*, 145-156.

Boules, M., Li, Z., Smith, K., Fredrickson, P., and Richelson, E. (2013). Diverse roles of neurotensin agonists in the central nervous system. Frontiers in endocrinology *4*, 36.

Brouillette, C.G., Anantharamaiah, G.M., Engler, J.A., and Borhani, D.W. (2001). Structural models of human apolipoprotein A-I: a critical analysis and review. Biochimica et biophysica acta *1531*, 4-46.

Carpenter, B., Nehme, R., Warne, T., Leslie, A.G., and Tate, C.G. (2016). Structure of the adenosine A(2A) receptor bound to an engineered G protein. Nature *536*, 104-107.

Carpenter, B., and Tate, C.G. (2016). Engineering a minimal G protein to facilitate crystallisation of G protein-coupled receptors in their active conformation. Protein engineering, design & selection : PEDS *29*, 583-594.

Casiraghi, M., Point, E., Pozza, A., Moncoq, K., Baneres, J.L., and Catoire, L.J. (2019). NMR analysis of GPCR conformational landscapes and dynamics. Molecular and cellular endocrinology *484*, 69-77.

Cherezov, V., Rosenbaum, D.M., Hanson, M.A., Rasmussen, S.G., Thian, F.S., Kobilka, T.S., Choi, H.J., Kuhn, P., Weis, W.I., Kobilka, B.K.*, et al.* (2007). High-resolution crystal structure of an engineered human beta2-adrenergic G protein-coupled receptor. Science *318*, 1258-1265.

Coleman, D.E., Berghuis, A.M., Lee, E., Linder, M.E., Gilman, A.G., and Sprang, S.R. (1994). Structures of active conformations of Gi alpha 1 and the mechanism of GTP hydrolysis. Science *265*, 1405-1412.

Day, P.W., Rasmussen, S.G., Parnot, C., Fung, J.J., Masood, A., Kobilka, T.S., Yao, X.J., Choi, H.J., Weis, W.I., Rohrer, D.K.*, et al.* (2007). A monoclonal antibody for G protein-coupled receptor crystallography. Nature methods *4*, 927-929.

Denisov, I.G., and Sligar, S.G. (2016). Nanodiscs for structural and functional studies of membrane proteins. Nature structural & molecular biology *23*, 481-486.

74

Denisov, I.G., and Sligar, S.G. (2017). Nanodiscs in Membrane Biochemistry and Biophysics. Chemical reviews *117*, 4669-4713.

Downes, G.B., and Gautam, N. (1999). The G protein subunit gene families. Genomics *62*, 544-552.

Draper-Joyce, C.J., Khoshouei, M., Thal, D.M., Liang, Y.L., Nguyen, A.T.N., Furness, S.G.B., Venugopal, H., Baltos, J.A., Plitzko, J.M., Danev, R.*, et al.* (2018). Structure of the adenosine-bound human adenosine A1 receptor-Gi complex. Nature *558*, 559-563.

Dror, R.O., Arlow, D.H., Borhani, D.W., Jensen, M.O., Piana, S., and Shaw, D.E. (2009). Identification of two distinct inactive conformations of the beta2-adrenergic receptor reconciles structural and biochemical observations. Proceedings of the National Academy of Sciences of the United States of America *106*, 4689-4694.

Dror, R.O., Mildorf, T.J., Hilger, D., Manglik, A., Borhani, D.W., Arlow, D.H., Philippsen, A., Villanueva, N., Yang, Z., Lerch, M.T.*, et al.* (2015). SIGNAL TRANSDUCTION. Structural basis for nucleotide exchange in heterotrimeric G proteins. Science *348*, 1361-1365.

Eddy, M.T., Gao, Z.G., Mannes, P., Patel, N., Jacobson, K.A., Katritch, V., Stevens, R.C., and Wuthrich, K. (2018a). Extrinsic Tryptophans as NMR Probes of Allosteric Coupling in Membrane Proteins: Application to the A2A Adenosine Receptor. Journal of the American Chemical Society *140*, 8228-8235.

Eddy, M.T., Lee, M.Y., Gao, Z.G., White, K.L., Didenko, T., Horst, R., Audet, M., Stanczak, P., McClary, K.M., Han, G.W.*, et al.* (2018b). Allosteric Coupling of Drug Binding and Intracellular Signaling in the A2A Adenosine Receptor. Cell *172*, 68-80 e12.

Egloff, P., Deluigi, M., Heine, P., Balada, S., and Pluckthun, A. (2015). A cleavable ligand column for the rapid isolation of large quantities of homogeneous and functional neurotensin receptor 1 variants from E. coli. Protein expression and purification *108*, 106-114.

Egloff, P., Hillenbrand, M., Klenk, C., Batyuk, A., Heine, P., Balada, S., Schlinkmann, K.M., Scott, D.J., Schutz, M., and Pluckthun, A. (2014). Structure of signaling-competent neurotensin receptor 1 obtained by directed evolution in Escherichia coli. Proceedings of the National Academy of Sciences of the United States of America *111*, E655-662.

Flock, T., Ravarani, C.N.J., Sun, D., Venkatakrishnan, A.J., Kayikci, M., Tate, C.G., Veprintsev, D.B., and Babu, M.M. (2015). Universal allosteric mechanism for Galpha activation by GPCRs. Nature *524*, 173-179.

Förster, T. (1948). Zwischenmolekulare Energiewanderung und Fluoreszenz. Annalen der Physik *437*, 55-75.

Fredriksson, R., Lagerstrom, M.C., Lundin, L.G., and Schioth, H.B. (2003). The G-protein-coupled receptors in the human genome form five main families. Phylogenetic analysis, paralogon groups, and fingerprints. Molecular pharmacology *63*, 1256-1272.

Garcia-Nafria, J., Lee, Y., Bai, X., Carpenter, B., and Tate, C.G. (2018a). Cryo-EM structure of the adenosine A2A receptor coupled to an engineered heterotrimeric G protein. eLife *7*.

Garcia-Nafria, J., Nehme, R., Edwards, P.C., and Tate, C.G. (2018b). Cryo-EM structure of the serotonin 5-HT1B receptor coupled to heterotrimeric Go. Nature *558*, 620-623.

Gardner, K.H., and Kay, L.E. (1998). The use of 2H, 13C, 15N multidimensional NMR to study the structure and dynamics of proteins. Annual review of biophysics and biomolecular structure *27*, 357-406.

Gilman, A.G. (1987). G proteins: transducers of receptor-generated signals. Annual review of biochemistry *56*, 615-649.

Goricanec, D., and Hagn, F. (2019). NMR backbone and methyl resonance assignments of an inhibitory G-alpha subunit in complex with GDP. Biomolecular NMR assignments *13*, 131-137.

Goricanec, D., Stehle, R., Egloff, P., Grigoriu, S., Pluckthun, A., Wagner, G., and Hagn, F. (2016). Conformational dynamics of a G-protein alpha subunit is tightly regulated by nucleotide binding. Proceedings of the National Academy of Sciences of the United States of America *113*, E3629-3638.

Granier, S., Manglik, A., Kruse, A.C., Kobilka, T.S., Thian, F.S., Weis, W.I., and Kobilka, B.K. (2012). Structure of the delta-opioid receptor bound to naltrindole. Nature *485*, 400-404.

Greenfield, N., and Fasman, G.D. (1969). Computed circular dichroism spectra for the evaluation of protein conformation. Biochemistry *8*, 4108-4116.

Greenfield, N.J. (2006a). Using circular dichroism collected as a function of temperature to determine the thermodynamics of protein unfolding and binding interactions. Nature protocols *1*, 2527-2535.

Greenfield, N.J. (2006b). Using circular dichroism spectra to estimate protein secondary structure. Nature protocols *1*, 2876-2890.

Greentree, W.K., and Linder, M.E. (2004). Purification of recombinant G protein alpha subunits from Escherichia coli. Methods in molecular biology *237*, 3-20.

Gully, D., Canton, M., Boigegrain, R., Jeanjean, F., Molimard, J.C., Poncelet, M., Gueudet, C., Heaulme, M., Leyris, R., Brouard, A., *et al.* (1993). Biochemical and pharmacological profile of a potent and selective nonpeptide antagonist of the neurotensin receptor. Proceedings of the National Academy of Sciences of the United States of America *90*, 65-69.

Hagn, F., Etzkorn, M., Raschle, T., and Wagner, G. (2013). Optimized phospholipid bilayer nanodiscs facilitate high-resolution structure determination of membrane proteins. Journal of the American Chemical Society *135*, 1919-1925.

Hagn, F., Nasr, M.L., and Wagner, G. (2018). Assembly of phospholipid nanodiscs of controlled size for structural studies of membrane proteins by NMR. Nature protocols *13*, 79-98.

Hauser, A.S., Attwood, M.M., Rask-Andersen, M., Schioth, H.B., and Gloriam, D.E. (2017). Trends in GPCR drug discovery: new agents, targets and indications. Nature reviews Drug discovery *16*, 829-842.

Holzwarth, G., and Doty, P. (1965). The Ultraviolet Circular Dichroism of Polypeptides. Journal of the American Chemical Society *87*, 218-228.

Horst, R., Liu, J.J., Stevens, R.C., and Wuthrich, K. (2013). beta(2)-adrenergic receptor activation by agonists studied with (1)(9)F NMR spectroscopy. Angewandte Chemie *52*, 10762-10765.

Huang, W., Manglik, A., Venkatakrishnan, A.J., Laeremans, T., Feinberg, E.N., Sanborn, A.L., Kato, H.E., Livingston, K.E., Thorsen, T.S., Kling, R.C., *et al.* (2015). Structural insights into micro-opioid receptor activation. Nature *524*, 315-321.

Isogai, S., Deupi, X., Opitz, C., Heydenreich, F.M., Tsai, C.J., Brueckner, F., Schertler, G.F., Veprintsev, D.B., and Grzesiek, S. (2016). Backbone NMR reveals allosteric signal transduction networks in the beta1-adrenergic receptor. Nature *530*, 237-241.

Kang, Y., Kuybeda, O., de Waal, P.W., Mukherjee, S., Van Eps, N., Dutka, P., Zhou, X.E., Bartesaghi, A., Erramilli, S., Morizumi, T., *et al.* (2018). Cryo-EM structure of human rhodopsin bound to an inhibitory G protein. Nature *558*, 553-558.

Kato, H.E., Zhang, Y., Hu, H., Suomivuori, C.M., Kadji, F.M.N., Aoki, J., Krishna Kumar, K., Fonseca, R., Hilger, D., Huang, W., *et al.* (2019). Conformational transitions of a neurotensin receptor 1-Gi1 complex. Nature *572*, 80-85.

Kenakin, T. (2011). Functional selectivity and biased receptor signaling. The Journal of pharmacology and experimental therapeutics *336*, 296-302.

Kenakin, T. (2013). New concepts in pharmacological efficacy at 7TM receptors: IUPHAR review 2. British journal of pharmacology *168*, 554-575.

Khan, S.M., Sleno, R., Gora, S., Zylbergold, P., Laverdure, J.P., Labbe, J.C., Miller, G.J., and Hebert, T.E. (2013). The expanding roles of Gbetagamma subunits in G protein-coupled receptor signaling and drug action. Pharmacological reviews *65*, 545-577.

Kitabgi, P. (2002). Targeting neurotensin receptors with agonists and antagonists for therapeutic purposes. Current opinion in drug discovery & development *5*, 764-776.

Klopfer, K., and Hagn, F. (2019). Beyond detergent micelles: The advantages and applications of non-micellar and lipid-based membrane mimetics for solution-state NMR. Prog Nucl Magn Reson Spectrosc *114-115*, 271-283.

Koehl, A., Hu, H., Maeda, S., Zhang, Y., Qu, Q., Paggi, J.M., Latorraca, N.R., Hilger, D., Dawson, R., Matile, H., *et al.* (2018). Structure of the micro-opioid receptor-Gi protein complex. Nature *558*, 547-552.

Kofuku, Y., Ueda, T., Okude, J., Shiraishi, Y., Kondo, K., Mizumura, T., Suzuki, S., and Shimada, I. (2014). Functional dynamics of deuterated beta2 -adrenergic receptor in lipid bilayers revealed by NMR spectroscopy. Angewandte Chemie *53*, 13376-13379.

Krishna Kumar, K., Shalev-Benami, M., Robertson, M.J., Hu, H., Banister, S.D., Hollingsworth, S.A., Latorraca, N.R., Kato, H.E., Hilger, D., Maeda, S.*, et al.* (2019). Structure of a Signaling Cannabinoid Receptor 1-G Protein Complex. Cell *176*, 448-458 e412.

Kruse, A.C., Hu, J., Pan, A.C., Arlow, D.H., Rosenbaum, D.M., Rosemond, E., Green, H.F., Liu, T., Chae, P.S., Dror, R.O.*, et al.* (2012). Structure and dynamics of the M3 muscarinic acetylcholine receptor. Nature *482*, 552-556.

Kruse, A.C., Ring, A.M., Manglik, A., Hu, J., Hu, K., Eitel, K., Hubner, H., Pardon, E., Valant, C., Sexton, P.M.*, et al.* (2013). Activation and allosteric modulation of a muscarinic acetylcholine receptor. Nature *504*, 101-106.

Lakowicz, J.R. (2013). Principles of Fluorescence Spectroscopy.

Latorraca, N.R., Venkatakrishnan, A.J., and Dror, R.O. (2017). GPCR Dynamics: Structures in Motion. Chemical reviews *117*, 139-155.

Lee, W., Tonelli, M., and Markley, J.L. (2015). NMRFAM-SPARKY: enhanced software for biomolecular NMR spectroscopy. Bioinformatics *31*, 1325-1327.

Liang, Y.L., Khoshouei, M., Radjainia, M., Zhang, Y., Glukhova, A., Tarrasch, J., Thal, D.M., Furness, S.G.B., Christopoulos, G., Coudrat, T.*, et al.* (2017). Phase-plate cryo-EM structure of a class B GPCR-G-protein complex. Nature *546*, 118-123.

Liu, J.J., Horst, R., Katritch, V., Stevens, R.C., and Wuthrich, K. (2012). Biased signaling pathways in beta2-adrenergic receptor characterized by 19F-NMR. Science *335*, 1106-1110.

Maeda, S., Qu, Q., Robertson, M.J., Skiniotis, G., and Kobilka, B.K. (2019). Structures of the M1 and M2 muscarinic acetylcholine receptor/G-protein complexes. Science *364*, 552-557.

Majumdar, S., and Devi, L.A. (2018). Strategy for making safer opioids bolstered. Nature *553*, 286-288.

Manglik, A., Kobilka, B.K., and Steyaert, J. (2017). Nanobodies to Study G Protein-Coupled Receptor Structure and Function. Annual review of pharmacology and toxicology *57*, 19-37.

Manglik, A., Lin, H., Aryal, D.K., McCorvy, J.D., Dengler, D., Corder, G., Levit, A., Kling, R.C., Bernat, V., Hubner, H.*, et al.* (2016). Structure-based discovery of opioid analgesics with reduced side effects. Nature *537*, 185-190.

Markby, D.W., Onrust, R., and Bourne, H.R. (1993). Separate GTP binding and GTPase activating domains of a G alpha subunit. Science *262*, 1895-1901.

McConnell, H.M. (1958). Reaction Rates by Nuclear Magnetic Resonance. The Journal of chemical physics *28*, 430-431.

Miehling, J., Goricanec, D., and Hagn, F. (2018). A Split-Intein-Based Method for the Efficient Production of Circularized Nanodiscs for Structural Studies of Membrane Proteins. Chembiochem : a European journal of chemical biology *19*, 1927-1933.

Milligan, G., and Kostenis, E. (2006). Heterotrimeric G-proteins: a short history. British journal of pharmacology *147 Suppl 1*, S46-55.

Morris, G.A., and Freeman, R. (1979). Enhancement of nuclear magnetic resonance signals by polarization transfer. Journal of the American Chemical Society *101*, 760-762.

Mustain, W.C., Rychahou, P.G., and Evers, B.M. (2011). The role of neurotensin in physiologic and pathologic processes. Current opinion in endocrinology, diabetes, and obesity *18*, 75-82.

Nalivaiko, E., Michaud, J.C., Soubrie, P., and Le Fur, G. (1998). Electrophysiological evidence for putative subtypes of neurotensin receptors in guinea-pig mesencephalic dopaminergic neurons. Neuroscience *86*, 799-811.

Nasr, M.L., Baptista, D., Strauss, M., Sun, Z.J., Grigoriu, S., Huser, S., Pluckthun, A., Hagn, F., Walz, T., Hogle, J.M.*, et al.* (2017). Covalently circularized nanodiscs for studying membrane proteins and viral entry. Nature methods *14*, 49-52.

Nehme, R., Carpenter, B., Singhal, A., Strege, A., Edwards, P.C., White, C.F., Du, H., Grisshammer, R., and Tate, C.G. (2017). Mini-G proteins: Novel tools for studying GPCRs in their active conformation. PloS one *12*, e0175642.

Neudecker, P., Lundstrom, P., and Kay, L.E. (2009). Relaxation dispersion NMR spectroscopy as a tool for detailed studies of protein folding. Biophysical journal *96*, 2045-2054.

Oldham, W.M., and Hamm, H.E. (2006). Structural basis of function in heterotrimeric G proteins. Quarterly reviews of biophysics *39*, 117-166.

Oldham, W.M., and Hamm, H.E. (2008). Heterotrimeric G protein activation by G-protein-coupled receptors. Nature reviews Molecular cell biology *9*, 60-71.

Palczewski, K., Kumasaka, T., Hori, T., Behnke, C.A., Motoshima, H., Fox, B.A., Le Trong, I., Teller, D.C., Okada, T., Stenkamp, R.E.*, et al.* (2000). Crystal structure of rhodopsin: A G protein-coupled receptor. Science *289*, 739-745.

Pervushin, K., Riek, R., Wider, G., and Wuthrich, K. (1997). Attenuated T2 relaxation by mutual cancellation of dipole-dipole coupling and chemical shift anisotropy indicates an avenue to NMR structures of very large biological macromolecules in solution. Proceedings of the National Academy of Sciences of the United States of America *94*, 12366-12371.

Peterson, Y.K., and Luttrell, L.M. (2017). The Diverse Roles of Arrestin Scaffolds in G Protein-Coupled Receptor Signaling. Pharmacological reviews *69*, 256-297.

Proudfoot, A., Frank, A.O., Frommlet, A., and Lingel, A. (2019). Selective Methyl Labeling of Proteins: Enabling Structural and Mechanistic Studies As Well As Drug Discovery Applications by Solution-State NMR. Methods in enzymology *614*, 1-36.

Qi, X., Liu, H., Thompson, B., McDonald, J., Zhang, C., and Li, X. (2019). Cryo-EM structure of oxysterol-bound human Smoothened coupled to a heterotrimeric Gi. Nature *571*, 279-283.

Rasmussen, S.G., Choi, H.J., Fung, J.J., Pardon, E., Casarosa, P., Chae, P.S., Devree, B.T., Rosenbaum, D.M., Thian, F.S., Kobilka, T.S.*, et al.* (2011a). Structure of a nanobody-stabilized active state of the beta(2) adrenoceptor. Nature *469*, 175-180.

Rasmussen, S.G., Choi, H.J., Rosenbaum, D.M., Kobilka, T.S., Thian, F.S., Edwards, P.C., Burghammer, M., Ratnala, V.R., Sanishvili, R., Fischetti, R.F.*, et al.* (2007). Crystal structure of the human beta2 adrenergic G-protein-coupled receptor. Nature *450*, 383-387.

Rasmussen, S.G., DeVree, B.T., Zou, Y., Kruse, A.C., Chung, K.Y., Kobilka, T.S., Thian, F.S., Chae, P.S., Pardon, E., Calinski, D.*, et al.* (2011b). Crystal structure of the beta2 adrenergic receptor-Gs protein complex. Nature *477*, 549-555.

Religa, T.L., Ruschak, A.M., Rosenzweig, R., and Kay, L.E. (2011). Site-directed methyl group labeling as an NMR probe of structure and dynamics in supramolecular protein systems: applications to the proteasome and to the ClpP protease. Journal of the American Chemical Society *133*, 9063-9068.

Ring, A.M., Manglik, A., Kruse, A.C., Enos, M.D., Weis, W.I., Garcia, K.C., and Kobilka, B.K. (2013). Adrenaline-activated structure of beta2-adrenoceptor stabilized by an engineered nanobody. Nature *502*, 575-579.

Rodriguez Camargo, D.C., Korshavn, K.J., Jussupow, A., Raltchev, K., Goricanec, D., Fleisch, M., Sarkar, R., Xue, K., Aichler, M., Mettenleiter, G.*, et al.* (2017). Stabilization and structural analysis of a membrane-associated hIAPP aggregation intermediate. eLife *6.*

Rosenbaum, D.M., Cherezov, V., Hanson, M.A., Rasmussen, S.G., Thian, F.S., Kobilka, T.S., Choi, H.J., Yao, X.J., Weis, W.I., Stevens, R.C.*, et al.* (2007). GPCR engineering yields high-resolution structural insights into beta2-adrenergic receptor function. Science *318*, 1266-1273.

Salzmann, M., Pervushin, K., Wider, G., Senn, H., and Wuthrich, K. (1998). TROSY in triple-resonance experiments: new perspectives for sequential NMR assignment of large proteins. Proceedings of the National Academy of Sciences of the United States of America *95*, 13585-13590.

Salzmann, M., Wider, G., Pervushin, K., Senn, H., and Wüthrich, K. (1999). TROSY-type Triple-Resonance Experiments for Sequential NMR Assignments of Large Proteins. Journal of the American Chemical Society *121*, 844-848.

Santos, R., Ursu, O., Gaulton, A., Bento, A.P., Donadi, R.S., Bologa, C.G., Karlsson, A., Al-Lazikani, B., Hersey, A., Oprea, T.I., *et al.* (2017). A comprehensive map of molecular drug targets. Nature reviews Drug discovery *16*, 19-34.

Sarkar, C.A., Dodevski, I., Kenig, M., Dudli, S., Mohr, A., Hermans, E., and Pluckthun, A. (2008). Directed evolution of a G protein-coupled receptor for expression, stability, and binding selectivity. Proceedings of the National Academy of Sciences of the United States of America *105*, 14808-14813.

Sattler, M., Schleucher, J., and Griesinger, C. (1999). Heteronuclear multidimensional NMR experiments for the structure determination of proteins in solution employing pulsed field gradients. Progress in Nuclear Magnetic Resonance Spectroscopy *34*, 93-158.

Schlinkmann, K.M., Hillenbrand, M., Rittner, A., Kunz, M., Strohner, R., and Pluckthun, A. (2012). Maximizing detergent stability and functional expression of a GPCR by exhaustive recombination and evolution. Journal of molecular biology *422*, 414-428.

Schwieters, C.D., Kuszewski, J.J., Tjandra, N., and Clore, G.M. (2003). The Xplor-NIH NMR molecular structure determination package. Journal of magnetic resonance *160*, 65-73.

Shimada, I., Ueda, T., Kofuku, Y., Eddy, M.T., and Wuthrich, K. (2019). GPCR drug discovery: integrating solution NMR data with crystal and cryo-EM structures. Nature reviews Drug discovery *18*, 59-82.

Smith, J.S., Lefkowitz, R.J., and Rajagopal, S. (2018). Biased signalling: from simple switches to allosteric microprocessors. Nature reviews Drug discovery *17*, 243-260.

Smrcka, A.V. (2008). G protein betagamma subunits: central mediators of G protein-coupled receptor signaling. Cellular and molecular life sciences : CMLS *65*, 2191-2214.

Soergel, D.G., Subach, R.A., Burnham, N., Lark, M.W., James, I.E., Sadler, B.M., Skobieranda, F., Violin, J.D., and Webster, L.R. (2014). Biased agonism of the mu-opioid receptor by TRV130 increases analgesia and reduces on-target adverse effects versus morphine: A randomized, double-blind, placebo-controlled, crossover study in healthy volunteers. Pain *155*, 1829-1835.

Solt, A.S., Bostock, M.J., Shrestha, B., Kumar, P., Warne, T., Tate, C.G., and Nietlispach, D. (2017). Insight into partial agonism by observing multiple equilibria for ligand-bound and Gs-mimetic nanobody-bound beta1-adrenergic receptor. Nature communications *8*, 1795.

Spera, S., and Bax, A. (1991). Empirical correlation between protein backbone conformation and C.alpha. and C.beta. 13C nuclear magnetic resonance chemical shifts. Journal of the American Chemical Society *113*, 5490-5492.

Sprang, S.R. (1997). G protein mechanisms: insights from structural analysis. Annual review of biochemistry *66*, 639-678.

Steyaert, J., and Kobilka, B.K. (2011). Nanobody stabilization of G protein-coupled receptor conformational states. Current opinion in structural biology *21*, 567-572.

Susac, L., Eddy, M.T., Didenko, T., Stevens, R.C., and Wuthrich, K. (2018). A2A adenosine receptor functional states characterized by (19)F-NMR. Proceedings of the National Academy of Sciences of the United States of America *115*, 12733-12738.

Thal, D.M., Glukhova, A., Sexton, P.M., and Christopoulos, A. (2018). Structural insights into G-protein-coupled receptor allostery. Nature *559*, 45-53.

Tjandra, N., and Bax, A. (1997). Direct measurement of distances and angles in biomolecules by NMR in a dilute liquid crystalline medium. Science *278*, 1111-1114.

Toyama, Y., Kano, H., Mase, Y., Yokogawa, M., Osawa, M., and Shimada, I. (2017). Dynamic regulation of GDP binding to G proteins revealed by magnetic field-dependent NMR relaxation analyses. Nature communications *8*, 14523.

Tugarinov, V., Hwang, P.M., Ollerenshaw, J.E., and Kay, L.E. (2003). Cross-correlated relaxation enhanced 1H[bond]13C NMR spectroscopy of methyl groups in very high molecular weight proteins and protein complexes. Journal of the American Chemical Society *125*, 10420-10428.

Tugarinov, V., Kanelis, V., and Kay, L.E. (2006). Isotope labeling strategies for the study of high-molecular-weight proteins by solution NMR spectroscopy. Nature protocols *1*, 749-754.

Van Eps, N., Preininger, A.M., Alexander, N., Kaya, A.I., Meier, S., Meiler, J., Hamm, H.E., and Hubbell, W.L. (2011). Interaction of a G protein with an activated receptor opens the interdomain interface in the alpha subunit. Proceedings of the National Academy of Sciences of the United States of America *108*, 9420-9424.

Venkatakrishnan, A.J., Deupi, X., Lebon, G., Heydenreich, F.M., Flock, T., Miljus, T., Balaji, S., Bouvier, M., Veprintsev, D.B., Tate, C.G.*, et al.* (2016). Diverse activation pathways in class A GPCRs converge near the G-protein-coupling region. Nature *536*, 484-487.

Venyaminov, S., Baikalov, I.A., Shen, Z.M., Wu, C.S., and Yang, J.T. (1993). Circular dichroic analysis of denatured proteins: inclusion of denatured proteins in the reference set. Analytical biochemistry *214*, 17-24.

Vincent, J.P., Mazella, J., and Kitabgi, P. (1999). Neurotensin and neurotensin receptors. Trends in pharmacological sciences *20*, 302-309.

Wacker, D., Stevens, R.C., and Roth, B.L. (2017). How Ligands Illuminate GPCR Molecular Pharmacology. Cell *170*, 414-427.

Weis, W.I., and Kobilka, B.K. (2018). The Molecular Basis of G Protein-Coupled Receptor Activation. Annual review of biochemistry *87*, 897-919.

White, J.F., Noinaj, N., Shibata, Y., Love, J., Kloss, B., Xu, F., Gvozdenovic-Jeremic, J., Shah, P., Shiloach, J., Tate, C.G.*, et al.* (2012). Structure of the agonist-bound neurotensin receptor. Nature *490*, 508-513.

Wu, Z., Martinez-Fong, D., Tredaniel, J., and Forgez, P. (2012). Neurotensin and its high affinity receptor 1 as a potential pharmacological target in cancer therapy. Frontiers in endocrinology *3*, 184.

Xu, J., Hu, Y., Kaindl, J., Risel, P., Hubner, H., Maeda, S., Niu, X., Li, H., Gmeiner, P., Jin, C.*, et al.* (2019). Conformational Complexity and Dynamics in a Muscarinic Receptor Revealed by NMR Spectroscopy. Molecular cell *75*, 53-65 e57.

Yao, X.Q., Malik, R.U., Griggs, N.W., Skjaerven, L., Traynor, J.R., Sivaramakrishnan, S., and Grant, B.J. (2016). Dynamic Coupling and Allosteric Networks in the alpha Subunit of Heterotrimeric G Proteins. The Journal of biological chemistry *291*, 4742-4753.

Ye, L., Van Eps, N., Zimmer, M., Ernst, O.P., and Prosser, R.S. (2016). Activation of the A2A adenosine G-protein-coupled receptor by conformational selection. Nature *533*, 265-268.

Zhang, Y., Sun, B., Feng, D., Hu, H., Chu, M., Qu, Q., Tarrasch, J.T., Li, S., Sun Kobilka, T., Kobilka, B.K.*, et al.* (2017). Cryo-EM structure of the activated GLP-1 receptor in complex with a G protein. Nature *546*, 248-253.

Zhao, L.H., Ma, S., Sutkeviciute, I., Shen, D.D., Zhou, X.E., de Waal, P.W., Li, C.Y., Kang, Y., Clark, L.J., Jean-Alphonse, F.G.*, et al.* (2019). Structure and dynamics of the active human parathyroid hormone receptor-1. Science *364*, 148-153.

Zweckstetter, M. (2008). NMR: prediction of molecular alignment from structure using the PALES software. Nature protocols *3*, 679-690.

Zweckstetter, M., and Bax, A. (2001). Characterization of molecular alignment in aqueous suspensions of Pf1 bacteriophage. Journal of biomolecular NMR *20*, 365-377.

List of publications

Goricanec, D., and Hagn, F. (2019). NMR backbone and methyl resonance assignments of an inhibitory G-alpha subunit in complex with GDP. Biomolecular NMR assignments *13*, 131-137.

Goricanec, D., Stehle, R., Egloff, P., Grigoriu, S., Pluckthun, A., Wagner, G., and Hagn, F. (2016). Conformational dynamics of a G-protein alpha subunit is tightly regulated by nucleotide binding. Proceedings of the National Academy of Sciences of the United States of America *113*, E3629-3638.

Miehling, J., **Goricanec, D**., and Hagn, F. (2018). A Split-Intein-Based Method for the Efficient Production of Circularized Nanodiscs for Structural Studies of Membrane Proteins. Chembiochem : a European journal of chemical biology *19*, 1927-1933.

Rodriguez Camargo, D.C., Korshavn, K.J., Jussupow, A., Raltchev, K., **Goricanec, D**., Fleisch, M., Sarkar, R., Xue, K., Aichler, M., Mettenleiter, G*., et al.* (2017). Stabilization and structural analysis of a membrane-associated hIAPP aggregation intermediate. eLife *6*.

Acknowledgements